# Physico-Chemical Phenomena Governing the Behaviour of Radioactive Substances. Site-specific characteristics

Restoration Strategies for Radioactively Contaminated
Sites and their Close Surroundings
RESTRAT - WP2

*Vinzenz Brendler*
*Forschungszentrum Rossendorf, Institute of Radiochemistry*
*P.O.Box. 51 01 19, D-01314 Dresden, Germany*

RESTRAT-TD.5

18 August 1999 - Issue 2:d

Project FI4P-CT95-0021a ( PL 950128 )
co-funded by the Nuclear Fission Safety Programme of the European Commission

## Summary

This technical deliverable of the EC project RESTRAT summarizes the work performed in working package WP 2.2: "Physico-Chemical Phenomena Governing the Behaviour of Radioactive Substances". For all five sites that are investigated in the framework of the RESTRAT project, a detailed description of the proposed compartment structure for the modelling with the PRISM / BIOPATH package [Gardner *et al.*, 1983; Bergström *et al.*, 1982] is shown for five selected sites. This is accompanied by a summary of the main physico-chemical parameters for all relevant aqueous phases in contact with minerals. All analytical results have been checked by chemical speciation modelling with EQ3/6 [Wolery, 1995] to reveal data gaps and inconsistencies. Thus attained additional insight into the physico-chemical characteristics of the example sites, together with some speciation patterns for the main contaminants are also presented. Further section deal with the establishment of the thermodynamic data base for complexation and hydrolysis reactions, mineral precipitation and dissolution, and surface complexation. The resulting input files for the newly developed combination of MINTEQA2 [Allison *et al.*, 1991] with PRISM / BIOPATH are given also. Finally, the new approach is tested after verifying the data sets and compartment structure, including a comprehensive test of the model implementation. The results thereof make up the last part of this report. The software itself is issued in RESTRAT TD 7 [Brendler *et al.*, 1999].

## Table of Contents

## List of Tables

## List of Figures

## List of Appendices

# 1. Introduction

The main objective of the overall RESTRAT project is to develop a generic methodology for the ranking of restoration techniques as a function of site and contamination characteristics. The work has been broken down into several working packages. This technical deliverable, as required by the contract, summarizes the work performed in working package WP 2: Physico-chemical phenomena during Phase 2: Site-specific characteristics. It pursues the Technical Deliverable RESTRAT TD 2 [Brendler, 1999], which summarized the state-of-the-art of chemical speciation and migration modelling, leading to the conclusion that it is necessary to unfold the wide-spread $K_d$-concept of distribution coefficients. $K_d$ values have generally both large uncertainties and important effects on the risk assessment predictions, particularly as models are often sensitive towards changes in $K_d$. Hence an unfolding makes it possible to perform more detailed sensitivity analysis, to find the most critical parameters, to reduce parameter space, and finally to pave the way for more reliable models. In its last parts, TD 2 described data structures and data flows for the proposed strategy of a $K_d$ unfolding. Here in TD 5 the focus will be on concrete models for surface complexation, their application in the MINTEQA2 code [Allison *et al.*, 1991] and the specific situation with regard to each site of the RESTRAT project.

# 2. Overview About Thermodynamic Databases

## 2.1. Complex stability constants (including hydrolysis) and solubilities

For the sites considered in the RESTRAT project the elements Mn, Co, Ni, Cs, Th, U, Pu, and Am (or radioisotopes thereof) are classified as contaminants. A detailed assignment to the sites is given in the sections dealing with the respective site-specific characteristics. Foundation of the thermodynamic data base used in this project was the data base distributed together with MINTEQA2, which is in turn based on the WATEQ3 [Ball *et al.*, 1981] data base as developed by the U.S. Geological Survey. This data base has been updated from various other sources. A number of databases have been scanned for their respective thermodynamic data concerning hydrolysis (if applicable), complexation and precipitation / dissolution reactions:

- OECD Nuclear Energy Agency - Thermodynamic Database (NEA TDDB) Recommendations for Uranium as of 1992 [Grenthe *et al.*, 1992] with the corrections included in the corresponding Americium volume [Silva *et al.*, 1995];
- LLNL Gembochs COM Data Base in Version 8 Release 2, as distributed with EQ3/6 Version 7.2b from August 1995, it includes also the NEA TDDB values for Uranium [Wolery, 1995];
- LLNL Gembochs ALT Data Base, which is in large parts identical to the COM data base (see above), but already taking into account the NEA TDDB recommendations for Neptunium und Plutonium [Wolery, 1995];
- FZR extensions to the LLNL Gembochs COM data base;
- NAGRA Chemical Thermodynamic Database: Redox coupled version for EQ3/6 and PHREEQE, version from August 1994 [Pearson and Berner, 1991; Pearson *et al.*, 1991; Pearson, 1994];
- NIST Critically Selected Stability Constants, Version 4.0 from December 1997 [Smith *et al.*, 1997];
- CHEMVAL 6.S data base as described in: CHEMVAL 2: Final Report EUR 16648, 1996 [Falck *et al.*, 1996];
- ZZ-Hatches database, NEA Release 9 from November 1996 [Cross and Ewart, 1991; Bond *et al.*, 1992; Bond *et al.*; 1996].

However, it should always be kept in mind, that the speciation of the contaminants (as minor components, for a complete list for all example sites see Table 1) also strongly depends on the pH, Eh, and the concentration of other major ionic components of the solution, like potassium, magnesium, sodium, carbonate, sulfate or chloride. And for those elements, the quality of the available data sets is often much lower than for the radionuclides, which have attracted considerable research and reviewing efforts especially during the last decade.

Table 1: List of relevant contaminants for all RESTRAT example sites.

| Site | Contaminants |
|---|---|
| Drigg | U, $^{137}$Cs, $^{239}$Pu, and $^{241}$Am |
| Ranstad Tailing | U, Mn, and Ni |
| Molse Nete | $^{60}$Co, $^{137}$Cs, $^{239}$Pu, and $^{241}$Am |
| Ravenglass Estuary | $^{137}$Cs, $^{239}$Pu, and $^{241}$Am |
| Lake Tranebärssjön | U, Mn, and Ni |

For all project example sites, several chemical speciation models were computed to verify the consistency of the analytical data and to extract information, when possible, about minerals in equilibrium with the solution. The geochemical speciation software EQ3/6 [Wolery, 1995] was used, together with the accompanying LLNL Gembochs ALT data base. This data base was corrected for several erroneous entries (e.g., uranyl sulfates). Moreover, the aqueous complex species $Ca_2UO_2(CO_3)_3$ [Bernhard *et al.*, 1997] and $UO_2(SO_4)_3^{4-}$ [Geipel *et al.*, 1997] were added. The MINTEQA2 software, used in the integrated model for $K_d$ computations, comes with its own database, derived from the WATEQ3 compilation [Ball *et al.*, 1983]. This database is outdated concerning the actinides Plutonium, Neptunium, and Americium, and therefore was adapted to the NEA recommendations using the ALT database of EQ3/6. Also, Cobalt and its compounds had to be added to the MINTEQA2 database, here the data from Smith *et al.*, 1997, were used to be consistent with the data set applied by Dzombak and Morel to derive the SCM complexation constants for Cobalt.

## 2.2. Sorption Parameters

There is in general a lack of sorption parameters in the literature, the data coverage is by far more sparse than in case of the complex stability constants discussed above. There are some older compilations of sorption data available [Higgo, 1987; Higgo, 1988], but they exclusively focus on the $K_d$ concept and are therefore of less value to this project. That means in order to get the thermodynamic parameters necessary to model sorption processes, one has to survey the primary literature. The concept of surface complexation models (SCM) was introduced first at the end of the seventies, and because it took some time until more researchers were attracted by this development, most of the experimental work was only quite recently published. With regard to the sites investigated under the RESTRAT project, the following publications about SCM parameter sets are of importance:

- a rather comprehensive collection about SCM for hydrous ferric oxides is issued by Dzombak and Morel [Dzombak and Morel, 1990];
- iron ions sorbing on sphalerite (ZnS) were investigated by Zhang [Zhang *et al.*, 1995a; Zhang *et al.*, 1995b];
- surface properties of hydrous fluorapatite ($Ca_{10}(PO_4)_6F_2$) were determined by Wu [Wu *et al.*, 1991];
- uranium(VI) sorption onto ferrihydrite was explained with SCM by Hsi and Langmuir [Hsi and Langmuir, 1985] and by Waite [Waite *et al.*, 1994] and;
- complexation of carbonate species on goethite surfaces was investigated by van Geen [van Geen *et al.*, 1994];
- surface properties of carbonates of iron, manganese and calcium were determined by van Cappellen [van Cappellen *et al.*, 1993];
- sulfate complexation at goethite surfaces was studied by Persson and Lövgren [Persson and Lövgren, 1996];
- thorium complexation at amorphous silica was studied by Östhols [Östhols, 1995] and by Olin and Lehikoinen [Olin and Lehikoinen, 1997];
- the sorption of nickel on quartz, manganese oxide, kaolinite and goethite were also investigated by Olin and Lehikoinen [Olin and Lehikoinen, 1997];
- surface properties of goethite were interpreted in terms of SCM by Lumsdon and Evans [Lumsdon and Evans, 1994];
- the sorption of copper on anatase ($TiO_2$) was studied by Ludwig and Schindler [Ludwig and Schindler, 1994];
- surface properties of goethite ($\alpha$-FeOOH), alumina ($\alpha$-$Al_2O_3$) and rutile ($TiO_2$) were investigated by Hayes [Hayes *et al.*, 1990];

- sorption of lead and cadmium onto goethite was investigated by Hayes and Leckie [Hayes and Leckie, 1987];
- sorption of mercury chloride onto goethite was studied by Gunneriusson and Sjöberg [Gunneriusson and Sjöberg, 1993];
- sorption of uranium(VI) on a variety of iron oxides (hydrous ferric oxide, goethite and haematite) was studied by Dicke and Smith [Dicke and Smith, 1996];

The obvious lack of suitable parameter sets has several consequences: Best would be in most cases to perform own experiments to determine the missing values. However, this is often hampered by restrictions in personnel, money and time. So it may be necessary to use analogies both between various ions in the aqueous phase, and also between minerals, to transfer surface complexation parameters from an experimental investigated system to the own system of interest. This can be done by simple oxidation state analogies as often used for actinides. Another way is to utilize Linear Free Energy Relationships (LFER) to derive stability constants for the species of interest from experimental results for other components, see Dzombak and Morel, 1990 for a more detailed explanation and also some nice applications. If such estimations of thermodynamic parameters required for SCM is not applicable, then one should be able to fall back to simpler approaches like the $K_d$ model. This is ensured by the MINTEQA2 software as outlined in TD 2 [Brendler, 1999].

### 2.2.1. Intrinsic surface properties

Before explaining the data base for the surface complexation reactions, a few words are necessary to the intrinsic surface properties such as specific surface area $\mathbf{S_A}$, the number of distinct site types, the surface site density $\Gamma$ or the electrostatic properties (capacities $\mathbf{C_n}$ of the various surface layers). Whereas the specific surface area $\mathbf{S_A}$ generally is given in $m^2$ / g, there is a variety of distinct surface site density terms in use. Table 2 lists them, together with the conversion into a surface site density given in mole per litre solution, as it is required by MINTEQA2.

Table 2: Various representations of surface site densities and their mutual conversion.

| Variable | Unit | Conversion to $\Gamma_M$ |
|---|---|---|
| $\Gamma$ | mol / $m^2$ surface | $\Gamma_M = \Gamma \cdot S_A \cdot C_S$ |
| $\Gamma_N$ | sites / $nm^2$ surface | $\Gamma_M = \Gamma_N \cdot S_A \cdot C_S \cdot F_C / N_A$ |
| $\Gamma_M$ | mol / L solution | – |
| $\Gamma_X$ | mol / mol metal | $\Gamma_M = \Gamma_X \cdot C_S \cdot \nu_M / M_S$ |
| $\Gamma_W$ | mol / g solid | $\Gamma_M = \Gamma_W \cdot C_S$ |

$\mathbf{C_S}$ is the concentration of the sorbing solid in the solution (in g / L), $\mathbf{F_C}$ is the conversion factor from $nm^2$ to $m^2$ ($10^{18}$), $\mathbf{N_A}$ is Avogadro's number ($6.022045 \cdot 10^{23}$ $mol^{-1}$), $\nu_\mathbf{M}$ is the stoichiometric factor of the binding metal in the solid, and $\mathbf{M_S}$ is the molar mass of the solid. Whereas the solid concentration $\mathbf{C_S}$ can be determined easily and directly in aqueous suspensions, the question is more difficult in aquifers consisting of porous rocks. To derive a "solid concentration in a solution", the following approximation (assuming a density of one for the water in the aquifer) can be used:

$$C_S = \frac{\rho \cdot (1 - P)}{P} \quad \textbf{(1)}$$

where ρ is the rock density and **P** is the porosity. Densities of rocks and minerals relevant for this project are taken from various sources as summarized in Table 3. For various surfaces, more than one surface type has been postulated, with different properties (binding strength, site density, protonation constant).

Table 3: Densities of important minerals

| Mineral | Density in g / cm$^3$ | Reference |
|---|---|---|
| Calcite ($CaCO_3$) | 2.71 | [Altmann *et al.*, 1984] |
| Quartz ($SiO_2$) | 2.66 | [Altmann *et al.*, 1984] |
| Goethite (α-FeOOH) | 4.26 | [Schwertmann and Cornell, 1991] |
| Muscovite (also Illite) | 2.77 - 2.88 *Mean: 2.81* | [Strübel and Zimmer, 1991] |
| Kaolinite | 2.61 - 2.68 *Mean: 2.64* | [Strübel and Zimmer, 1991] |
| K-Feldspar (Orthoclase - $K[AlSi_3O_8]$) | 2.54 - 2.63 *Mean: 2.58* | [Strübel and Zimmer, 1991] |
| Pyrite ($FeS_2$) | 4.87 | [Altmann *et al.*, 1984] |
| Graphite | 2.08 - 2.23 *Mean: 2.15* | [Strübel and Zimmer, 1991] |
| Ferrihydrite | 3.96 | [Schwertmann and Cornell, 1991] |
| Chlorite | 2.5 - 3.3 *Mean: 2.9* | [Strübel and Zimmer, 1991] |

### 2.2.2. SCM data base for hydrous ferric oxides (HFO)

A data base in the MINTEQA2 format for surface reactions on hydrous ferric oxides (HFO) has been established applying the Diffuse Double Layer model. This data base (HFO_DDL.DBS) was used whenever appropriate in the combined PRISM / BIOPATH / MINTEQA2 model. The assumed stoichiometry for HFO was $Fe(OH)_3$, which corresponds to $Fe_2O_3 \cdot 3H_2O$, but it should be kept in mind that the stoichiometry is not really constant. Depending on the chemical environment, the precipitation process, and the aging time the water content may change between one and three moles. Also the density varies between 2.2 and 4.0 g / cm$^3$ [Schwertmann and Cornell, 1991]. HFO are the natural precursors of other thermodynamically more stable iron minerals, such as Goethite, Lepidocrocite and Haematite, when precipitation in oversaturated solutions starts. HFO do not show a regular crystal lattice, and have an considerably larger

surface than other iron minerals, 600 $m^2$ / g [Davies and Leckie, 1978] compared, e.g., with 35 - 52 $m^2$ / g for Goethite [Hayes and Leckie, 1987; Puukko and Hakanen, 1997]. This huge surface in turn promotes any sorption processes. The data base HFO_DDL.DBS must be used in conjunction with a given set of intrinsic surface properties. In conformity with Dzombak and Morel, 1990 two distinct binding sites are postulated: a strong one with a site density of 0.09 µmol / $m^2$ and a weak one with 3.75 µmol / $m^2$. The protonation constants are equal for both site types:

$$\equiv Fe-OH_2^+ \rightleftarrows \equiv Fe-OH + H^+ \qquad \log\beta_1 = -7.29 \qquad \textbf{(2)}$$

$$\equiv Fe-OH \rightleftarrows \equiv Fe-O^- + H^+ \qquad \log\beta_2 = -8.93 \qquad \textbf{(3)}$$

Table 4 gives the intrinsic reaction constants for the surface complexation of various cations and anions, based on the diffuse double layer model. It is indicated whether the given reaction is for a strong or weak sorption site, and whether the value was derived from a linear free energy relationship (LFER).

Table 4: Thermodynamic database for sorption onto hydrous ferric oxides described with the diffuse double layer surface complexation model.

| Ion | Reaction | log $K_{intr}$ | Reference | Remark |
|---|---|---|---|---|
| $UO_2^{2+}$ | $\equiv FeOH + UO_2^{2+} + H_2O \rightleftarrows \equiv FeO\text{-}UO_2(OH) + 2\,H^+$<br>$\equiv FeOH + UO_2^{2+} + H_2O \rightleftarrows \equiv FeO\text{-}UO_2(OH) + 2\,H^+$ | -3.12<br>-5.00 | Dicke & Smith 1996 | Strong<br>Weak |
| $PuO_2^{2+}$ | $\equiv FeOH + PuO_2^{2+} \rightleftarrows \equiv FeO\text{-}PuO_2^+ + H^+$<br>$\equiv FeOH + PuO_2^{2+} \rightleftarrows \equiv FeO\text{-}PuO_2^+ + H^+$ | 5.4<br>3.0 | Dzombak & Morel 1990 | Strong, LFER<br>Weak, LFER |
| $Pu^{4+}$ | $\equiv FeOH + Pu^{4+} + 3\,CO_3^{2-} + H^+ \rightleftarrows \equiv FeOH_2\text{-}Pu(CO_3)_3^-$ | 58.0 | Baston *et al.* 1995 | Strong |
| $Ca^{2+}$ | $\equiv FeOH + Ca^{2+} \rightleftarrows \equiv FeOH\text{-}Ca^{2+}$<br>$\equiv FeOH + Ca^{2+} \rightleftarrows \equiv FeO\text{-}Ca^+ + H^+$ | 4.97<br>-5.85 | Dzombak & Morel 1990 | Strong<br>Weak |
| $Mg^{2+}$ | $\equiv FeOH + Mg^{2+} \rightleftarrows \equiv FeO\text{-}Mg^+ + H^+$ | -4.6 | Dzombak & Morel 1990 | Weak, LFER |
| $Co^{2+}$ | $\equiv FeOH + Co^{2+} \rightleftarrows \equiv FeO\text{-}Co^+ + H^+$<br>$\equiv FeOH + Co^{2+} \rightleftarrows \equiv FeO\text{-}Co^+ + H^+$ | -0.46<br>-3.01 | Dzombak & Morel 1990 | Strong<br>Weak |
| $Mn^{2+}$ | $\equiv FeOH + Mn^{2+} \rightleftarrows \equiv FeO\text{-}Mn^+ + H^+$<br>$\equiv FeOH + Mn^{2+} \rightleftarrows \equiv FeO\text{-}Mn^+ + H^+$ | -0.4<br>-3.5 | Dzombak & Morel 1990 | Strong, LFER<br>Weak, LFER |
| $Am^{3+}$ | $\equiv FeOH + Am^{3+} + 2\,CO_3^{2-} + H^+ \rightleftarrows \equiv FeO\text{-}Am(HCO_3)_2$ | 29.0 | Baston *et al.* 1995 | Strong |
| $SO_4^{2-}$ | $\equiv FeOH + SO_4^{2-} + H^+ \rightleftarrows \equiv Fe\text{-}SO_4^- + H_2O$<br>$\equiv FeOH + SO_4^{2-} \rightleftarrows \equiv FeOH\text{-}SO_4^{2-}$ | 7.78<br>0.79 | Dzombak & Morel 1990 | LFER<br>LFER |
| $SiO_3^{2-}$ | $\equiv FeOH + SiO_3^{2-} + H^+ \rightleftarrows \equiv Fe\text{-}SiO_3^- + H_2O$<br>$\equiv FeOH + SiO_3^{2-} \rightleftarrows \equiv FeOH\text{-}SiO_3^{2-}$ | 15.9<br>8.3 | Dzombak & Morel 1990 | LFER |

The simple cations $Na^+$, $K^+$, and $Cs^+$ and the anions $CO_3^{2-}$, $Cl^-$ and $NO_3^-$ are considered to be non-sorbing. This means that the contaminant $^{137}Cs$, present in three of the examples cases, can not be dealt with in the framework of the SCM, here other approaches such as ion exchange equilibria must be used. There were no data available for $Al^{3+}$, but an omission of $Al^{3+}$ is not so critical, because the sorption of the contaminants is mainly competing with the major cationic components $Ca^{2+}$ and $Mg^{2+}$. Anions, as already outlined in TD 2 [Brendler, 1999], section 8.2, are considered to sorb on strong and weak sites with the same stability constants.

### 2.2.3. SCM data base for clays

In comparison to HFO the SCM data pool for clays is less well established. However, as is it was first investigated by Cremers and Maes, 1985, even in clay material minor parts (below 5% of total mass) of iron oxides and hydroxides can play a dominant in sorption. This means that also for clay minerals the content of HFO should be carefully analysed, and either a combination of HFO and clay sorption data bases, or even a sole consideration of HFO may lead to the most realistic speciation and transport model. A successful application of this approach can be found in Bond *et al.*, 1990.

The intrinsic surface properties of alumosilicates reported so far in the literature dealing with SCM cover a range of more than one order of magnitude (all values in $m^2/g$): Kaolinite 11.38, Muscovite 1.4, Montmorillonite 9.7, Biotite 1.3, Feldspars 0.3 - 0.7, Chlorite 1.6, and Phyllite 4. The Diffuse Double Layer model had only been applied to sorption experiments of uranium onto Montmorillonite, whereas the Constant Capacitance model was used to interpret sorption of nickel onto Kaolinite. To create a useful SCM data base for the modelling with MINTEQA2, data for different alumosilicates had to combined, but at the moment the accessible data base is to sparse to do so.

# 3. Site-specific Characteristics

At present, the aqueous phases important for the various compartments of each site are rather well characterized. The main problem is a similar description of the dominant solid phases, i.e. a geochemical-mineralogical characterization of the relevant rocks and minerals. Here the available data is insufficient, own investigations are complicated and time-consuming, but they are under way for the Drigg site at least.

The following conventions apply to all the tables about physico-chemical analytics: "n.d." stands for "not determined", a value of zero stands for "value was determined to be below detection limit". Furthermore, superscript [1)] indicates values (most often redox potentials) assigned to compartments based on a speciation modelling with EQ3/6 [Wolery, 1995], as explained in the respective sections. Superscript [2)] marks values set arbitrarily to define an oxidizing state, where there is no information about the real redox potential available at the moment. All values based on approximations explained in detail in the paragraphs preceding a table are labelled with the superscript [3)]. Finally, superscript [4)] is reserved for those data selection based on charge balance considerations.

If a figure contains several speciation diagrams, but only one legend listing the species, then this legends applies to all diagrams in the figure.

All modellings, both with the geochemical speciation code EQ3/6 and with the new integrated model PRISM / MINTEQA2 / BIOPATH, were performed using the thermodynamic databases as explained in detail in chapter 2. For each site, also the input files for the integrated model are given in the appendix. Their syntax is explained in full detail in the Technical Deliverable TD 2 [Brendler, 1999].

## 3.1. Drigg Site

### 3.1.1. Compartment Structure

The compartment structure is given in Fig. 1, from the scheme the following heterogeneous phase equilibria can be derived:

- between the aqueous phase inside the trenches and the solids therein;
- between the aqueous phase of the Drain and suspended solids;
- between the aqueous phase of the Drigg stream and its sediment.

There is nearly no information available about the exact composition of the solid phase (which is very heterogeneous due to the different amount and origin of the waste dumped there over the years, for details see RESTRAT TD 9 [Bousher, 1999a]) and the aqueous phase inside the trenches. This leaves two distinct aqueous-solid phase equilibria for the Drigg site, i.e., two $K_d$ values are required by the BIOPATH model and must therefore be computed with MINTEQA2.

### 3.1.2. Physico-Chemical Characteristics

The geology of Drigg consists of a complex heterogeneous sequence of glacial sediments overlying an irregular bedrock surface of Triassic sandstone (St Bees Sandstone). The glacial sediments range from compact boulder clays, through silts to coarse, highly permeable, sands and gravels. The site is everywhere underlain by at least one clay horizon. Clays will restrict the downward percolation of surface infiltration but create the potential for lateral groundwater flow. There are only rather general mineralogical investigations for this site published. General conclusions to be drawn from such information, partly supported by

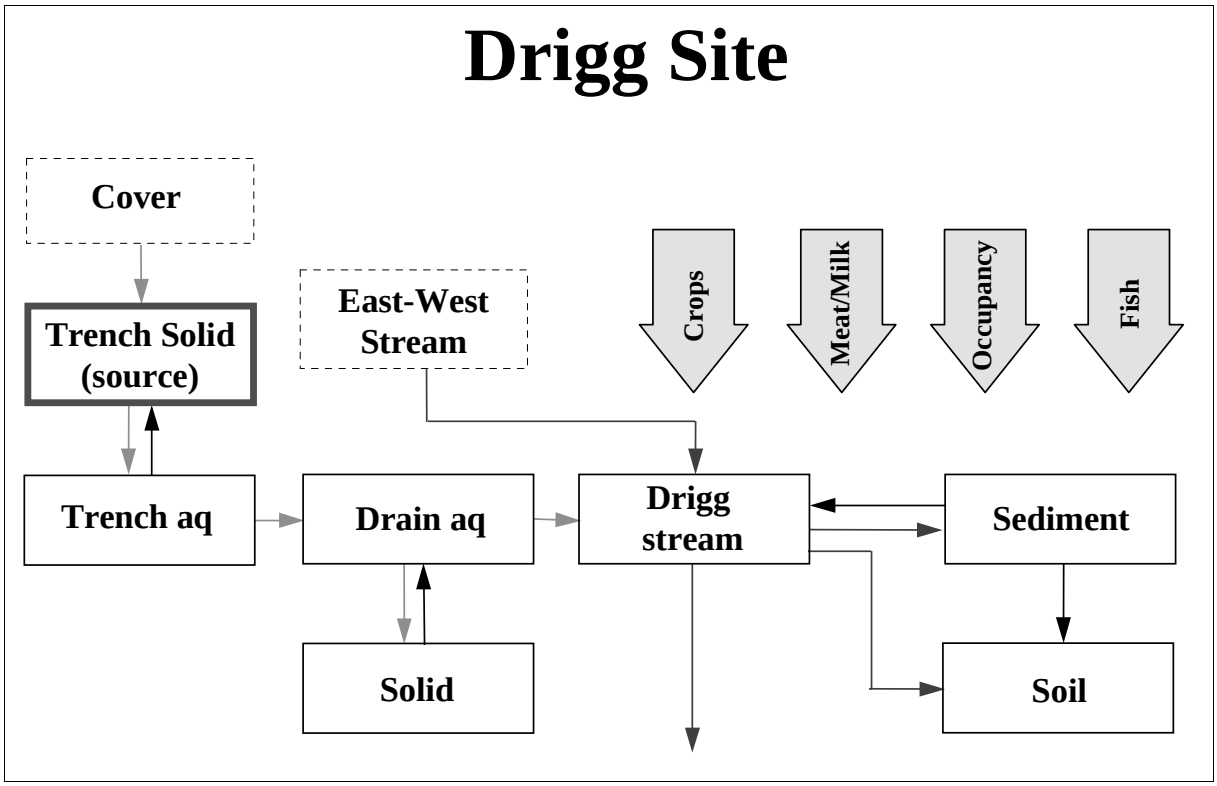


**Figure 1**: BIOPATH compartment structure for the Drigg Site

modelling results, indicate, that the sediments in contact with the aqueous phase are mostly mixtures of a dominant fraction of quartz with some weathered alumosilicates. Information from the RESTRAT TD12 [Bousher, 1999b] about the mineralogical composition of glacial tills (with references to Kelly and Emptage, 1992) allows the derivation of an approximate composition of the clay fraction of 67 % Illite, 6 % Chlorite and 13 % Kaolinite. The high colloidal portion of Iron found in the aqueous samples also points at the presence of Iron oxides / hydroxides.

The site is crossed by several small streams, the most important ones being the 'East-West-Stream' and the 'Drigg Stream', which takes in the former one. The main Drigg stream flows off-site (c. $1x10^6$ $m^3$ / year) through cattle grazed pasture, before joining the River Irt and flowing to the confluent estuary at Ravenglass. Three phases of the Drigg stream are recognized:

1. Input reach (the stretch from the point of origin through the northern half of the site)
2. Flow gauge area (from the confluence with the East-West stream through the southern part of the site)
3. Tidal reach (the whole stretch from the flow gauge to the confluence with the River Irt)

The following radioisotopes have been identified to be of most concern: $^{238}U$, $^{239}Pu$, $^{241}Am$, and $^{137}Cs$. Water samples were taken from the East-West stream just outside the Drigg Site and from the Drigg Stream after leaving the site, also rain water samples were analysed. BNFL did not allow sampling directly on the ground of the site. The samples have been analysed in parallel by the FZ Rossendorf and Westlakes Research Institute, showing a good conformity inside the experimental uncertainties.

All results for the two compartments relevant for $K_d$ computations are summarized in Table 5, this already takes into account the modelling results discussed in the following section. Refer again to the RESTRAT

TD 9 [Bousher, 1999a] for more details about the experimental analytical data. See the beginning of this chapter for explanations of the superscripts.

Table 5: Selected best set of analytical values for the Drigg Site, all concentrations are in mol / L.

| **Compartment:** | **Drain** | | **Drigg Stream** | |
|---|---|---|---|---|
| **Component:** | *Mean* | *STD* | *Mean* | *STD* |
| F- | | | 4.545E-07 | - |
| PO43- | 2.001E-06 | 4.212E-07 | 1.259E-06 | 1.346E-06 |
| NO3- | 7.096E-05 | 5.483E-05 | 4.720E-04 | 2.675E-04 |
| NO2- | 3.695E-07 | 1.087E-07 | 3.036E-06 | 2.771E-06 |
| NH3 | 2.877E-05 | 2.349E-06 | 1.687E-05 | 1.486E-05 |
| SO42- | 5.674E-04 | 3.123E-05 | 4.015E-04 | 4.469E-05 |
| CO32- | 7.410E-03 [4)] | | 2.870E-03 [4)] | |
| Cl- | 2.398E-03 | 1.692E-04 | 1.629E-03 | 7.184E-05 |
| SiO2 | 1.714E-04 | 3.329E-06 | 1.262E-04 | 1.326E-05 |
| K+ | 1.228E-04 | 2.558E-06 | 2.107E-04 | 3.876E-05 |
| Na+ | 2.358E-03 | 1.740E-05 | 1.435E-03 | 1.714E-04 |
| Ca2+ | 1.854E-03 | 1.372E-04 | 1.302E-03 | 1.975E-04 |
| Mg2+ | 5.513E-04 | 1.234E-05 | 3.058E-04 | 6.895E-05 |
| Fe3+ | 4.118E-05 | 7.162E-06 | 1.561E-05 | 2.631E-05 |
| Al3+ | 1.731E-04 | 3.706E-07 | 1.931E-06 | 2.721E-06 |
| Zn2+ | | | 3.370E-07 | 4.402E-07 |
| U | 8.132E-08 [3)] | | 8.132E-08 | 1.354E-07 |
| Th | | | 8.862E-08 | 1.150E-07 |
| Pb2+ | | | 3.517E-08 | 6.008E-08 |
| Ni2+ | | | 3.087E-07 | 3.409E-07 |
| Mn2+ | | | 1.000E-07 | 1.732E-07 |
| Cd2+ | | | 4.326E-08 | 7.339E-08 |
| As5+ | | | 7.071E-08 | 7.575E-08 |
| Pu4+ | 2.0E-14 [3)] | | 2.0E-14 [3)] | |
| Am3+ | 1.83E-15 [3)] | | 8.0E-16 [3)] | |
| Cs+ | 2.0E-5 [3)] | | 2.0E-5 [3)] | |
| pH: | 6.45 | - | 6.80 | 0.53 |
| Eh / mV: | 417 [1)] | - | 401 [1)] | - |

Concerning the contaminants, the data situation is not very clear. First it should be mentioned, that for the computation of a $K_d$ not the concentration of a single nuclide is required, but the total concentration of the respective element. On the other side the relative error in concentrations is less important for tracer elements compared to major constituents of the aqueous phase. For Uranium, there is no measured value for the drain on-site available, only the $\alpha$-activity over the sum of the nuclides $^{234}U$, $^{235}U$ and $^{238}U$. This can not be decomposed into individual concentrations, therefore as an approximation the value from the Drigg Stream was used. The situation with regard to Plutonium is similar (sum over $^{239}Pu$ and $^{240}Pu$), but the concentration values computed assuming pure nuclides differ only by less than 60 %. Thus, the average

of all available values was selected. For Americium, values for the activity are reported for both the Drain and the Drigg Stream. These could easily be transferred into concentrations, in this project the respective upper limits were chosen for all following computations. The most difficult problem concerns Cesium. Here the radionuclide $^{137}Cs$ is only in tracer amounts present compared to the non-radioactive Cesium. The latter value is not known, so as an approximation about 1% of the Sodium concentration was used, extrapolating the Cs / Na ratio as found in many surface waters.

The average temperature in the waters was estimated to 7±3 °C.

### 3.1.3. Chemical Speciation Modelling

The site is characterized by waters dominated by the anions $Cl^-$ and $HCO_3^-$ and the cations $Na^+$ and $Ca^{2+}$, with a comparatively high silicate content, corresponding to the dissolution equilibrium of quartz. Iron and Alumina are mostly present in colloidal form. The mineralization of the drain water (ionic strength = 0.01 M) is reduced after merging with the waters from the East-West stream. The resulting Drigg stream only has an ionic strength of about 0.006. The pH is in the neutral range. The redox potential deserves special discussion. It was measured to be +60 mV, which is surprisingly low for a flowing water with intense contact to open air. Of course degradation processes of organic material making up part of the waste, under the exclusion of oxygen occurring in the trenches, may lead to reducing condition. But the water later in the open Drain, and especially in the Drigg stream after mixing with the oxidized waters from the East-West stream can hardly keep this low redox potential. This contradiction and its consequences towards the species distribution was investigated with the help of modelling.

*Drain*

Taking into account the unexpected experimental values for the redox potential, the modelling results were checked for additional information. Based on analytical concentrations the potentials of the two redox couples $NO_3^-$ / $NO_2^-$ and $NO_3^-$ / $NH_4^+$ were computed to be +402 mV and +432 mV, respectively. This seems to be in better agreement with the actual situation. The mean of these two computed Eh values, +417 mV, was therefore used in several subsequent speciation models.

The carbonate content is obviously also not very well defined. Three scenarios were modelled, where the pH of 6.45 and the carbonate equilibria will lead to nearly equal amounts of $HCO_3^-$ and $CO_2$(aq) (aka $H_2CO_3$) anyway:

a) The measured value of the total carbonate concentration [$CO_3^{2-}$] is the true one. This implies a severe shortage of negative charges, meaning either the concentrations of some anions are strongly underestimated (or some important anions were not measured at all), or the concentrations of some cations are strongly overestimated. This is not a realistic assumption, however.
b) Carbonate is considered to be in equilibrium with the atmosphere (partial pressure of carbon dioxide at 0.03 bar). This would mean that the true total inorganic carbon content must be about two orders of magnitude lower than the measured one, an even more unrealistic scenario.
c) The concentrations of all other major constituents of the solution are considered to be more accurate than the carbonate determination, i.e. [$CO_3^{2-}$] is allowed to float to maintain the charge balance in the system. This results in [$CO_3^{2-}$]$_{total}$ being twice the measured value, which is equal to the assumption that the measured value only represents [$HCO_3^-$], ignoring [$CO_3$(aq)]. This seems the most plausible scenario and was used for the speciation modelling, the related partial pressure of carbon dioxide is 0.06 bar (log $p_{CO2}$ = -1.22). But in addition, also the dependence of the speciation on the total carbonate content was investigated.

Modellings with EQ6, i.e. including the precipitation of mineral phases and the subsequent reduction of related aqueous concentrations, implied a strong oversaturation of the solution with regard to various iron and aluminium compounds. After excluding Goethite, Haematite, Diaspore, and Boehmite from the chemical model because they will not form from aqueous solutions under ambient conditions [Cornell and Schwertmann, 1996; Hsu, 1989], the precipitation of HFO, Kaolinite, and Gibbsite was modelled. This means that at thermodynamic equilibrium actually nearly 100 % of the total alumina, 82 % of the total iron, and 88 % of the total silica will be removed from the solution. Aging processes of HFO and the accompanying transition into Goethite will precipitate an even higher proportion of the iron. The redox potential at equilibrium is predicted to be +772 mV, whereas the pH will remain at the measured level of around 6.5 units.

The Uranium speciation was first computed as a function of the redox potential Eh, with the pH held constant at 6.45, and the concentration of the carbonate ion floating free to maintain the charge balance. Over wide ranges in Eh the speciation will be uniform, see Fig. 2C, with the transition from Uranium(VI)

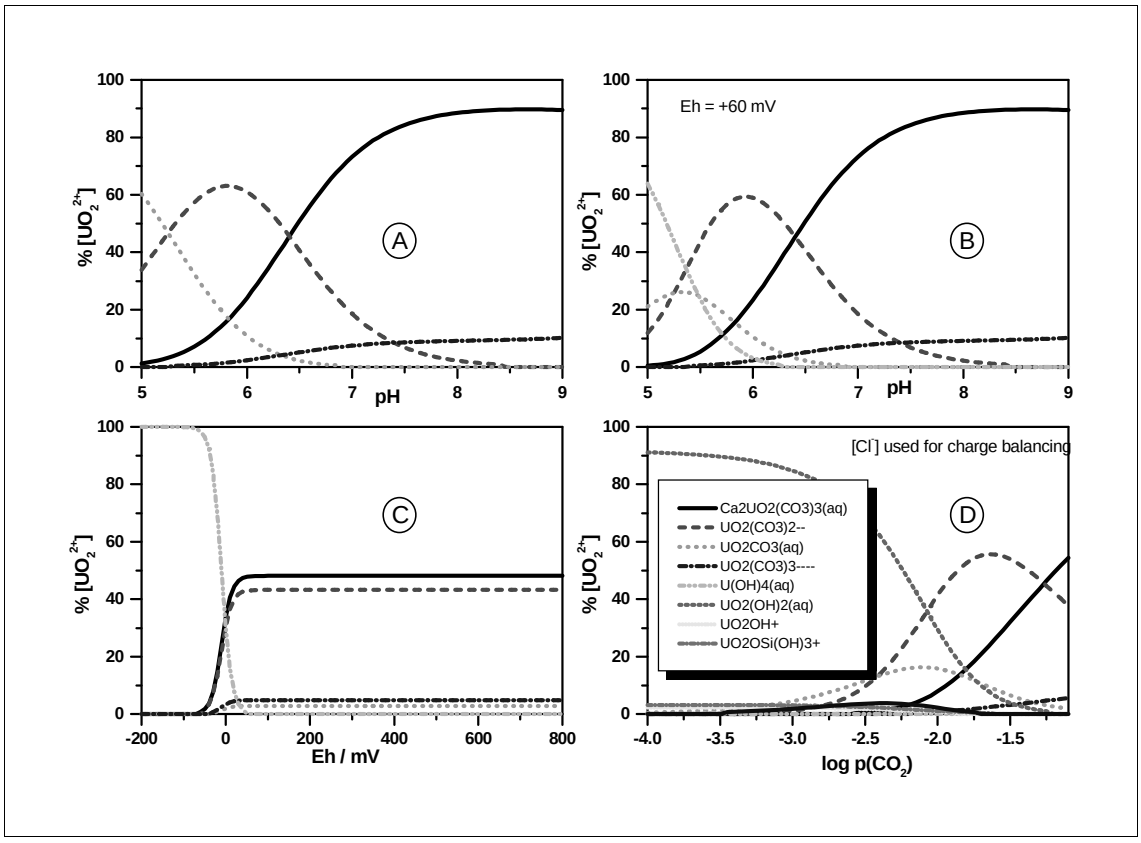


**Figure 2**: Uranium speciation in the drain water of the Drigg Site as function of pH, Eh, and $p_{CO2}$

to Uranium(IV) just starting around the measured redox potential of +60 mV. This transition is promoted at more acidic conditions. As illustrated in Fig. 2B, at pH = 5 and Eh = +60 mV the species $U(OH)_4(aq)$ makes up already 65 % of the total Uranium. But a comparison of Fig. 2A (Eh = +417 mV) and Fig. 2B (Eh = +60 mV) indicates, that at least around the system pH of 6.45 the Uranium speciation is redox-insensitive. So the large uncertainty of the real redox potential in the Drain should not be reflected in the $K_d$ computation. More critical is the dependence on the carbonate concentration, Fig. 2D shows the changing speciation patterns for log $p_{CO2}$ > -3.0, where (mixed) carbonate complexes become dominant. Here, the chloride ion concentration had to be used for charge balancing.

Plutonium, contrary to Uranium, does not form especially stable carbonate complexes, thus its speciation is not dependent on the carbonate content. However, the speciation is influenced by both redox potential and pH, as shown in Fig. 3. An increase in pH means a conversion from the dominant $Pu(HPO_4)_4^{4-}$ species into $Pu(OH)_5^-$, both representing Pu(IV). A decreasing pH, on the other hand, only at reducing conditions changes the speciation, when $Pu^{3+}$ and $PuSO_4^+$ are starting to form: the transition from Pu(IV) to Pu(III). Over wide ranges of the varied parameters the solid phase $PuO_2$ is oversaturated.

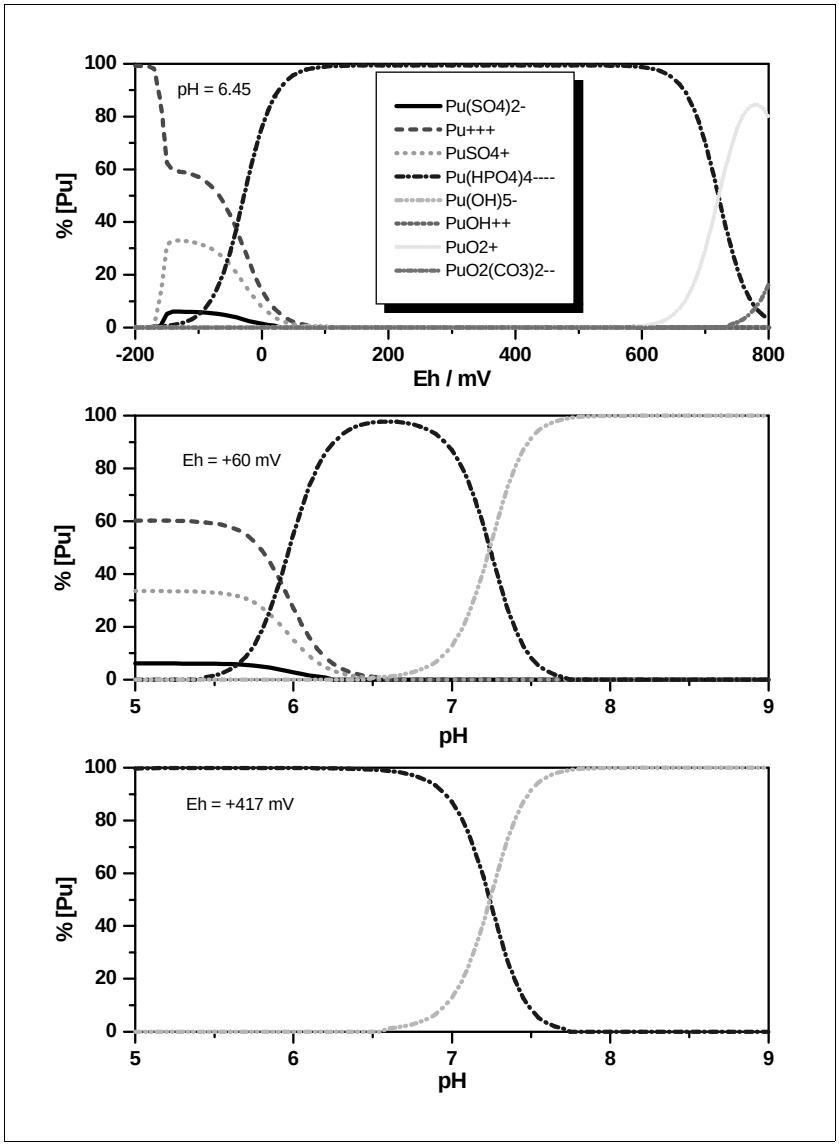


**Figure 3**: Plutonium speciation in the drain water at the Drigg site as function of pH and Eh

Americium will not leave its trivalent state throughout the whole redox potential range under discussion. Its speciation dependence on pH and carbonate content is given in Fig. 4. But over large ranges in both variables, $AmCO_3^+$ is the clearly dominating species.

For Cesium, finally, no dependence of the speciation on pH or on the carbonate content can be observed. Of course there is also no redox sensitivity of the Cesium speciation, which will always be present as a simple cation $Cs^+$.

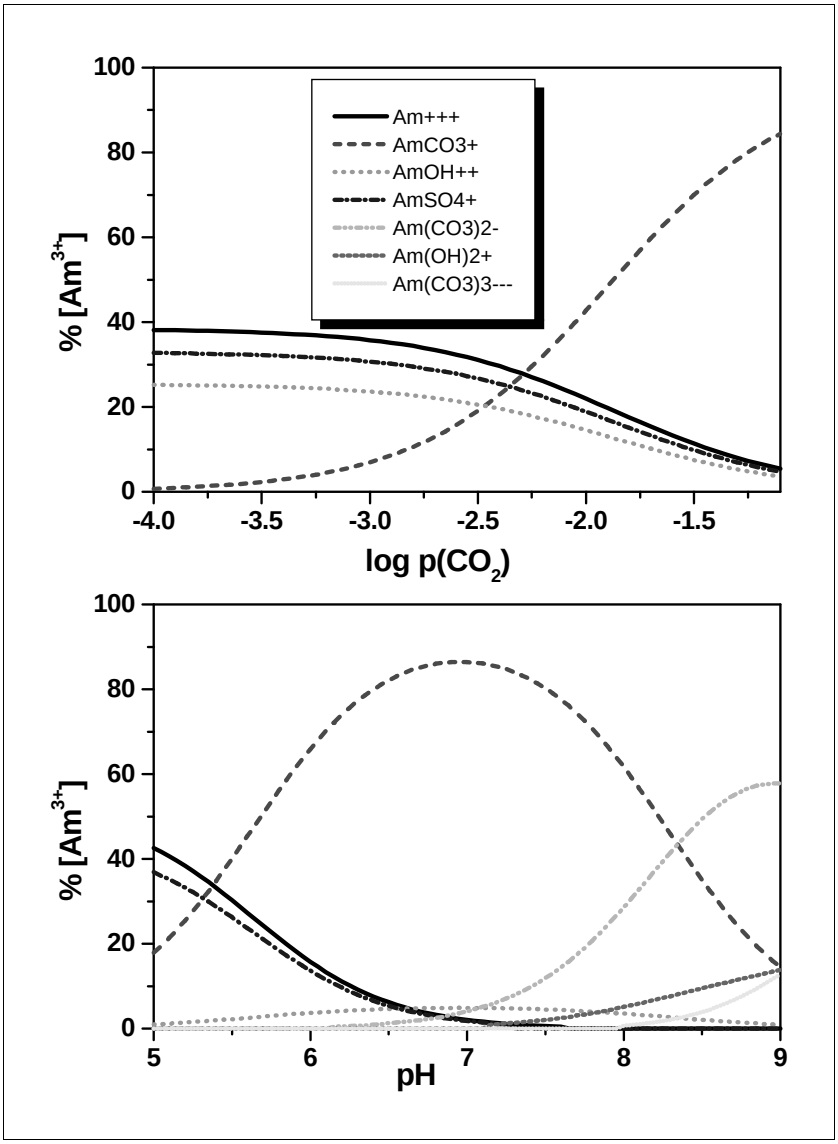


**Figure 4**: Americium speciation in the drain water at the Drigg Site as function of $p_{CO2}$ and pH

The speciation of all considered radioactive contaminants at the selected conditions as given in Table 5 is presented below in Table 6.

Table 6: Speciation of radioactive contaminants in the Drain of the Drigg Site, computed with EQ3NR.

| Uranium | Plutonium | Americium | Cesium |
|---|---|---|---|
| 48.0 % $Ca_2UO_2(CO_3)_3$(aq) | 96.9 % $Pu(HPO_4)_4^{4-}$ | 81.1 % $AmCO_3^+$ | 99.9 % $Cs^+$ |
| 43.1 % $UO_2(CO_3)_2^{2-}$ | 1.5 % $Pu^{3+}$ | 6.9 % $Am^{3+}$ | |
| 4.9 % $UO_2(CO_3)_3^{4-}$ | | 6.0 % $AmSO_4^+$ | |
| 2.7 % $UO_2CO_3$(aq) | | 4.6 % $AmOH^{2+}$ | |
| | | 1.1 % $Am(CO_3)_2^-$ | |

*Drigg stream*

Because the composition of the water in the Drigg stream does not vary that much from the water in the previously discussed Drain, the differences in speciation should also not be that dramatic. Again, a discussion of the redox potential seems necessary, because the measured value is much lower than should be expected from the water which had already contact with air over a range of several hundred metres, and, even more important, was mixed with a larger volume of oxidized water from the East-West stream. Again, the modelling of the redox pairs $NO_3^-$ / $NO_2^-$ and $NO_3^-$ / $NH_4^+$ suggested a redox potential much less reducing, at around +401 mV. This values was used subsequently in all following modellings. Besides, the difficulties with regard to the carbonate content in the water were smaller than in the case of the Drain, with the total carbonate content to be adjusted from the reported experimental value of $1.62 \cdot 10^{-3}$ M to the equilibrium value of $2.87 \cdot 10^{-3}$ M.

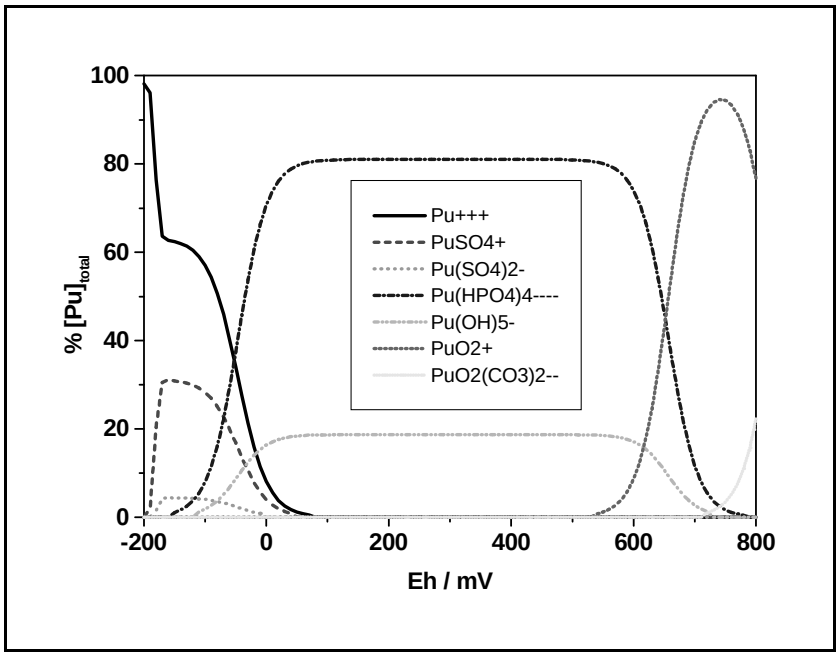


**Figure 5**: Plutonium speciation in the Drigg stream water at the Drigg Site as function of Eh.

The modelling results from EQ6 runs are similar to the ones for the Drain. After exclusion of Goethite, Haematite, Diaspore, and Boehmite the following minerals precipitated in the model: Fluorapatite, Quartz,

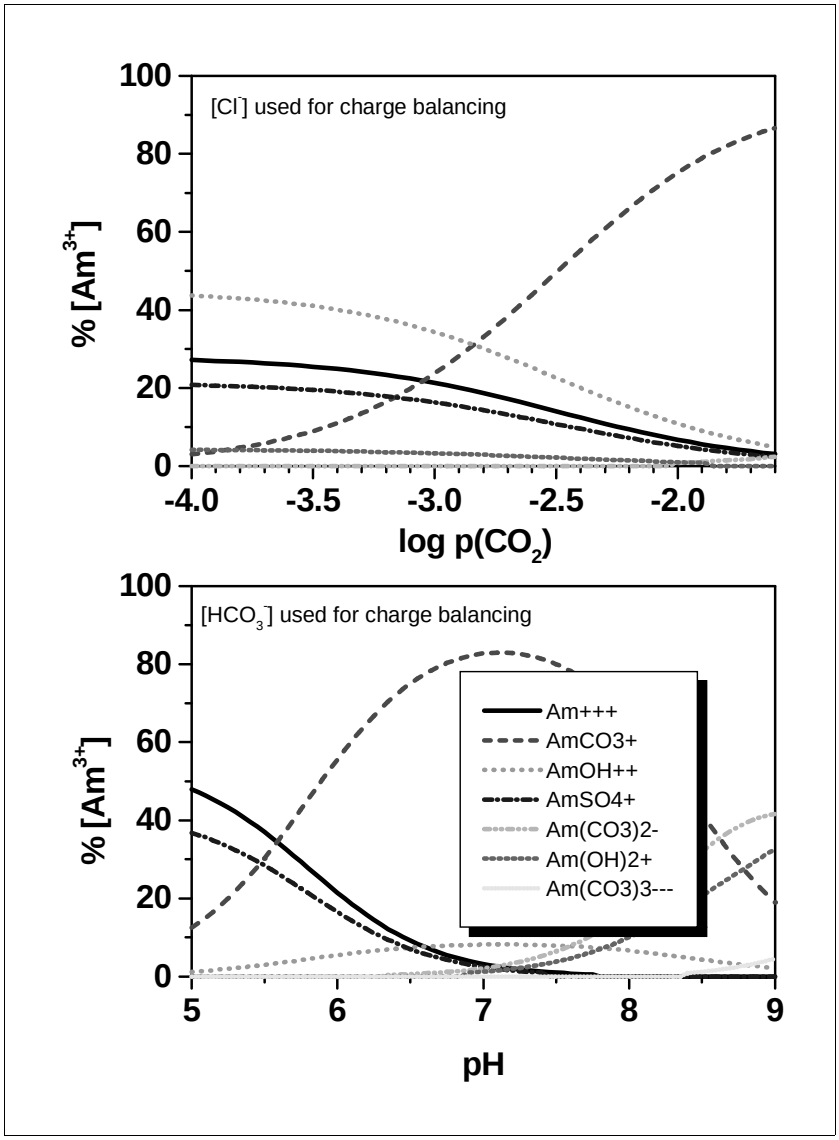


**Figure 6**: Americium speciation in the Drigg stream water at the Drigg Site as function of $p_{CO2}$ and pH

HFO, and Kaolinite, removing aluminium nearly quantitatively, 65 % of the total iron, 70 % of the total silica, 77 % of the total fluoride, and 83 % of the total phosphate. The pH kept its measured value of 6.8, with the Eh going up to +759 mV.

Concerning Uranium, the dependence of its speciation on pH, Eh, and $CO_2$ partial pressure is identical to the one in the Drain compartment.

The Plutonium speciation as a function of pH or $CO_2$ partial pressure is also similar to the situation in the Drain. However, compared to the Drain, there is a higher content of the $Pu(OH)_5^-$ species with up to 19 % of the total Plutonium. Fig. 5 shows how a variation of the redox potential Eh influences the speciation. The sharp perturbation of the speciation pattern around an Eh of -180 mV is assigned to the sulfate / sulfide redox equilibrium.

Americium exhibits only at higher pH speciation pattern different from the Drain waters, namely the content of $Am(OH)_2^+$ is increased. Whereas the speciation shows no dependence on the redox potential, there is a clear effect of a variation of the carbonate content, the differences to the Drain water speciation can be seen in Fig. 6.

Cesium, as already noted in the previous section, is always nearly quantitatively present as the simple $Cs^+$ cation under the given experimental conditions.

### 3.1.4. $K_d$ Computations for the Basic Scenario

*Chemical data set*

Based on the values presented in Table 5, further simplifications were introduced to create the data set used for the computations of the distribution coefficients. This input parameter set was then translated into the file model.chem (required by the integrated model, for syntax questions see again [Brendler, 1999]) that is presented in Appendix A for the case of Plutonium. The input files for Americium and Uranium are similar, with an exchange of *PuO2+2* by *Am+3* and *UO2+2*, respectively, and the appropriate contaminant concentrations being adapted.

Fluoride, nitrate, nitrite, and ammonia were removed from the set of analysed anions because they neither form strong complexes with the contaminants, nor do they contribute significantly to the ionic strength. Thus their omission will not really influence the speciation of Uranium, Plutonium, Americium, and Cesium. For the same reasons, all cations with concentrations lower than $10^{-6}$ M were not considered in the speciation modelling. Because a decreasing pH means the loss of carbonate from any aqueous solutions due to the fact that $H_2CO_3$ is only a weak acid, the parameters *pH* and *$HCO_3^-$ concentration* were coupled through a correlation of 0.6, which is a very conservative assumption. Due to a lack of SCM parameters for the sorption of Cesium its distribution coefficients could not be calculated, see also the appropriate note at the end of section 2.2.2.

According to the speciation modelling results discussed above, for both compartments silica and alumina were defined to be in equilibrium with Quartz and Kaolinite, respectively. Due to a program peculiarity of MINTEQA2, the minerals Pyrophyllite, Diaspore, and Leonhardite had to be suppressed to ensure these equilibria.

*Surface properties*

Concerning the solid phase, the total solid concentration in the Drain was taken from the RESTRAT TD 9 [Bousher, 1999a] to be a suspension of 45±19 mg / L. Because the site is mainly composed of sandy clays, the suspended material is mostly Quartz, with 5 % HFO as the sorbing admixture, as supported by the high content of colloidal iron found in several samples. Thus a sorbate concentration of 2.25±0.95 mg / L is derived. Using the specific site densities for HFO as given in Section 2.2.2., the following concentrations in mol / L for strong and weak binding sites were obtained for the Drain: $(1.2\pm0.5)\cdot10^{-7}$ and $(5.1\pm2.1)\cdot10^{-6}$, respectively.

There were no values for the porosity of the Drigg Stream sediments available, so a default value of 90 % was applied. According to Section 3.1.2, the composition of the Drigg Stream sediment is approximated by Illite. Applying Eqn. 1, Table 3 and an average HFO content of 5 %, this yields a sorbate concentration of 15.6 mg / L. Applying the same approach as for the Drain, the respective concentrations in mol / L for the Drigg Stream are $8.43 \cdot 10^{-7}$ (strong binding sites) and $3.51 \cdot 10^{-5}$ (weak binding sites).

*Results*

The computed $K_d$ values and their error distributions for the contaminants Uranium, Americium, and Plutonium are given in Fig. 7. The box elements lower horizontal line, lower box border, middle line, upper box border, and upper horizontal line, mark the 5th, 25th, 50th, 75th, and 95th percentile, respectively. Additional box elements are already explained in the graph legend.

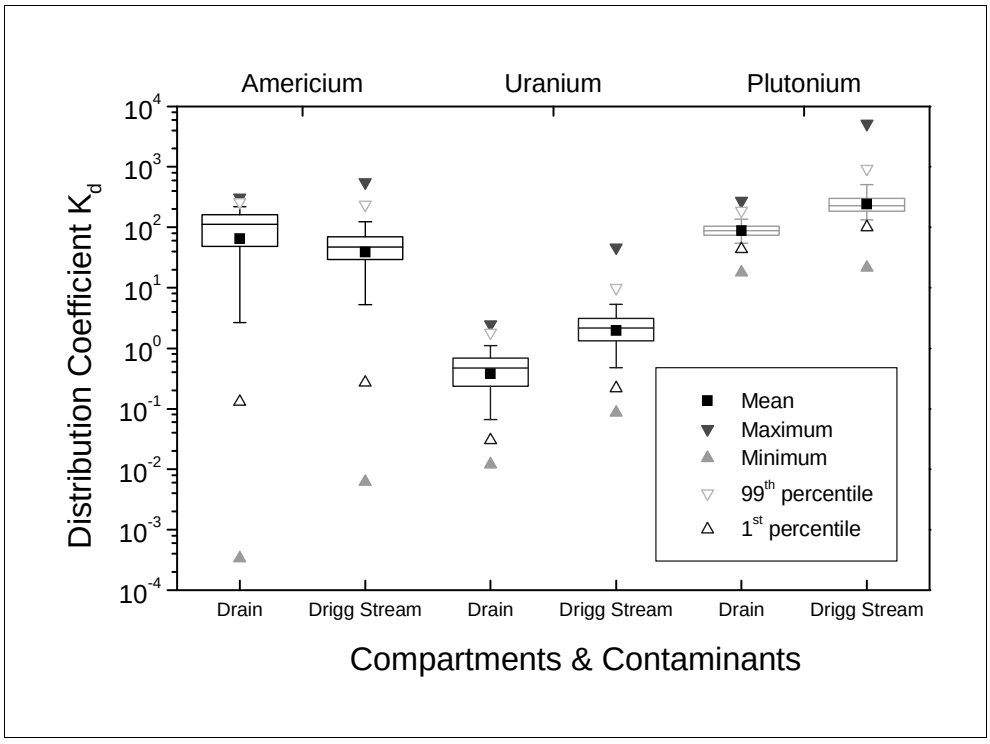


**Figure 7**: Computed $K_d$ values and their error distribution for the Drigg Site

The results obtained for the $K_d$ values of the major contaminants (U, Am, and Pu), each averaging a run with 1000 parameter variations, are summarized in Table 7. So far only estimates of the distribution coefficient were used, with a logtriangular distribution, see RESTRAT TD 9 [Bousher, 1999a] for details. The computed $K_d$ values exhibit a lognormal distribution, so the geometric mean was taken as the best approximator for the true mean value. This equals the antilog of the mean of the logarithms of each data point.

Table 7: Comparison of computed and estimated distribution coefficients in $m^3$ / kg for Uranium, Americium and Plutonium at the Drigg Site.

| **$K_d$ in $m^3$ / kg** | **Computed** | | | | **Default** | | |
|---|---|---|---|---|---|---|---|
| **Compart-ment:** | *log $K_d \pm \sigma$* | *Geometric Mean* | *$5^{th}$ Percentile* | *$95^{th}$ Percentile* | *Mean* | *Lower Limit* | *Upper Limit* |
| Uranium | | | | | | | |
| Drain | -0.42 ± 0.38 | 0.38 | 0.07 | 1.11 | 10 | 1 | 100 |
| Drigg Stream | 0.29 ± 0.32 | 1.94 | 0.48 | 5.31 | | | |
| Americium | | | | | | | |
| Drain | 1.81 ± 0.66 | 64.6 | 2.7 | 218.6 | 100 | 1 | 600 |
| Drigg Stream | 1.59 ± 0.48 | 38.5 | 5.3 | 122 | | | |
| Plutonium | | | | | | | |
| Drain | 1.94 ± 0.12 | 88 | 54.8 | 137.1 | 100 | 1 | 600 |
| Drigg Stream | 2.38 ± 0.19 | 240.8 | 132 | 499 | | | |

Whereas the computed $K_d$ values for Plutonium and Americium fall well into the ranges used so far for modelling (values taken from Smith *et al.*, 1998), the Uranium values are positioned at the lower limit. However, it must be pointed out, that for the latter actinide there are no on-site $K_d$ data available at all. So, the default value range used so far was a generic one. The computed values for Americium exhibit the largest uncertainties.

The next table lists those parameters influencing most heavily the overall uncertainty of the computed distribution coefficients, ***C*** stands for a concentration (of the solid or a chemical component). They were obtained from a ranked regression. In all cases, the concentration of the solid, the pH value, and the carbonate concentration are the most sensitive input factors.

Table 8: Parameters responsible for the uncertainty of computed Uranium, Americium and Plutonium distribution coefficients for the Drigg Site.

| **Compartment:** | **1st Factor** | **$R^2$ Improvement** | **2nd Factor** | **$R^2$ Improvement** |
|---|---|---|---|---|
| Uranium | | | | |
| Drain | $C(HCO_3^-)$ | 71.7 % | pH | 8.9 % |
| Drigg Stream | pH | 36.1 % | C(solid) | 27.4 % |
| Americium | | | | |
| Drain | pH | 66.9 % | $C(HCO_3^-)$ | 11.9 % |
| Drigg Stream | C(solid) | 21.5 % | $C(HCO_3^-)$ | 14.1 % |
| Plutonium | | | | |
| Drain | $C(HCO_3^-)$ | 63.6 % | C(solid) | 10.9 % |
| Drigg Stream | C(solid) | 67.0 % | $C(HCO_3^-)$ | 8.8 % |

### 3.2. Ranstad Tailing Site

#### 3.2.1. Compartment Structure

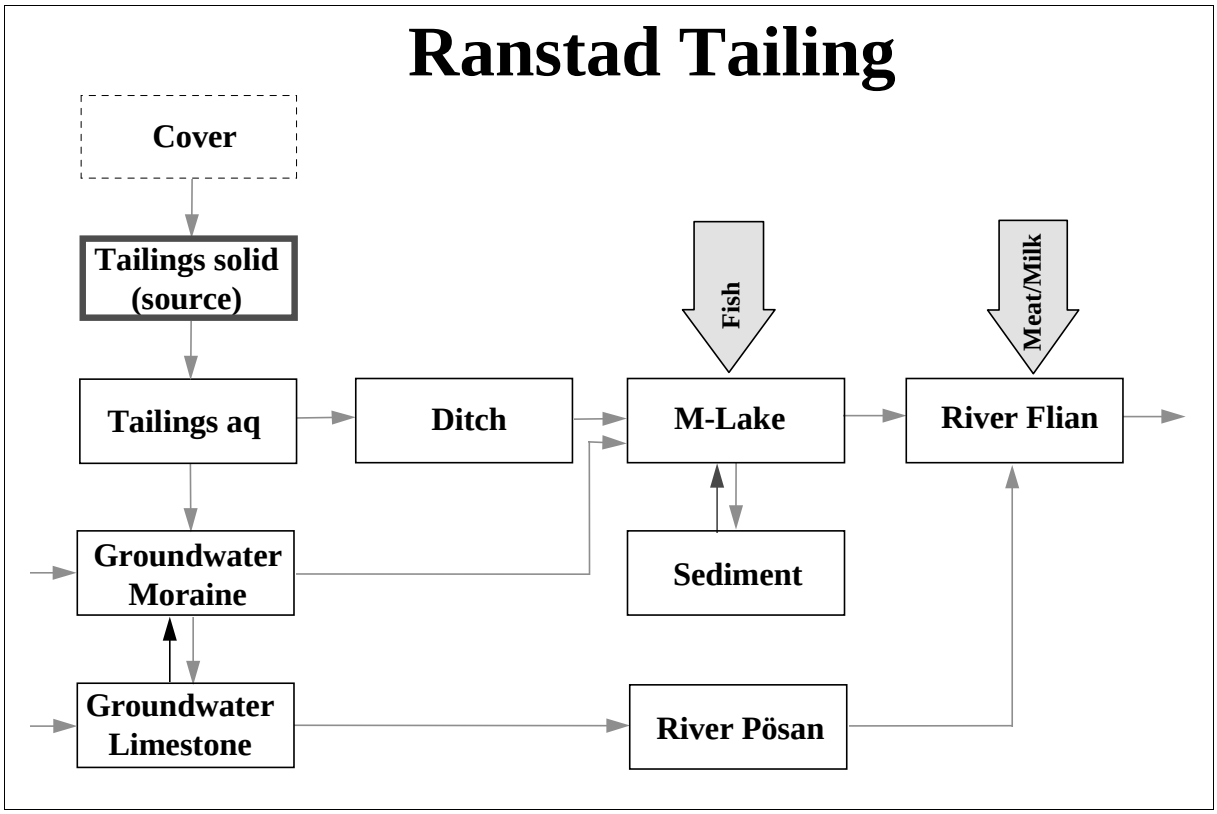


**Figure 8**: BIOPATH compartment structure for the Ranstad Tailing Site

The compartment structure is given in Fig. 8 above. It is derived from the site characterization as specified in the RESTRAT TD 10 [Stiglund, 1999a]. From this scheme the following four heterogeneous phase equilibria can be derived:

- between infiltrating water and the solids in the tailing;
- between the aqueous phase of the moraine and the moraine itself;
- between the aqueous phase of the limestone and the limestone itself;
- between the water of the M-Lake (Magasineringssjön = Storage Pond) and its sediments.

The contact between water and sediment in the ditches around the tailing heap is limited to a very short time scale, so no chemical equilibrium can be established there. This finally leads to four different $K_d$ values required by BIOPATH.

#### 3.2.2. Physico-Chemical Characteristics

The mill tailing consists of crushed alum shale from which uranium has been extracted by leaching. About $10^6$ $m^3$ of tailings have been deposited, covering an area of 230,000 $m^2$. They are covered by a sealing system of various layers of soil-moraine (thickness 0.2 m), moraine (1.2 m), crushed limestone (0.2 m),

and clay-moraine mixtures (0.2 m). The tailing itself (leached alum shale with a thickness of 6 to 10 m) has Quartz, Illite, Feldspars and Pyrite as main constituents, with about 22 % organics. The underlying layers of the tailing site consist of moraine and limestone.

The tailing is shaped into stable slopes which allow efficient drainage of the surface water. A system of ditches, surrounding the tailing deposit, collects both surface water and leachate. All the ditch water is purified in a small purification plant, after passing several collection ponds helping sedimentation. The purified water flows into the river Flian.

The (upper) moraine layer and the (lower) limestone layer are aquifers and will take up the part of the leaching water that penetrates the tailing. The waters will eventually enter the river Flian, either directly (from the moraine layer) or through the river Pösan (from the limestone layer).

As a contaminant not only the radionuclide $^{238}U$ must be considered, but there is also a significant level of the chemical-toxical elements Mn and Ni present.

There have been extensive measurements covering the whole area of the tailing site and its surrounding, extending over several years. Thus this site can be regarded as the best documented example. While the water tables inside the tailing and the moraine layers (and also the pond waters) are dominated by sulfates of magnesium and calcium, the limestone layer water as expected mainly contains the respective carbonates. Especially the moraine layer contains significant amounts of manganese and nickel. There is a pH gradient from the pond waters downwards through tailing and moraine layers till the limestone aquifer. The redox conditions are reducing in general.

A summary of the analytical values used for all modellings is given in Table 9, for a detailed compilation of all site-relevant data refer to RESTRAT TD 10 [Stiglund, 1999b]. Average values (MEAN) and standard deviations (STD) were calculated assigning equal weights to all listed values. Exceptions are alumina and iron, where only the values from analyses at FZR, performed after filtering, were taken into consideration. Here the older measurements clearly gave much too high concentrations, indicating strong oversaturation with respect to many minerals. Obviously those samples were not filtered properly, so the analytical value incorporated fine-disperse and colloidal material. The values from filtered samples show, that both dissolved iron and alumina are only trace components. The following data selection criteria were applied:

- Tailing layer: values from the FZR analysis and from bore hole 111L were averaged, with the exception of Fe, Al, Pb, and Th, where only the FZR analysis was used.
- Moraine layer: values from bore hole 105M were used (105M is defined as reference for the moraine layer in Sundblad *et al.*, 1996), with the exception of Fe, Al, Th and all anions other than sulfate, where only the FZR analysis was used.
- Limestone layer: values from bore holes 101K were averaged (101K is defined as reference for the limestone layer in Sundblad *et al.*, 1996), with the exception of Fe, Al, and Th, where only the FZR analysis was used.
- M-Lake: values from the FZR analysis and from the sampling point station 5 were averaged.
- W-Ditch: values from the sampling point station 2 (Western Ditch) were used.

The usage of anion concentrations for the moraine layer based on FZR analysis is just an intermediate solution. These samples were drawn from boreholes that are drilled inside the tailing area, and therefore are more or less influenced by the overlaying tailing layer, i.e., the analytical values for the anions are not consistent with the values for the cations. Thus it is necessary to analyse new samples from the respective reference bore hole 105M. See the beginning of this chapter for explanations of the superscripts.

Table 9: Selected best set of analytical values for the Ranstad Tailing Site, all concentrations are in mol / L.

| **Compartment** | **Tailing** | | **Moraine** | | **Limestone** | | **M-Lake** | | **W-Ditch** | |
|---|---|---|---|---|---|---|---|---|---|---|
| **Abbreviation** | **L** | | **M** | | **K** | | **S** | | **D** | |
| **Component** | *Mean* | *STD* | *Mean* | *STD* | *Mean* | *STD* | *Mean* | *STD* | *Mean* | *STD* |
| F- | 1.088E-04 | 3.70E-05 | | 2.47E-05 | 7.106E-06 | 2.61E-06 | | | | |
| PO43- | 1.959E-06 | 1.03E-06 | *< 2.1E-05* | 4.93E-05 | 5.328E-07 | 5.25E-07 | 3.159E-08 | | 1.474E-07 | |
| NO3- | 1.188E-04 | 8.48E-05 | *1.097E-05* | 7.14E-05 | 7.139E-05 | | 1.840E-05 | 7.42E-06 | 8.967E-06 | |
| NO2- | 3.189E-06 | 1.77E-06 | *< 1.1E-05* | 1.78E-07 | 2.856E-07 | 2.02E-07 | 2.826E-07 | | 3.043E-07 | |
| NH4+ | 4.450E-04 | 2.30E-05 | | 3.21E-05 | 7.139E-06 | | 1.663E-05 | | 1.502E-04 | |
| SO42- | 2.293E-02 | 2.23E-03 | 2.567E-04 | 7.30E-03 | 5.350E-04 | 7.29E-05 | 5.815E-03 | 5.65E-04 | 1.028E-02 | 7.63E-04 |
| CO32- | 3.584E-03 | 1.10E-03 | *3.715E-03* | 9.30E-03 | 2.991E-03 | 5.79E-05 | 1.593E-03 | 1.35E-03 | 4.835E-04 | |
| Cl- | 5.639E-04 | 6.47E-05 | *3.798E-04* | 2.68E-04 | 3.244E-04 | 1.99E-05 | 2.191E-04 | 8.14E-06 | 1.912E-04 | |
| SiO2 | 6.834E-05 | 1.28E-05 | 4.593E-04 | 7.05E-05 | 2.464E-04 | 3.51E-05 | 3.270E-05 | 6.19E-06 | 2.154E-04 | |
| K+ | 1.175E-03 | 8.91E-05 | 3.363E-05 | 8.14E-06 | 3.775E-05 | 9.18E-06 | 3.954E-04 | 2.59E-05 | 9.962E-04 | 1.14E-04 |
| Na+ | 8.647E-04 | 4.44E-05 | 2.736E-04 | 9.66E-05 | 2.913E-04 | 2.26E-05 | 1.139E-03 | 4.26E-04 | 5.850E-04 | 2.15E-05 |
| Ca2+ | 1.075E-02 | 2.15E-03 | 1.643E-03 | 3.62E-04 | 1.696E-03 | 3.17E-04 | 5.291E-03 | 1.05E-04 | 9.294E-03 | 1.59E-04 |
| Mg2+ | 1.038E-02 | 3.33E-04 | 1.446E-04 | 3.46E-05 | 2.092E-04 | 2.85E-05 | 7.634E-04 | 6.75E-05 | 2.580E-03 | 1.75E-04 |
| Fe | 3.581E-07 | | 3.581E-07 | | 3.581E-07 | | | | | |
| Al3+ | 1.223E-07 | 5.77E-08 | 2.038E-07 | | 7.042E-08 | | 1.112E-07 | 4.50E-07 | | |
| Zn2+ | 4.590E-07 | 4.28E-07 | 3.228E-06 | 4.50E-06 | 7.158E-08 | 3.91E-08 | 1.652E-07 | 1.62E-07 | 2.983E-07 | |
| U | 1.004E-06 | 2.36E-07 | 5.128E-09 | 4.57E-09 | 4.887E-09 | 1.15E-09 | 3.033E-08 | 1.02E-09 | 1.012E-07 | |
| Th | 1.293E-09 | | 3.232E-09 | | 3.080E-07 | | 1.293E-09 | | | |
| Pb2+ | 1.977E-08 | 3.13E-08 | 5.772E-08 | 7.26E-08 | 8.517E-09 | 5.85E-09 | 2.823E-09 | | 3.224E-09 | |
| Ni2+ | 6.275E-07 | 1.96E-07 | 5.182E-07 | 6.57E-07 | 7.491E-08 | 9.13E-09 | 1.337E-07 | 1.29E-07 | 1.755E-06 | |
| Mn2+ | 8.670E-05 | 2.98E-05 | 5.646E-06 | 5.45E-06 | 7.077E-06 | 2.72E-06 | 8.513E-06 | 5.38E-06 | 6.888E-05 | |
| Cd2+ | 4.183E-09 | 8.83E-10 | 1.299E-09 | 1.43E-09 | 3.034E-10 | 1.12E-10 | 3.096E-09 | | 3.567E-09 | |
| As | 2.456E-08 | 1.96E-08 | 1.615E-08 | 1.38E-08 | 1.041E-08 | 2.58E-09 | 3.377E-08 | 5.10E-09 | 5.112E-08 | |
| pH | 7.46 | 0.15 | 6.93 | | 7.85 | 0.12 | 7.80 | | 6.88 | |
| T (in °C) | 8.8 | | 9.0 | | 9.0 | | 7.9 | | 8.5 | |
| Eh (in mV) | 346 [1)] | | 800 [2)] | | 800 [2)] | | 318 [1)] | | 374 [1)] | |

### 3.2.3. Chemical Speciation Modelling

The modelling was done separately for the three main layers of the tailing: the proper tailing layer (the residues of the mining & milling activities), the underlying moraine layer, and the lowest layer consisting of limestone. Also the speciation in the W-Ditch and the M-Lake were calculated.

*Tailing Layer*

For all further computations, performed either as scans over a free parameter with EQ3NR, or as reaction path modellings with EQ6, the (kinetically hindered) precipitation of Dolomite was suppressed. Also, iron-containing minerals others than $Fe(OH)_3$ (or HFO - hydrous ferric oxides) were not allowed to precipitate,

because their formation kinetics is far too low in relation to the flow rate of the water inside the layers. Finally, the redox state was set to the mean value of the potential of the two redox couples $NO_3^-$ / $NO_2^-$ and $NO_3^-$ / $NH_4^+$, i.e. Eh was fixed at 346 mV. Speciation scans for the homogeneous aqueous phase with EQ3NR, as shown below, revealed that actually the system is redox-indifferent over a wide range of the redox potential, only below an Eh of 0.0 mV the speciation of uranium changes with the appearance of U(IV) species. Concerning Manganese the situation is similar, and Nickel does not occur in different oxidation states at all. Thus the approximation of the Eh as discussed above is fully justified.

Based on the above remarks, the uranium speciation was calculated with EQ3NR: as function of the pH, of the partial pressure of carbon dioxide $p_{CO2}$, and of the redox potential Eh. The thus obtained speciation

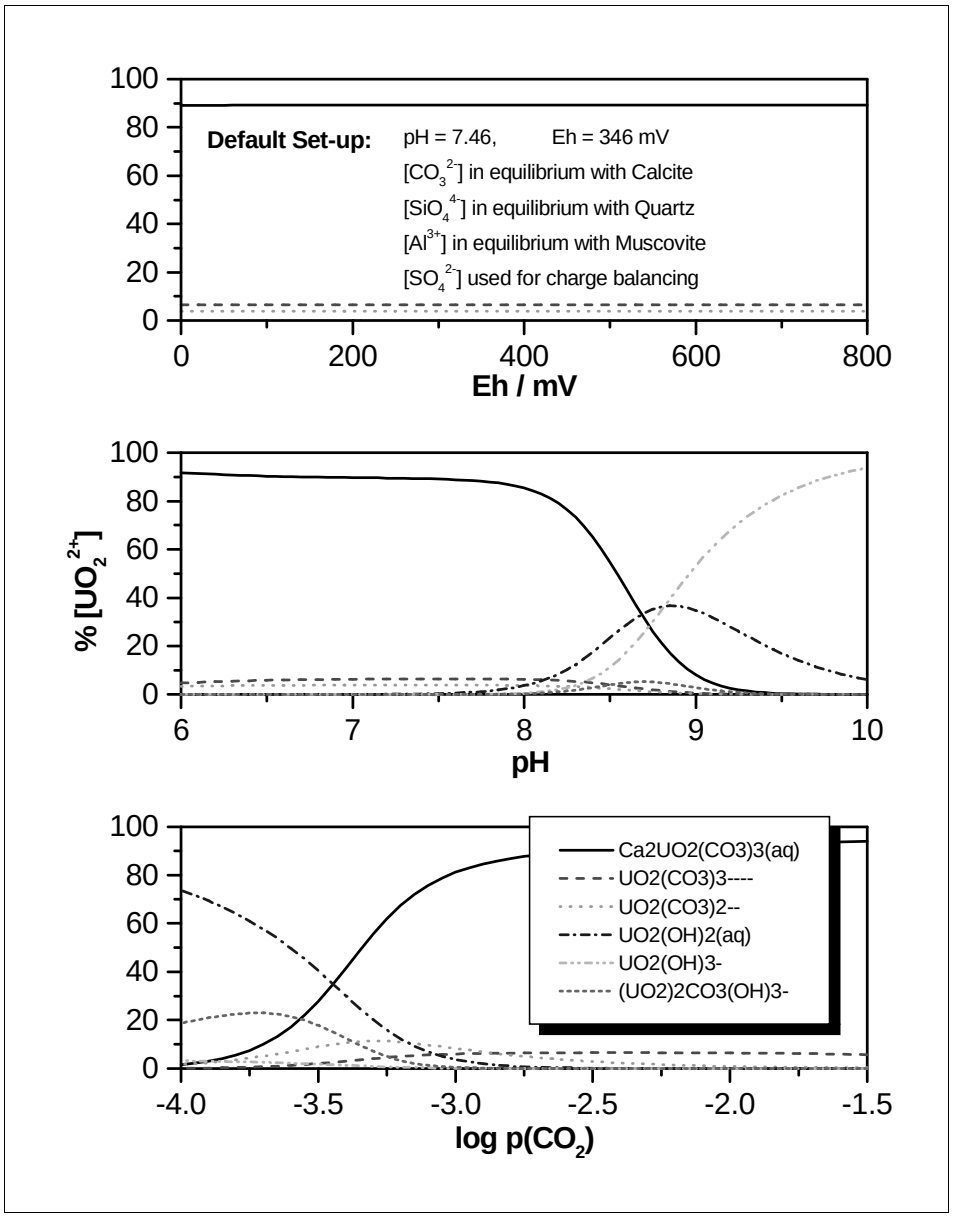


**Figure 9**: Uranium speciation as function of Eh, pH and $p_{CO2}$ for the Ranstad Tailing Site (Tailing Layer)

patterns are shown in Fig. 9. As already mentioned before, there is no dependence on the redox potential. Over large ranges in pH (up to 8.6) and in $p_{CO2}$ the neutral aqueous complex $Ca_2UO_2(CO_3)_3(aq)$ comprises nearly all of the uranium. At higher pH values a negatively charged hydrolysis species, $UO_2(OH)_3^-$, becomes dominant, whereas at very low carbon dioxide contents the respective neutral hydrolysis product, $UO_2(OH)_2(aq)$, is the main species.

In a next step, the speciations of Manganese and Nickel were also computed with EQ3NR as a function of pH, see Fig. 10 for the results. There is no speciation dependence on Eh in both cases at the system pH of 7.46, and both elements mostly occur as positively charged ions ($Mn^{2+}$ / $Mn_2(OH)_3^+$ and $Ni^{2+}$, respectively) over the whole modelled pH range.

Before discussing the main results from the EQ6 reaction path run, it must be mentioned that the species $N_2(aq)$, $N_3^-$, $HN_3(aq)$,and $UO_2(N_3)_x$ had to be excluded in this and all the other EQ6 runs in order to avoid that Eh shifts to very anoxic values around -200 mV. Also, thermodynamic stable solid phases such as

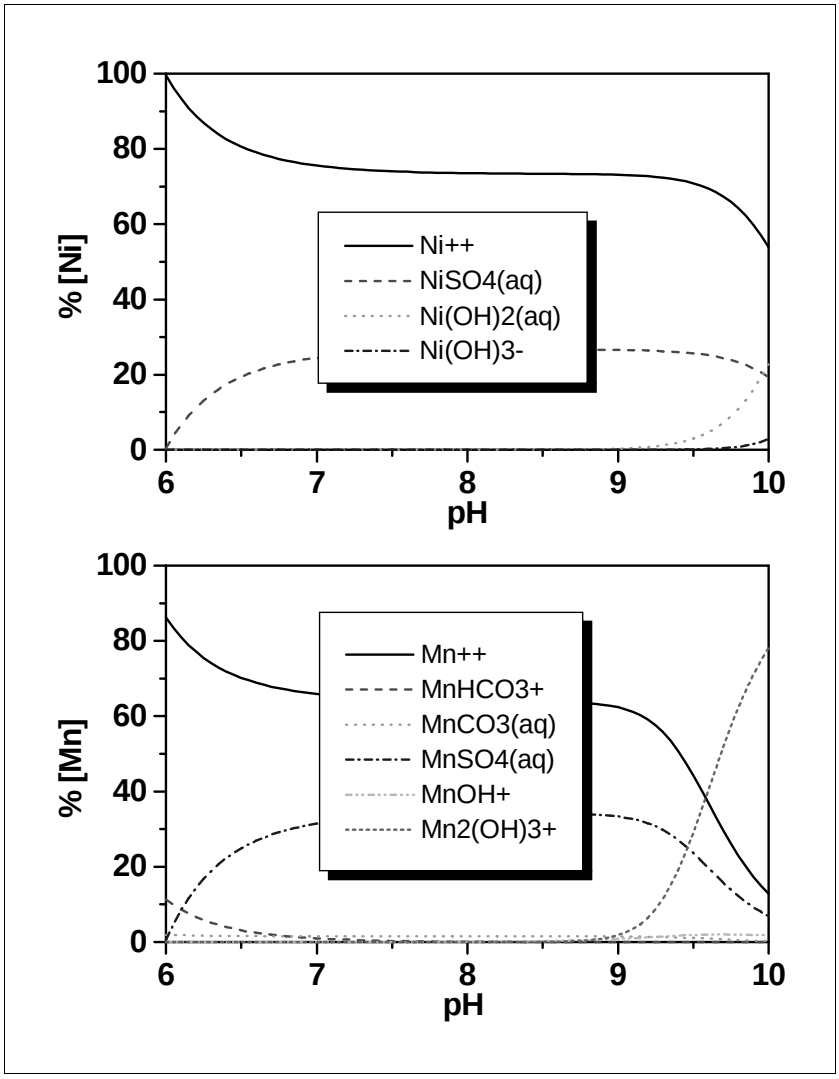


**Figure 10**: Nickel and Manganese speciation as function of pH for the Ranstad Tailing Site (Tailing Layer)

Ferrite-Zn, Goethite, Haematite, Magnetite, various Nontronites, and Trevorite were suppressed in all modellings because they do not form directly from oversaturated solutions due to kinetic hindering.

In case of thermodynamic equilibrium the minerals Calcite, Diaspore, Fluorapatite, Quartz, and Thorianite should eventually precipitate. This will remove phosphate and thorium nearly quantitatively from the solution, also 97 % of the alumina and 39 % of the silica. However, the assumed presence of Calcite instead of Dolomite reduces the measured content of calcium only by 0.9 %. For iron, the assumed stable phase of $Fe(OH)_3$ is not saturated. The modelled precipitations will decrease the pH to 7.21, and increase the redox potential Eh to 356 mV, which in both cases is still inside the uncertainty. The corresponding uranium speciation is given in Table 10. It is clearly dominated by the neutral complex species $Ca_2UO_2(CO_3)_3(aq)$.

Table 10: Uranium speciation computed with EQ6 at thermodynamic equilibrium (Tailing layer of Ranstad Tailing Site)

| Species | Molality | Mol % of Total U |
|---|---|---|
| $Ca_2UO_2(CO_3)_3(aq)$ | 8.9825E-07 | 89.5 |
| $UO_2(CO_3)_3^{4-}$ | 6.5215E-08 | 6.5 |
| $UO_2(CO_3)_2^{2-}$ | 3.9075E-08 | 3.9 |
| $UO_2(OH)_2(aq)$ | 9.9927E-10 | 0.1 |

For the tailing layer can be summarized, that modellings with EQ3NR and EQ6 demonstrated that the contents of Si, Al, Fe, Mn and Th measured in the solution are too high with respect to the saturation limits of many minerals. Probably the analysis also included colloidal or microcrystalline material. The saturation indices indicated, that:
- total Si content may be determined by equilibrium with Quartz;
- total Carbonate content may be determined by equilibrium with Calcite;
- total Al content may be determined by equilibrium with an alumosilicate, e.g. Muscovite.

*Moraine Layer*

The water in the moraine layer is similar to the one in the tailing layer, with higher contents of the alkaline metal ions. Because there is no information available about the redox state inside this layer, EQ3NR calculations were performed to check the speciation sensitivity with regard to the redox potential. No such dependence could be observed for either Uranium, Manganese or Nickel in the Eh range between 0 and 900 mV. Therefore the Eh was set to 844 mV, the value obtained from the EQ3NR computations. Fig. 11 gives the dependence of the Uranium speciation on the pH and on $p_{CO2}$. The pH scan was computed twice with varying ions ($HCO_3^-$ and $Ca^{2+}$) selected for charge balancing, but the observed differences are only minor ones. The neutral complex species $Ca_2UO_2(CO_3)_3(aq)$ dominates over wide ranges in pH and $p_{CO2}$. Only at high carbon dioxide contents or pH values below 6.5 a negatively charged aqueous uranyl complex - $UO_2(CO_3)_2^{2-}$ - becomes important, and at very low $CO_2$ partial pressures the neutral uranyl hydrolysis species $UO_2(OH)_2(aq)$ is the main species.

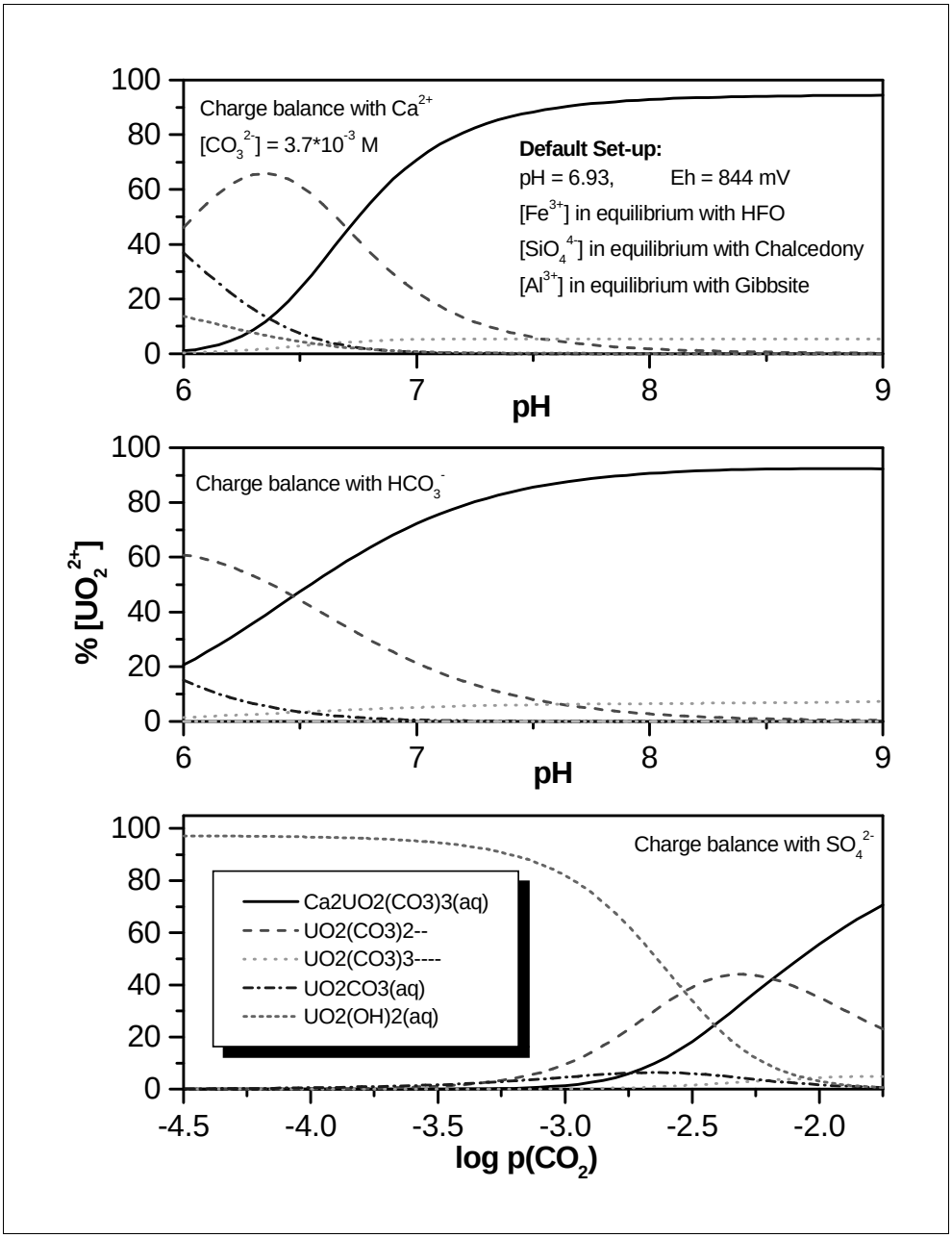


**Figure 11**: Uranium speciation as function of pH and $p_{CO2}$ for the Ranstad Tailing Site (Moraine Layer)

Again, the pH dependence of the Manganese and Nickel speciation were computed, with the latter showing no effect at all. But for Manganese, at pH 8.4 there is an important transition from the positively charged ion $Mn^{2+}$ at lower pH to the negatively charged $MnO_4^-$ ion, a nice example for a coupled effect of pH and Eh on speciation. The results are given in Fig. 12.

EQ6 computations indicated in case of thermodynamic equilibrium the precipitation of Diaspore, Hydrous Ferric Oxide, Pyrolusite, Quartz, and Thorianite. The latter again removes thorium nearly quantitatively from the solution. Also alumina and iron are quantitatively precipitated. In the case of Manganese

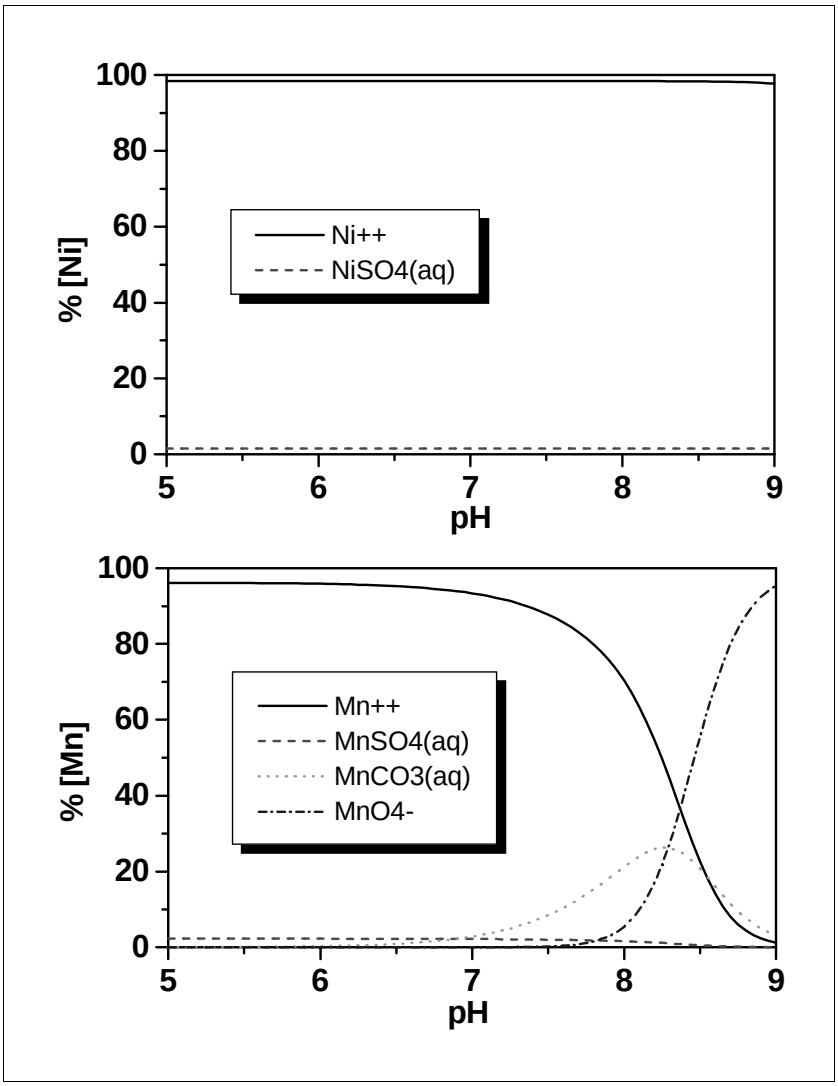


**Figure 12**: Nickel and Manganese speciation as function of pH for the Ranstad Tailing Site (Moraine Layer)

Pyrolusite has the same effect, however here is a strong Eh dependence, at redox potentials lower than 400 mV no Pyrolusite shall occur in the system. Moreover, this mineral usually does not form directly from oversaturated solutions but rather through transformations from other Mn-phases at higher temperatures. Therefore, Pyrolusite was removed from the list of minerals. Finally, the observed Quartz formation will decrease the silica content in the aqueous phase by about 90 %. The modelled precipitations will not shift the pH, and decrease the redox potential Eh only slightly to 829 mV, which is still well inside the range of an oxidized environment. The resulting uranium speciation is given in Table 11. It is, like in the tailing layer, dominated by the neutral complex species $Ca_2UO_2(CO_3)_3(aq)$, but now carbonate complexes play a stronger role.

Table 11: Uranium speciation computed with EQ6 at thermodynamic equilibrium (Moraine layer of the Ranstad Tailing Site)

| Species | Molality | % of Total U |
|---|---|---|
| $Ca_2UO_2(CO_3)_3(aq)$ | 3.3323E-09 | 65.0 |
| $UO_2(CO_3)_3^{4-}$ | 1.4394E-09 | 28.1 |
| $UO_2(CO_3)_2^{2-}$ | 2.5593E-10 | 5.0 |

*Limestone Layer*

The modelling for the limestone layer revealed, that the measured carbonate concentration was much too low, it should be approximately in equilibrium with the Calcite dominating the mineral composition of this limestone layer. The equilibrium between carbonate and Calcite was therefore forced in all following speciation modellings. Furthermore this relation rendered speciation scans based on a varied $CO_2$ partial pressure useless. Because also no Eh effects could be observed, only the pH dependence of the Uranium speciation was computed, with the results shown in Fig. 13. The silicate content of the solution was assumed to be determined by the dissolution of Quartz, which agrees with the computed mineral saturation index.

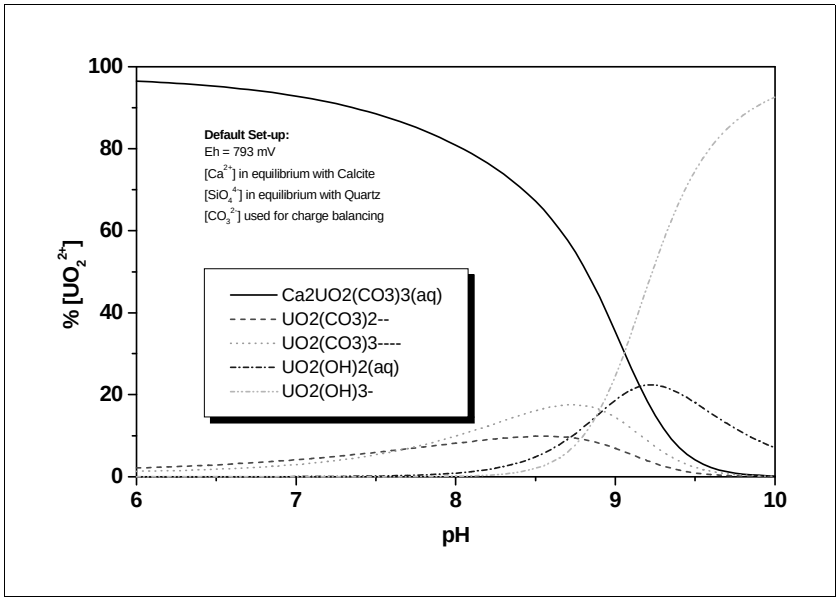


**Figure 13**: Uranium speciation as function of pH for the Ranstad Tailing Site (Limestone Layer)

Whereas the Uranium and Nickel speciation did not show any dependence on the redox state in the Eh range between 0 and 1000 mV, similar to the tailing and moraine layer, this is not true for the Manganese

speciation. When Eh increases over approximately 810 mV, the divalent $Mn^{2+}$ ion is nearly quantitatively transformed into the permanganate ion $MnO_4^-$. This, together with the pH effects on the Manganese and Nickel speciations are shown in Fig. 14.

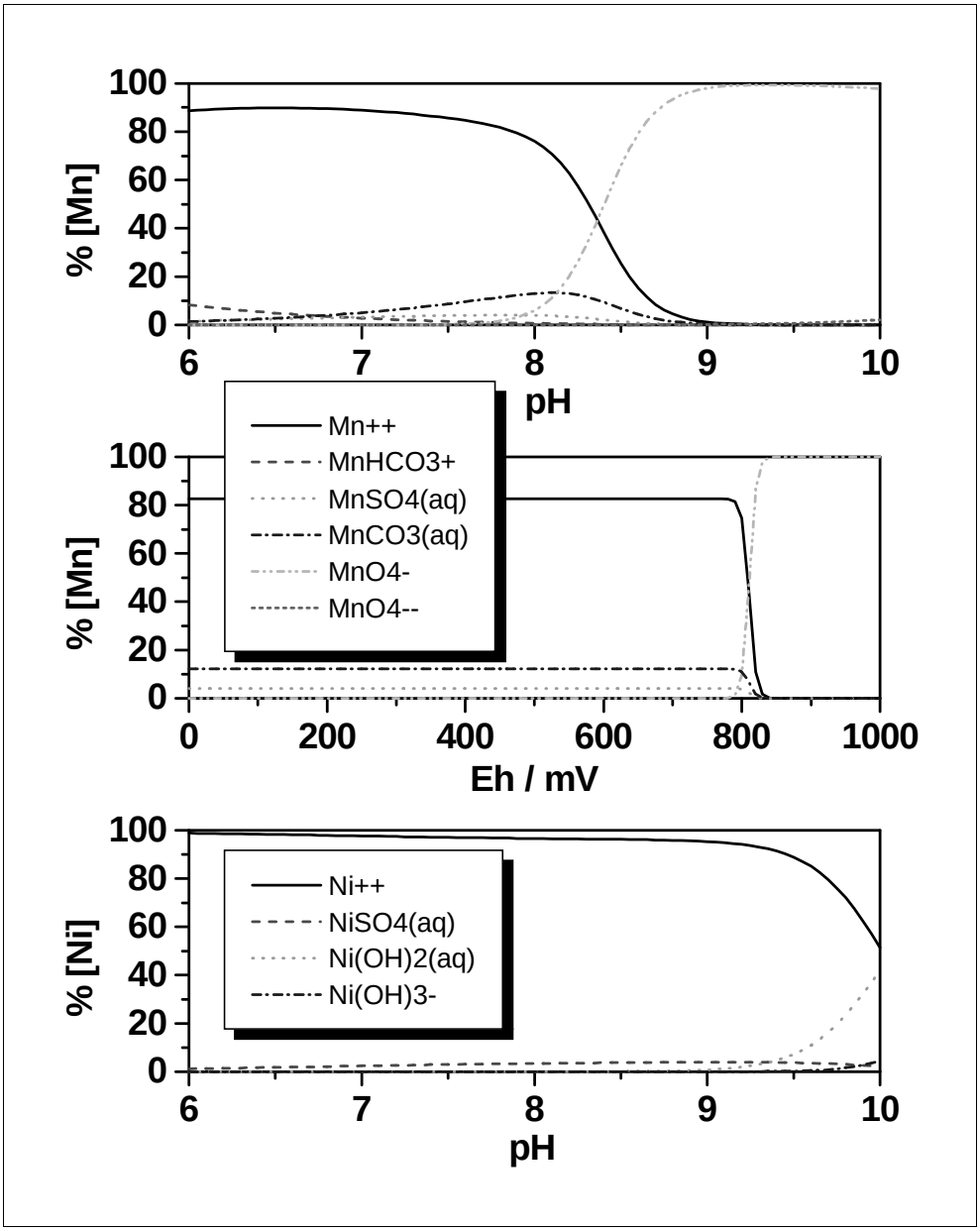


**Figure 14**: Nickel and Manganese speciation as function of pH and Eh for the Ranstad Tailing Site (Limestone Layer)

For the three investigated rock layers it can be summarized, that the speciation diagrams for the moraine and limestone layers do not differ significantly from the one presented above for the tailing layer. Due to the rather high carbonate and calcium content, in all three layers of the Ranstad tailing site the Uranium

speciation is dominated over wide pH ranges by the neutral complex $Ca_2(UO_2)(CO_3)_3(aq)$, whereas Manganese and Nickel are mostly present as the divalent cations $Mn^{2+}$ and $Ni^{2+}$, respectively.

*Western Ditch*

The speciation in the waters of the ditches surrounding the tailing somewhat different from the one inside the rock layers, due to the lower overall content of the major anions and cations. Also the lowest redox

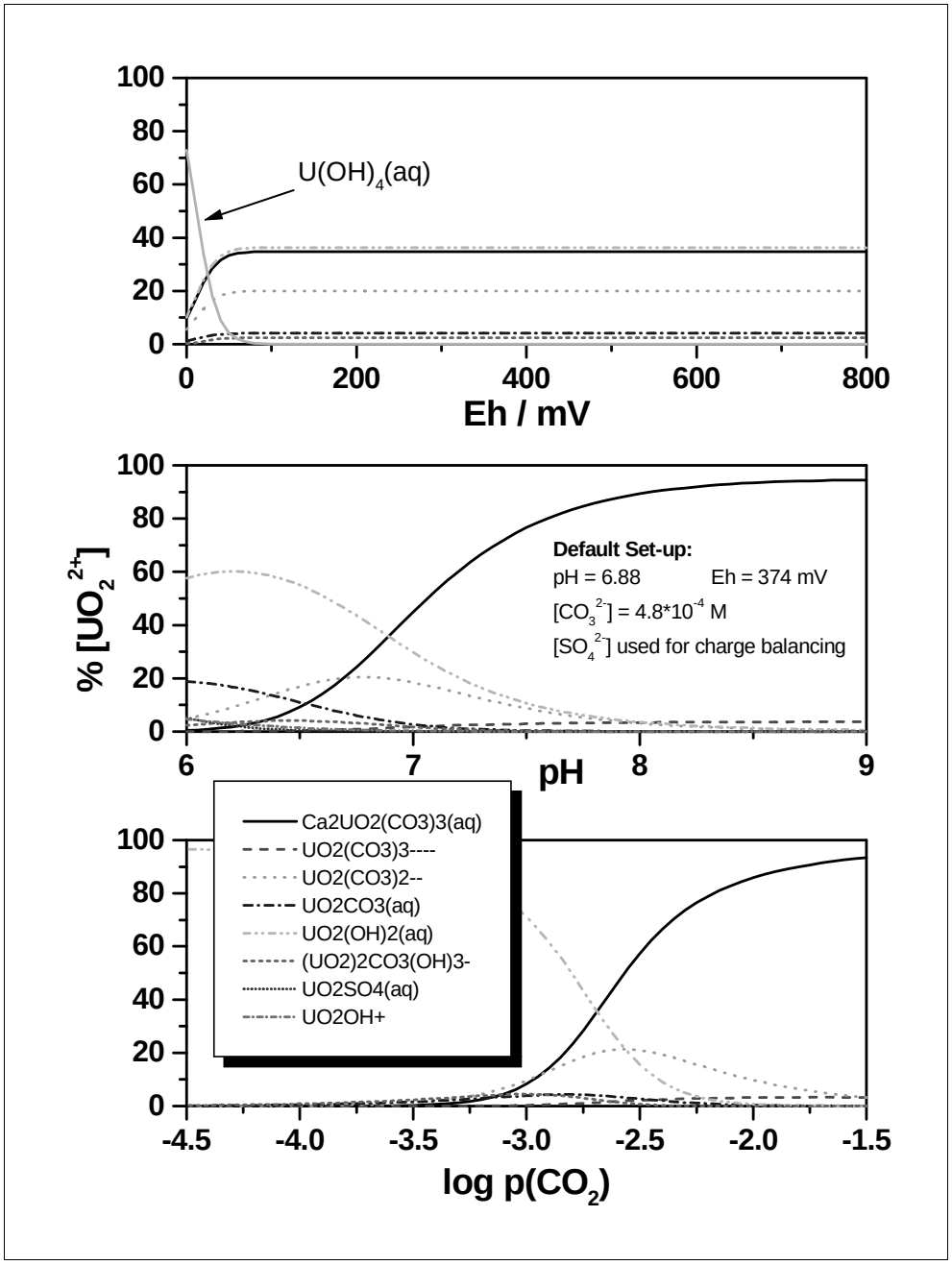


**Figure 15**: Uranium speciation as function of Eh, pH and $p_{CO2}$ for the Ranstad Tailing Site (Western Ditch)

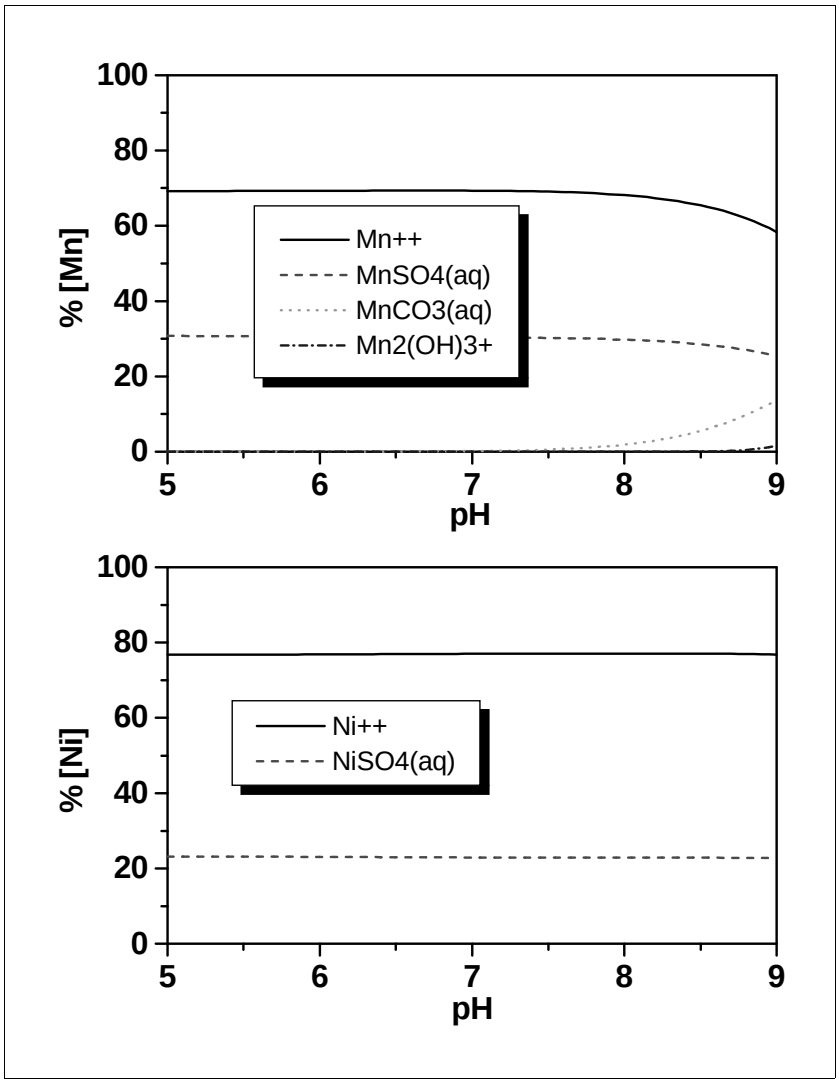


**Figure 16**: Nickel and Manganese speciation as function of pH for the Ranstad Tailing Site (Western Ditch)

potential were observed here. Results of EQ3NR scans over wide ranges in the pH, in the partial pressure of carbon dioxide $p_{CO2}$, and in the redox potential Eh are given in Fig. 15. A scan over pH for the Manganese and Nickel speciation led to the already well known picture of $Mn^{2+}$ and $Ni^{2+}$ as the major species, see Fig. 16.

*Magasineringssjön (Storage Pond - M-Lake)*

Finally, the speciation patterns in the M-Lake are reviewed. The ionic strength of the water is higher than in the ditches, but still lower than in the rock layers. Again, no Eh dependence of the speciation of Uranium, Manganese, or Nickel could be detected at the system pH of 7.80. The uranium speciation is shown in Fig. 17 at varied pH and $p_{CO2}$. Fig. 18 gives the pH dependence of the speciation of Manganese and Nickel.

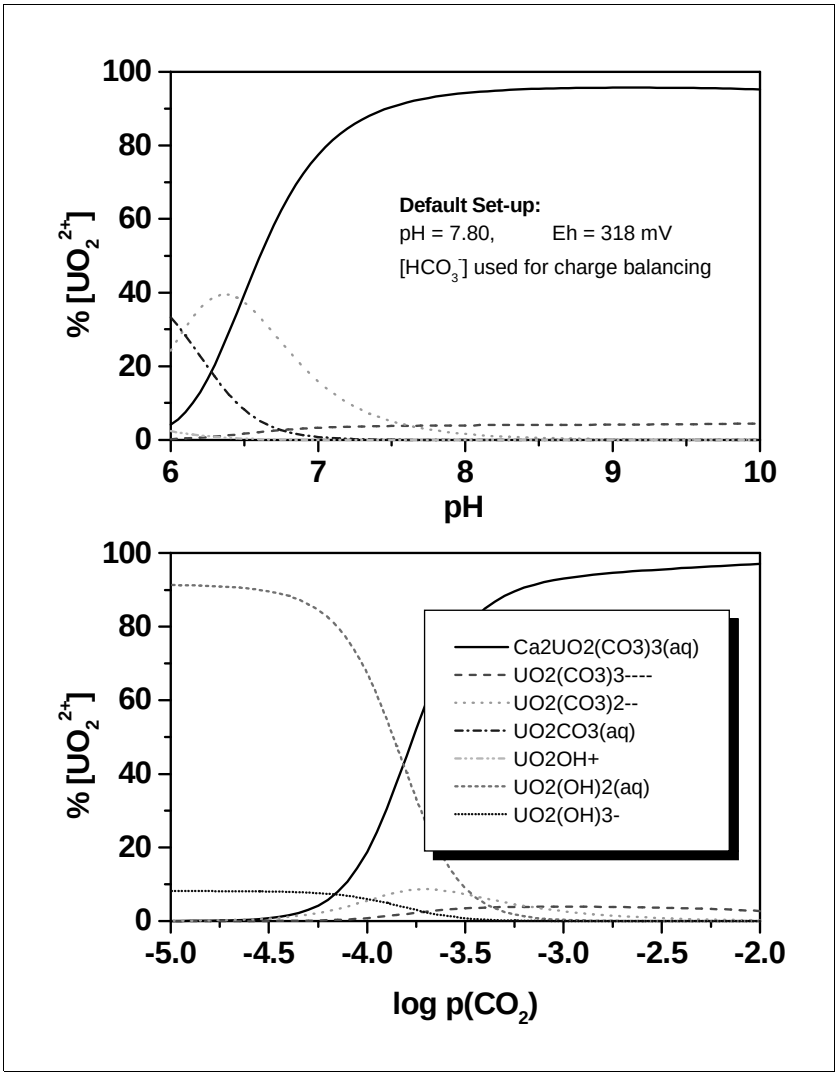


**Figure 17**: Uranium speciation as function of Eh, pH and $p_{CO2}$ for the Ranstad Tailing Site (Storage pond)

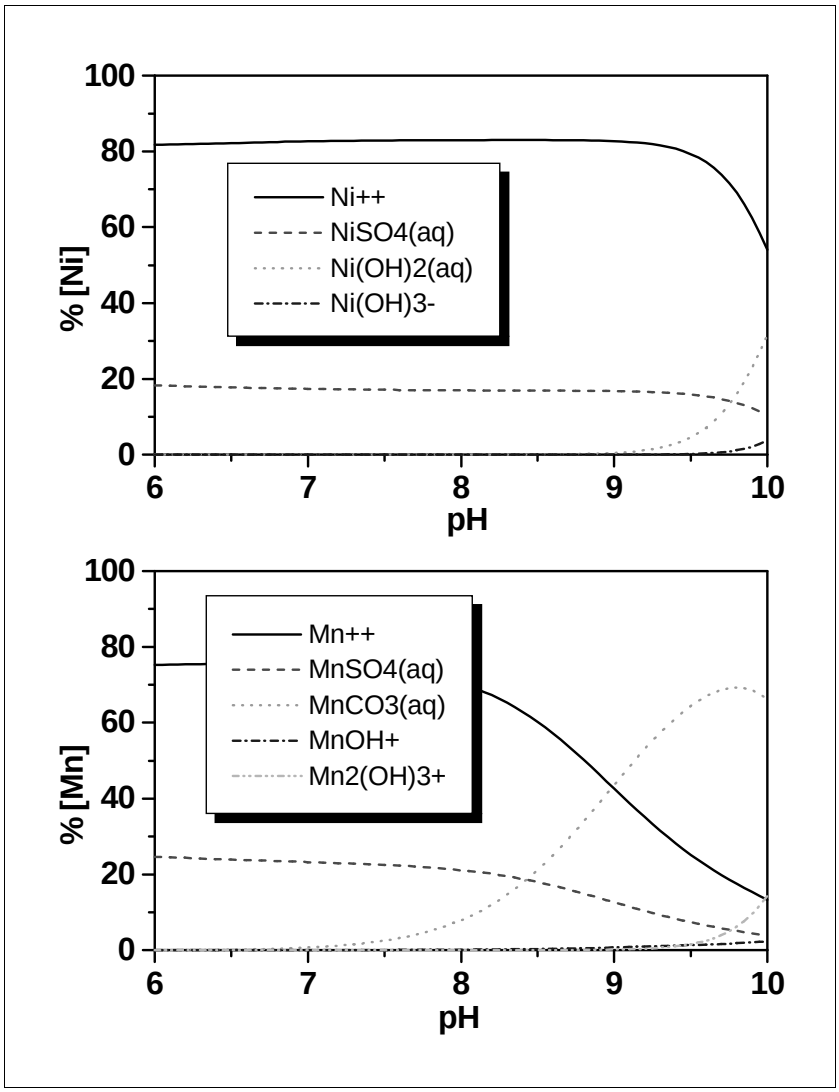


**Figure 18**: Nickel and Manganese speciation as function of pH for the Ranstad Tailing Site (Storage pond)

### 3.2.4. $K_d$ Computations for the Basic Scenario

*Chemical data set*

Based on the values presented in Table 9, further simplifications are introduced to create the data set used for the computations of the distribution coefficients for Uranium. Due to the present lack of a model suitable for a combined risks assessment for radioactive and non-radioactive source terms, the potential contamination caused by Nickel or Manganese has not been considered in this project. Thus no distribution coefficients are computed. The input parameter set for Uranium is translated into the file model.chem (required by the integrated model, for syntax questions see again [Brendler, 1999]) that is presented in Appendix B.

Fluoride, nitrite, and ammonia are removed from the set of analysed anions because they neither form strong complexes with the contaminants, nor do they contribute significantly to the ionic strength. Thus

their omission will not really influence the speciation of Uranium. For the same reasons, all cations with concentrations lower than $10^{-6}$ M are not considered in the speciation modelling. A correlation of the parameters *pH* and $HCO_3^-$ *concentration* does not give an improvement in the computation.

According to the speciation modelling results discussed above for the three aquifer compartments, silica, calcium and alumina are defined to be in equilibrium with Quartz, Calcite, and Muscovite, respectively. Due to a program peculiarity of MINTEQA2, the minerals Pyrophyllite, Diaspore, Hausmannite, Kaolinite and Leonhardite have to be suppressed then to ensure these equilibria.

*Surface properties*

The solid concentrations for the three tailing layers are computed according to Eqn. 1, with the densities calculated from Table 3 based on the solid phase composition for the Tailing Layer (yielding 2.81 g/cm$^3$), using the value for Quartz for the Moraine Layer, and using the Calcite value for the Limestone Layer. The porosities are 0.3, 0.2, and 0.05, respectively. In case of the M-Lake, an experimental value for the solid concentration is available. Finally, 5 % of the respective solid concentration are assigned to the complexing phase HFO in the case of the three aquifer compartments. The HFO content of the M-Lake suspension is much higher, therefore a value of 50 % is used. The finally resulting solid concentrations and binding site concentrations (for both strong and weak binding sites) can be extracted from Appendix B.

*Results*

The results (computed Uranium $K_d$ values and their error distributions) are summarized in Fig. 19, for explanations of the graph elements refer to the respective paragraph in the previous section about the Drigg Site. Above each column, the geometric mean of the computed $K_d$ is given. So far, a default $K_d$ value of 2 m$^3$ / kg was used for all compartments, with a log normal distribution extending from 0.01 to 100. The results are listed also in Table 12. As expected, the high carbonate content in the Limestone layer water leads to a considerable formation of soluble uranyl carbonates, thus strongly reducing the $K_d$. But also for the other aquifer compartments, the computed $K_d$ values are on the lower limit of the generic range, probably due to competition between Uranium and other metal ions for surface sites. On the other side, the increased iron content of the suspended material in the M-Lake is related to a especially high $K_d$ value for that compartment.

Table 12: Computed Uranium distribution coefficients for the Ranstad Tailing Site

| | **Computed $K_d$ in m$^3$ / kg** | | | |
|---|---|---|---|---|
| **Compartment:** | *log $K_d$ ± σ* | *Geometric Mean* | *5$^{th}$ Percentile* | *95$^{th}$ Percentile* |
| Tailing Layer | -2.16 ± 0.30 | 0.0069 | 0.0022 | 0.020 |
| Moraine Layer | -1.50 ± 0.28 | 0.0320 | 0.0097 | 0.081 |
| Limestone Layer | -4.69 ± 0.30 | 2.1E-5 | 6.9E-6 | 6.6E-5 |
| M-Lake | 1.50 ± 0.21 | 31.8 | 13.4 | 62.4 |

Table 13 identifies those parameters contributing most to the uncertainty of the various computed $K_d$ values: pH and solid concentration (and carbonate content for the M-Lake). They were obtained from a

ranked regression analysis. It gives a very homogeneous picture, with the pH clearly dominating the $K_d$ uncertainty, followed by the solid concentrations.

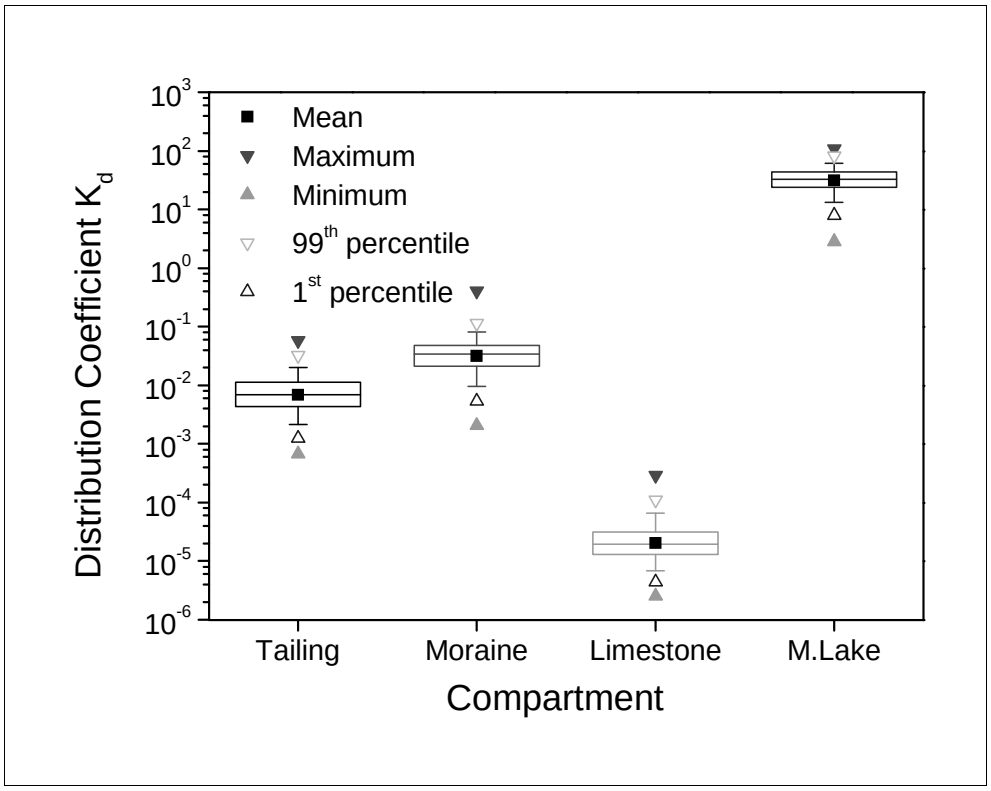


**Figure 19**: Computed $K_d$ values and their error distributions for the Ranstad Tailing Site

Table 13: Parameters responsible for the uncertainty of computed Uranium distribution coefficients for the Ranstad Tailing Site.

| **Compartment:** | **1st Factor** | **$R^2$ Improvement** | **2nd Factor** | **$R^2$ Improvement** |
|---|---|---|---|---|
| Tailing Layer | pH | 82.2 % | C(solid) | 11.0 % |
| Moraine Layer | pH | 79.3 % | C(solid) | 17.0 % |
| Limestone Layer | pH | 88.3 % | C(solid) | 9.8 % |
| M-Lake | pH | 69.5 % | C(solid) | 18.6 % |

### 3.3. Molse Nete River

#### 3.3.1. Compartment Structure

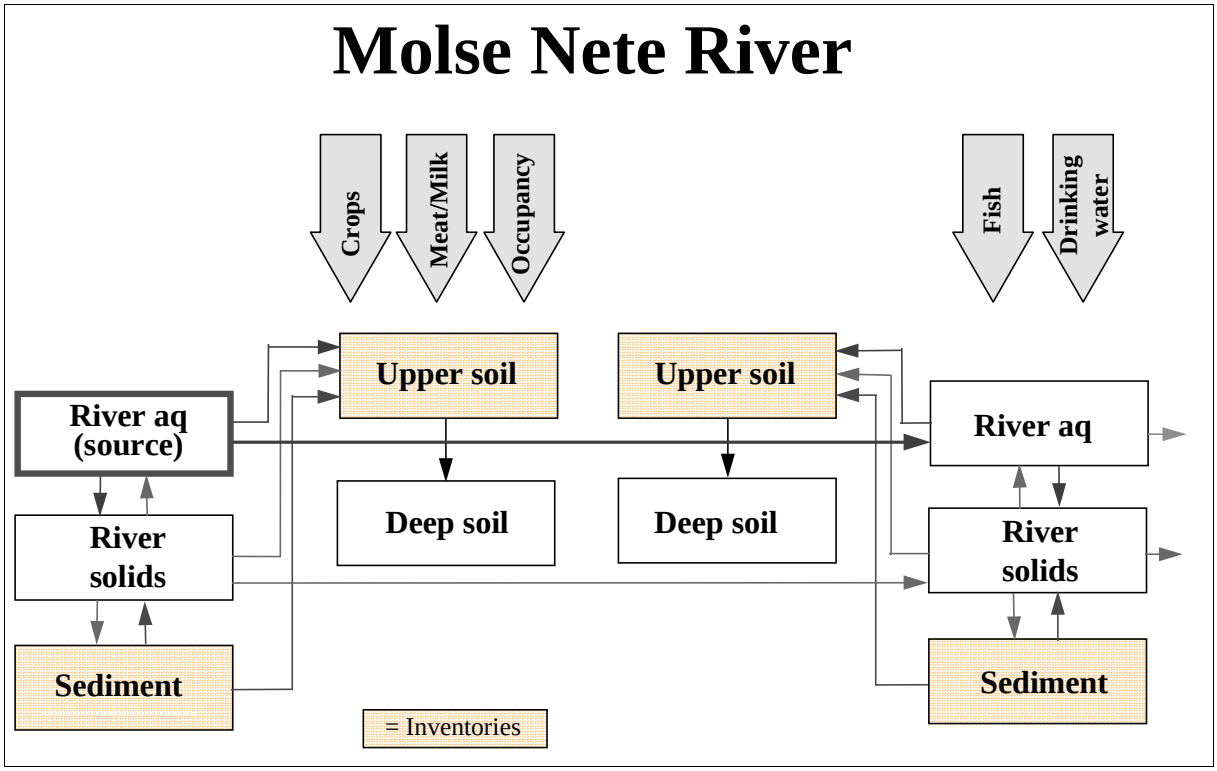


**Figure 20**: BIOPATH compartment structure for the Molse Nete River

For the complete compartment scheme refer to Fig. 20. The water in the river and the composition of its solids and sediments are considered to be homogeneous along the river section investigated in this project. Also the solids in the river are assumed to have a composition similar to the sediment. Therefore only one water-solid equilibrium must be taken into account, also the chemical speciation modelling requires only one scenario. For the interactions between the soil and infiltrating water no equilibrium or even steady state chemistry can be assumed, i.e. a chemical speciation followed by sorption coefficient computation is not applicable.

#### 3.3.2. Physico-Chemical Characteristics

At the Molse Nete site, the surface layer (quarternair, Pleistocene) is a fine, poorly glauconitic sand layer of 2 to 10 m thick. The underlying soil is constituted by the Kasterlee formation (Lower Pliocene), which is a homogeneous fine sand layer (mode : 150 µm) of about 15 m thick, containing micaceous and slightly glauconitic minerals. At the base of this formation, small flint pebbles and lenses of clay can be found. The Kasterlee formation is lying upon the Diest formation (Upper Miocene), which is about 120 m thick at the Molse Nete site and is formed by strongly glauconitic clayey and medium to very coarse-grained sands. Locally, thin layers of siderite and limonite appear.

The water table of the aquifer lies between one to two metres beneath ground level. The lower part of the Kasterlee formation contains a significant clay content which limits the water migration into the underlying Diestiaan aquifer.

The Molse Nete drains approximately 62 $km^2$, which is about 3 % of the Nete hydrographic basin. The relief of the region is flat and the slope of the Molse Nete is rather small, about 0.4%. The river has an average water velocity of 0.41 m/s (0.24 - 0.47 m/s) and a flow rate of 2.9 $m^3/s$ in the wet season and 0.28 $m^3/s$ in the dry season. The water balance of the Grote Nete, which is similar to the one of the Molse Nete, shows that nearly half of the precipitation will evapotransporated.

Analysis of the water samples from the two points of investigation did not reveal larger changes, so the water can be regarded as homogeneous throughout the course of the river, at least inside the defined site area. Main components are chlorides and (hydrogen)carbonates of sodium and calcium, under oxidizing redox conditions at neutral pH. The silicate content is rather high, whereas iron and alumina are only trace components, thereby not heavily influencing the contaminant speciation.

The critical radionuclides, discharged into the Molse Nete are $^{60}Co$, $^{137}Cs$, $^{239}Pu$ and $^{241}Am$. There are no analytical data for those contaminants in the river water. Some radiochemical determinations in the river sediment and from soil that was dredged from the river are reported. These values were used to estimate an upper limit for both the Americium and Plutonium content. Whereas the sorption behaviour of these elements will not show any dependence on their concentration at this very low tracer levels (below $10^{-10}$ mol / L), there are still some very insoluble solid phases, such as $AmPO_4$ or $PuO_2$, that may precipitate and thus contribute to the $K_d$. Taking the total maximum of the measured radionuclide activity in sediments and soils, an upper limit of their concentration was calculated. This was combined with the lower limit of the distribution coefficients as reported by Sweeck and Zeevaert, 1999, to yield upper concentration limits in the river water for Americium and Plutonium of $10^{-16}$ mol / L and $6 \cdot 10^{-14}$ mol / L, respectively. In the case of Cobalt and Cesium, the sorption properties will be dominated by the non-radioactive isotopes, thus the total concentration for these elements is required. Unfortunately, there are no analytical data available. In analogy to the procedure explained for the Drigg Site, a Cesium content amounting for 1 % of the Sodium content was assumed, giving $10^{-5}$ mol / L. The Cobalt content was assumed to be in the range of other two-valent heavy metals, giving $10^{-7}$ mol / L.

The results from various analytical investigations in the past (for details see RESTRAT TD 11 [Sweeck and Zeevaert, 1999]) are summarized in Table 14, together with additional measurements that were performed as part of the RESTRAT project to close gaps in the previous investigations, and to verify the accuracy of those measurements. Except for the data of 1978b, each parameter value is the mean of at least three independent measurements. Mean values and standard deviations were calculated giving equal weights to all listed values. Exceptions are zinc, alumina and iron, where only the values for the filtered samples from 1996 were taken into consideration, see below for an explanation.

A critical review of the data based on Table 14 shows, that for most of the major anions and cations the analytical values are in good agreement over the whole time range from 1977 till 1996. Remarkable exceptions are the content of zinc, iron and alumina. Here the older measurements clearly gave much too high concentrations, indicating strong oversaturation with respect to many minerals. Obviously those samples were not filtered, so the analytical value incorporated fine-disperse and colloidal material. The values from filtered samples from 1996 show, that both iron and alumina are only trace components, thereby not heavily influencing the contaminant speciation. There are no in-situ determinations of the redox state available, only some measurements of the oxygen content in the water without specifying the method and the measurement conditions. From these rather uncertain values (in the range between 2.5 and

11.2 mg $O_2$ / L), and from computations based on concentrations for the redox pairs $NO_3^-$ / $NH_4^+$ and $NO_2^-$ / $NH_4^+$, redox potentials of 810, 359, and 382 mV, respectively, were obtained. This means on average slightly oxidizing conditions, as to be expected from water of a river with free contact to atmosphere, but with significant redox disequilibria. Moreover, the observed ammonia and nitrate concentrations indicate that the water is slightly polluted. Also the Na concentration is rather high. The concentrations of most ions lie in the common range. Main components are chlorides and (hydrogen) carbonates of sodium and calcium, contributing to an ionic strength of about $6.5 \cdot 10^{-3}$ mol / L. The silica content seems to be determined by the dissolution of quartz, as could be concluded from speciation modelling. As can be seen in Table 14 the water maintains a neutral pH, varying between 6.7 and 7.5. For the solids in suspension also a seasonal variation is observed; in the summer about 9 mg / L solids (April till September) are in suspension, in winter (October till March) on an average, 28 mg / L suspended matter is measured. The fully analysed water samples gave suspension concentrations of 13.68, 15.94, and 23.0 mg / L.

Table 14: Summary of analysis of river water samples from the Molse Nete with the selected best set of analytical data, all concentrations are in mol / L.

| **Year** | **1977** | **1978 (a)** | **1978 (b)** | **1979** | **1980** | **1996*** | **1996**** | **Mean** | **Std.Dev.** |
|---|---|---|---|---|---|---|---|---|---|
| **Component** | mol / L | mol / L | mol / L | mol / L | mol / L | mol / L | mol / L | mol / L | mol / L |
| PO43- | 4.37E-06 | 5.69E-06 | | 2.11E-06 | | | | 4.05E-06 | 1.81E-06 |
| NO3- | 1.60E-04 | 1.50E-04 | 7.42E-05 | 2.31E-04 | | 3.29E-04 | 3.79E-04 | 2.20E-04 | 1.16E-04 |
| NO2- | 3.70E-05 | 6.74E-06 | 2.61E-06 | 1.80E-06 | 2.61E-06 | | | 1.01E-05 | 1.51E-05 |
| NH4+ | 2.38E-05 | 4.88E-06 | 1.55E-06 | 1.50E-06 | 1.11E-06 | | | 6.57E-06 | 9.77E-06 |
| SO42- | 9.47E-04 | 9.37E-04 | 9.06E-04 | 7.82E-04 | 7.60E-04 | 7.78E-04 | 9.90E-04 | 8.71E-04 | 9.53E-05 |
| HCO3- | 1.25E-03 | | 1.29E-03 | | | 1.56E-03 | 1.61E-03 | 1.43E-03 | 1.82E-04 |
| Cl- | 1.54E-03 | 9.59E-04 | 1.13E-03 | 8.46E-04 | 1.02E-03 | 1.46E-03 | 1.49E-03 | 1.21E-03 | 2.86E-04 |
| Si | | | 5.84E-05 | | | 1.84E-04 | 1.87E-04 | 1.43E-04 | 7.36E-05 |
| K+ | 2.35E-04 | 1.76E-04 | 2.48E-04 | 2.02E-04 | 1.46E-04 | 2.53E-04 | 3.02E-04 | 2.23E-04 | 5.24E-05 |
| Na+ | 1.39E-03 | 1.35E-03 | 1.22E-03 | 9.13E-04 | 1.30E-03 | 1.77E-03 | 1.82E-03 | 1.40E-03 | 3.15E-04 |
| Ca2+ | 1.41E-03 | 1.25E-03 | 1.05E-03 | 1.07E-03 | 1.05E-03 | 1.17E-03 | 1.27E-03 | 1.18E-03 | 1.36E-04 |
| Mg2+ | 2.47E-04 | 2.26E-04 | 3.37E-04 | 2.10E-04 | 1.97E-04 | 2.80E-04 | 3.86E-04 | 2.69E-04 | 7.01E-05 |
| Fe | | 1.70E-05 | 2.69E-06 | 2.95E-05 | | 8.95E-07 | 8.95E-07 | 8.95E-07 | |
| Al3+ | 1.59E-06 | 2.59E-06 | 9.64E-06 | 3.15E-06 | | 8.75E-08 | 8.01E-08 | 8.38E-08 | 4.00E-09 |
| Zn2+ | 6.35E-06 | 5.20E-06 | | 3.90E-06 | | 8.32E-07 | 3.30E-07 | 3.32E-06 | 2.65E-06 |
| U | | | | | | 2.48E-09 | 6.26E-09 | 4.37E-09 | 2.67E-09 |
| Pb2+ | 4.83E-09 | | | | | 2.41E-10 | 2.41E-10 | 1.77E-09 | 2.65E-09 |
| Ni2+ | | | | | | 1.46E-07 | 2.10E-07 | 1.78E-07 | 4.52E-08 |
| Mn2+ | | | | | | 2.26E-07 | 2.39E-06 | 1.31E-06 | 1.53E-06 |
| As | | | | | | 4.55E-08 | 4.27E-08 | 4.41E-08 | 1.98E-09 |
| Cd2+ | 1.25E-08 | | | | | | | 1.25E-08 | |
| pH | 6.6 - 8.0 | 7.2 | 6.7 | 7.0 - 7.2 | | 7.2 | 6.9 - 7.2 | 7.11 | 0.15 |
| T (°C) | 6 - 18 | | | | | | | 12 | 4 |
| Eh (mV) | | | | | | | | 500 | 300 |

* 3.7 km downstream from discharge pipe (filtered samples)
** 0.7 km downstream from discharge pipe (filtered samples)

There are no mineralogical investigations for this site available, only rather general descriptions of the geological state. They indicate, that the river sediments mostly consist of Quartz sands and clays based on Mica, Glauconite, and Flint. This is in good agreement with own observations based on X-ray diffraction measurements of samples from the river bed. Analysis is complicated by a considerable content of organic matter of various origin and in different state of degradation. The soil is based on Glauconite, and Fe-enriched Sandstone. A bulk composition of 77 % $SiO_2$, 3.7 % $Fe_2O_3$, 2 % $Al_2O_3$, 4.3 % ZnO, and 1.1 % CaO (mass precents, only the major constituents are given) was determined, the total carbon content amounts to about 3 %.

### 3.3.3. Chemical Speciation Modelling

The EQ3NR modelling of the chemical speciation in the river water revealed, that the available analytical data for the aqueous phase are of satisfactory quality. Only a small charge disequilibrium could be detected, with the $Cl^-$ anion (selected for charge balancing) increasing from $1.21 \cdot 10^{-3}$ to $1.37 \cdot 10^{-3}$ mol / L, i.e. $1.6 \cdot 10^{-4}$ equv / L positive charges or only 3.7 % of the total positive charges are not compensated for in the original analyses. The true ionic strength is computed to be $6.5 \cdot 10^{-3}$ mol / L. The equilibrium partial pressure of $CO_2$(g) is at $4.61 \cdot 10^{-3}$ bar, about 15 times the atmospheric value. Oversaturation with respect to 55 minerals is indicated, mostly iron minerals and alumosilicates. The dissolved Silica concentration of $SiO_2$(aq) seems to be determined by equilibrium with Quartz, the following saturation indices were computed:

- 0.449 Quartz
- 0.262 Tridymite
- 0.165 Chalcedony

More difficult is the situation with regard to the redox state. Various redox couple potentials are obviously not in equilibrium:

- default 0.829 V (this means all the iron is converted into $Fe^{III}$)
- $NO_2^-$ / $NH_3$(aq) 0.364 V
- $NO_3^-$ / $NH_3$(aq) 0.386 V
- $O_2$(aq) / $H_2O$ 0.815 V

But even with this large uncertainty in the system's redox potential, in general an oxidizing environment can be assumed. As shown later, actually the Eh is critical to the speciation for Plutonium only. The speciation of all considered radioactive contaminants at the selected conditions as given in Table 14 is presented below in Table 15.

Table 15: Speciation of radioactive contaminants in the Molse Nete river water, computed with EQ3NR.

| **Americium** | **Plutonium** | **Cobalt** | **Cesium** |
|---|---|---|---|
| 74.1 % $AmCO_3^+$ | 60.4 % $PuO_2CO_3$(aq) | 95.1 % $Co_2(OH)_3^+$ | 99.9 % $Cs^+$ |
| 12.1 % $AmOH^{2+}$ | 18.0 % $PuO_2HPO_4$(aq) | 2.5 % $Co^{2+}$ | |
| 6.2 % $AmSO_4^+$ | 10.1 % $PuO_2^+$ | 2.4 % $HCoO_2^-$ | |
| 3.7 % $Am^{3+}$ | 3.4 % $PuO_2(CO_3)_2^{2-}$ | | |
| 2.4 % $Am(OH)_2^+$ | 2.7 % $PuO_2OH^+$ | | |
| 1.5 % $Am(CO_3)_2^-$ | 2.7 % $PuO_2(OH)_2$(aq) | | |

In a second step using EQ6 the precipitation of minerals was allowed under the following premises: Due to kinetic reasons the formation of Diaspore and any Iron minerals other then HFO is suppressed. There, the pH decreases to 7.05 (which is well inside the error range) and the Eh now defaults to 813 mV. The following minerals precipitate:

| *Product* | *Log moles* | *Moles* |
|---|---|---|
| Kaolinite | -7.409 | 3.899E-08 |
| Pyrolusite | -5.883 | 1.310E-06 |
| Quartz | -4.083 | 8.258E-05 |

This means, that Manganese and Alumina precipitate quantitatively, and also 57.8 % of the Silica precipitates.

When looking at each contaminant separately, there is nothing exciting with the Cesium, it always occurs at the simple monovalent cation $Cs^{+}$.

In case of Cobalt, only variations in pH are reflected in the speciation, changes in Eh or the carbonate content as the other most variable environmental parameters have no influence. Fig. 21 gives the pH effect on Cobalt speciation in waters from the Molse Nete river. However, it must be noted that the quality of the thermodynamic data set for Cobalt is worse compared to the ones for Americium or Plutonium.

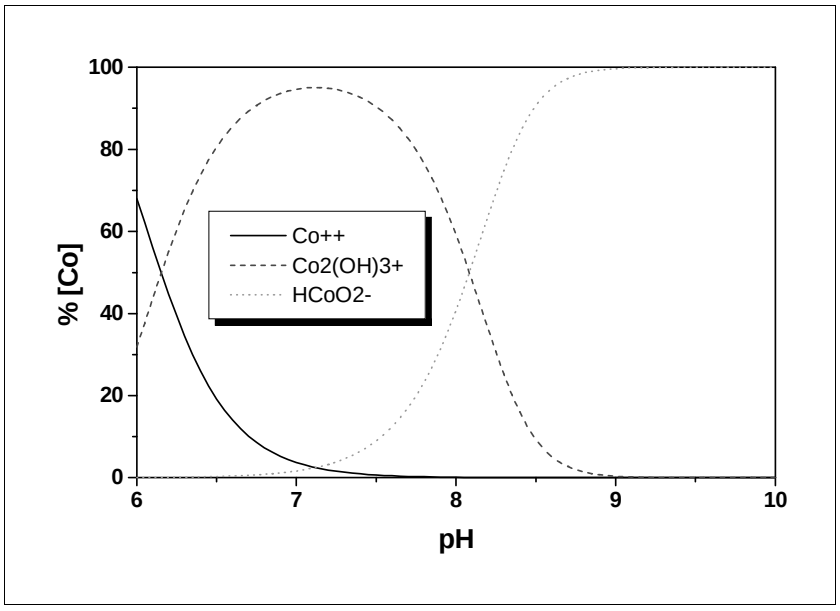


**Figure 21**: Cobalt speciation as a function of pH in river water of the Molse Nete

The modelling for Americium showed shifts in speciation both as a function of the pH and of the carbonate content. This is documented in Fig. 22.

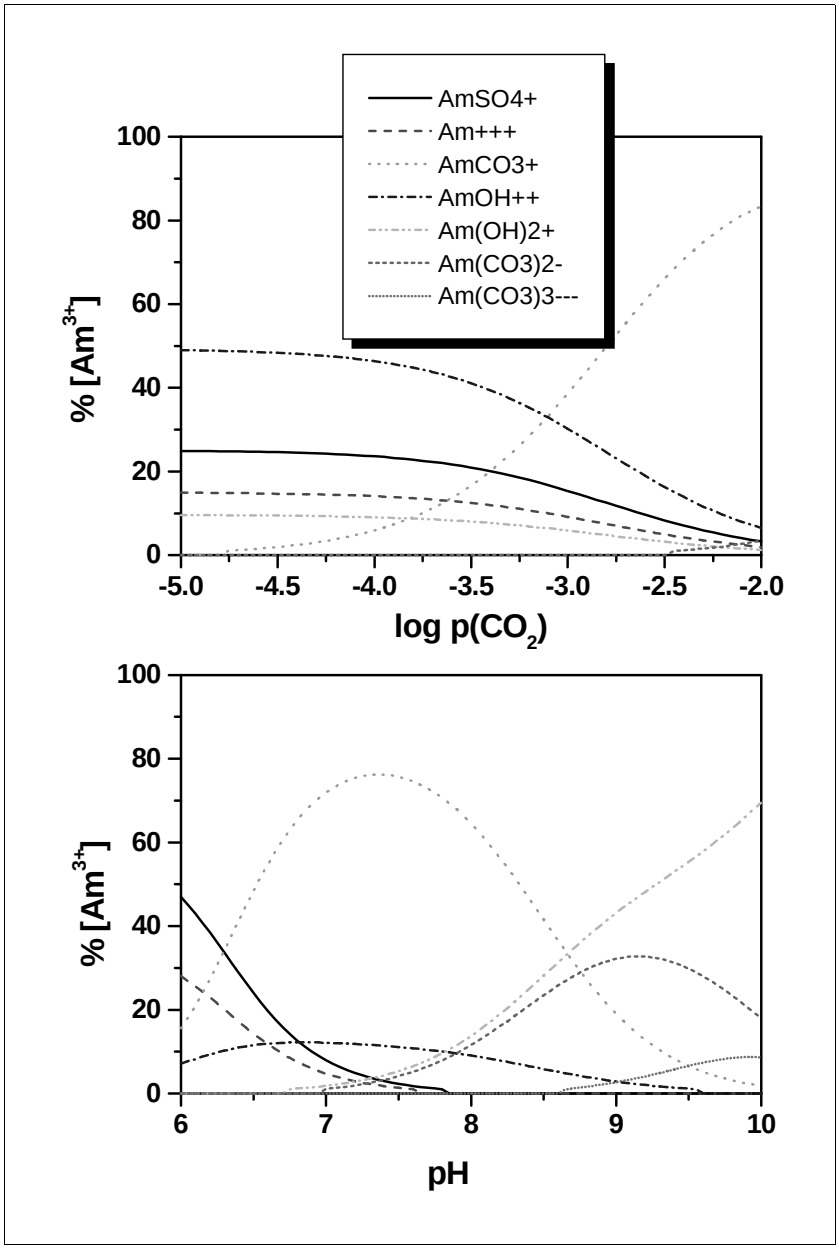


**Figure 22**: Americium speciation as function of pH and $p_{CO2}$ in river waters of the Molse Nete

Finally, as expected from the previous modellings for the Drigg Site, the Plutonium speciation is the most sensitive one. Therefore, Fig. 23 depicts the Plutonium speciation as function of all the three parameters pH, Eh, and carbonate content.

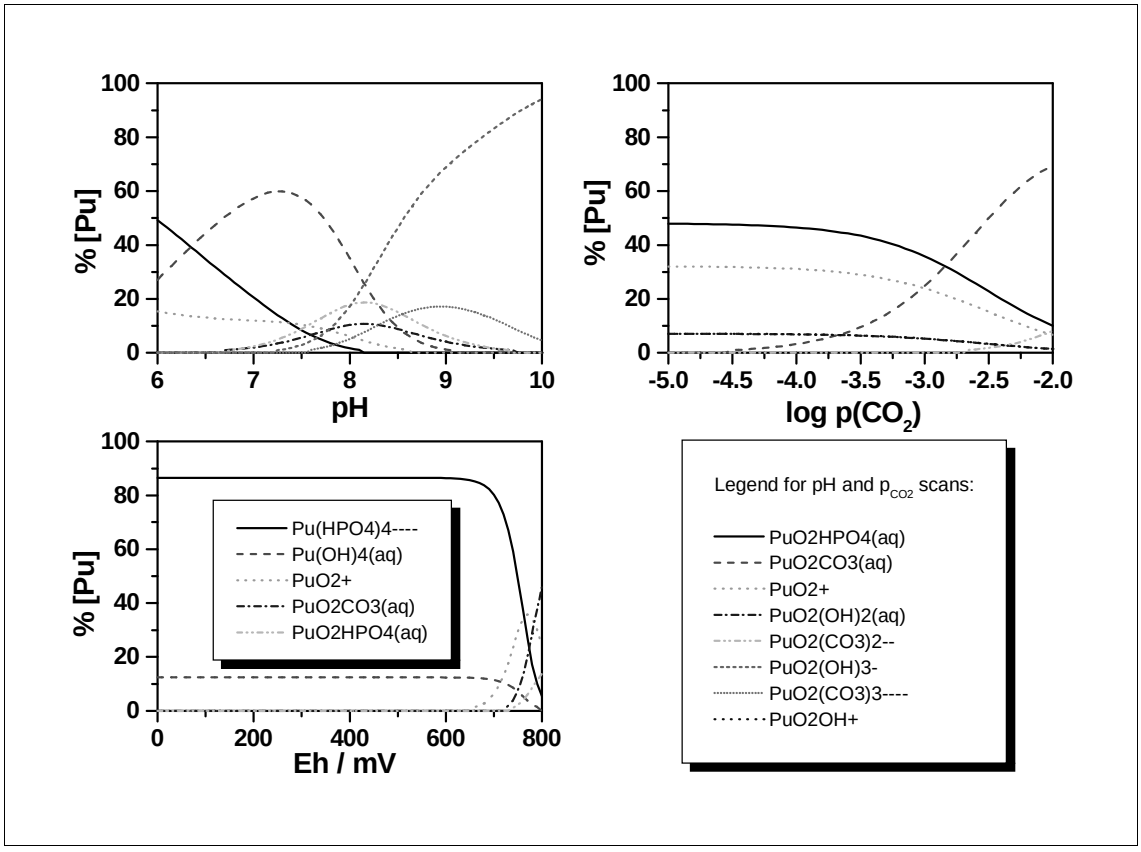


**Figure 23**: Plutonium speciation as function of pH, Eh and $p_{CO2}$ in river waters of the Molse Nete

### 3.3.4. $K_d$ Computations for the Basic Scenario

*Chemical data set*

Based on the chemical speciation modelling as discussed above, the input data set for the $K_d$ computations was composed from only the major anions (phosphate, chloride, sulfate and carbonate) and cations (Sodium, Potassium, Calcium, and Magnesium) with the concentrations given in Table 13. Additionally, Silica and Alumina were inserted as being determined by equilibrium with Quartz and Kaolinite, respectively. The following minerals had to be suppressed: Pyrophyllite, Diaspore, Hydroxylapatite and Leonhardite. Due to the pronounced redox dependency of the Plutonium speciation combined with the large uncertainty of the actual redox potential Eh, two scenarios for Plutonium were computed: A) $Pu^{4+}$ dominating at an Eh of 200±100 mV, and B) assuming $PuO_2^{2+}$ and 800±100 mV for the Eh.

*Surface properties*

Concerning the solid phase, the total solid concentration in the Molse Nete river was taken from the RESTRAT TD 11 [Sweeck and Zeevaert, 1999] to be a suspension of 17.5±4.0 mg / L. Because the site is mainly composed of sandy clays, the suspended material is mostly Quartz, with 4 % HFO as the sorbing admixture, as supported by the high content of colloidal iron found in several samples and the iron content from analysed sediment samples, see again RESTRAT TD 11. This gives a sorbate concentration $C_S$ of 0.7±0.1 mg / L. Using the specific site densities for HFO as given in Section 2.2.2., the following site concentrations $\Gamma_M$ in mol / L for strong and weak binding sites were obtained for the river water: $3.78 \cdot 10^{-8}$ and $1.575 \cdot 10^{-6}$, respectively. The resulting combined input parameter set was translated into the file model.chem as presented in Appendix C for the Cobalt case.

*Results*

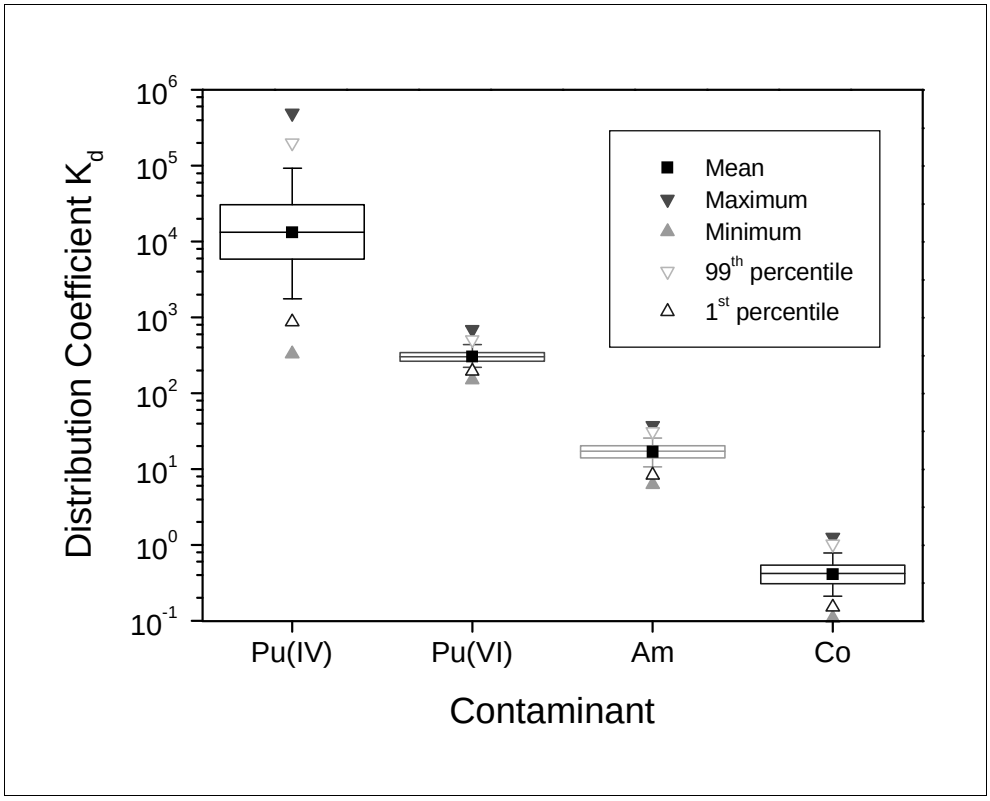


**Figure 24**: Computed $K_d$ values and their error distribution for the Molse Nete river

In Fig. 24, the results for three contaminants are summarized, with two scenarios (anoxic and oxic) for Plutonium as explained above. Please refer to Fig. 7 in section 3.1.4 for explanations of the graph elements.

Table 16 compares the computed and default $K_d$ values for the Molse Nete river. For both Cobalt and Americium, the generic values seem to be overestimating the site-specific $K_d$ values significantly, whereas for Plutonium the modelling based on $Pu^{VI}$ is in good coincidence with the default values used so far in the

risk assessment. As already observed for the Drigg Site, the computations assuming tetravalent $Pu^{4+}$ being the dominant Plutonium redox state yields unrealistic high $K_d$ values.

Table 16: Comparison of computed and estimated distribution coefficients in $m^3$ / kg for Cobalt, Americium and Plutonium in the Molse Nete river

| **$K_d$ in $m^3$ / kg** | **Computed** | | | | **Default** | | |
|---|---|---|---|---|---|---|---|
| **Contaminant:** | *log $K_d \pm \sigma$* | *Geometric Mean* | *$5^{th}$ Percentile* | *$95^{th}$ Percentile* | *Mean* | *Lower Limit* | *Upper Limit* |
| Cobalt | -0.38 ± 0.18 | 0.375 | 0.194 | 0.724 | 20 | 5 | 100 |
| Americium | 1.23 ± 0.12 | 17.0 | 10.8 | 25.9 | 1000 | 100 | 2000 |
| Plutonium (IV) | 4.13 ± 0.52 | 13362 | 1769 | 90476 | 250 | 100 | 1000 |
| Plutonium (VI) | 2.49 ± 0.09 | 308 | 222 | 441 | | | |

Table 17 presents the parameters strongest influencing the overall uncertainty of the distribution coefficients, derived from a ranked regression. As expected, pH, solid concentration and carbonate content are the major impact factors. A peculiarity is the strong dominance of the phosphate concentration (via the $Pu(HPO_4)_4^{4-}$ complex) in the case of tetravalent Plutonium.

Table 17: Parameters responsible for the uncertainty of computed distribution coefficients for the Molse Nete river.

| **Contaminant:** | **$1^{st}$ Factor** | **$R^2$ Improvement** | **$2^{nd}$ Factor** | **$R^2$ Improvement** |
|---|---|---|---|---|
| Cobalt | pH | 83.8 % | C(solid) | 11.9 % |
| Americium | $C(HCO_3^-)$ | 36.4 % | C(solid) | 30.1 % |
| Plutonium (IV) | $C(PO_4^{3-})$ | 69.2 % | pH | 12.1 % |
| Plutonium (VI) | C(solid) | 47.7 % | $C(HCO_3^-)$ | 19.9 % |

### 3.4. Ravenglass Estuary

#### 3.4.1. Compartment Structure

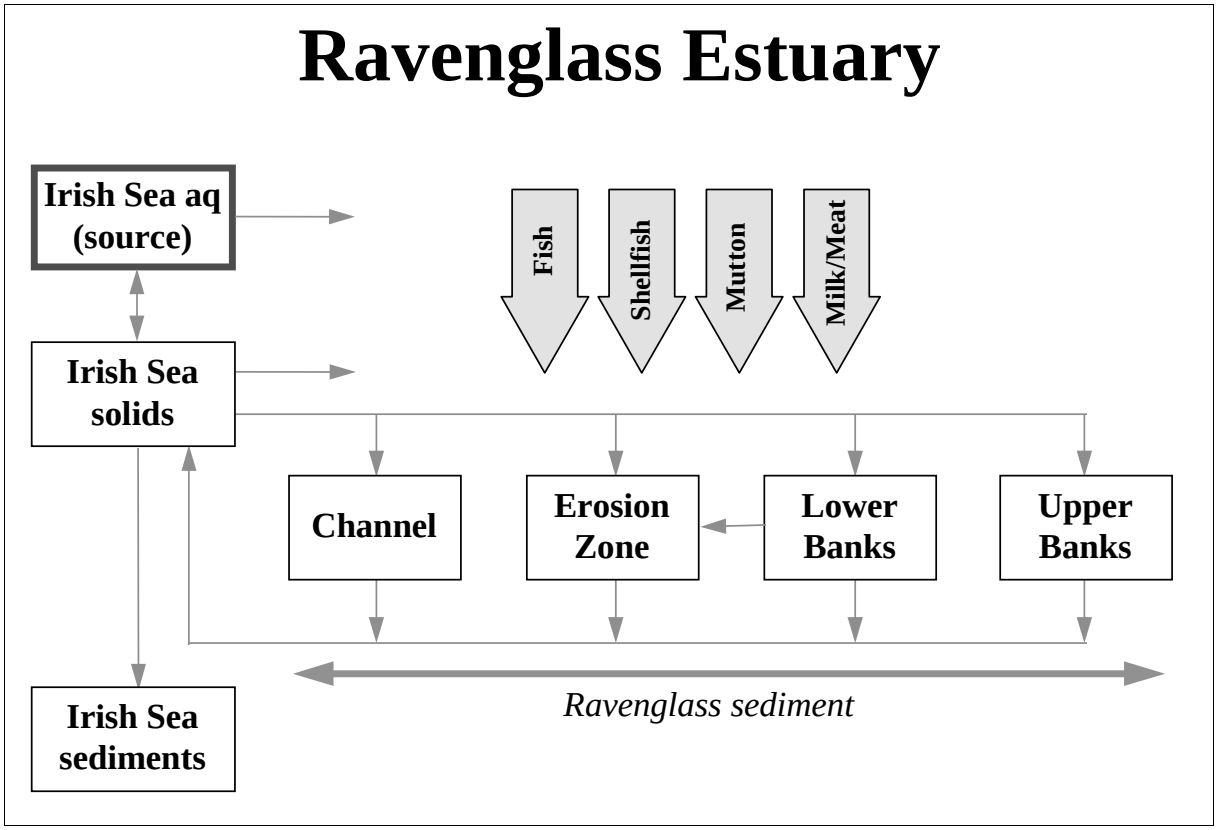


**Figure 25**: BIOPATH compartment structure for the Ravenglass Estuary

The compartment structure shown above indicates, that there exist equilibria between aqueous and solid phase for all compartments, but as will be shown later, only some of them have to be taken into account:

- between the upper banks of the rivers and its suspended solids in the river water;
- between the channel zone (as representative for those compartments that are strongly influenced by the Irish Sea) and its sediments;
- between the channel zone and the suspended solids in the estuarine water.

#### 3.4.2. Physico-Chemical Characteristics

The estuary is contaminated mainly via the Irish Sea from waste discharges from the Sellafield nuclear fuel reprocessing plant, but to a lesser degree also through the River Irt running off the Drigg site. The main radionuclides under consideration are $^{137}$Cs, $^{239}$Pu and $^{241}$Am. From the RESTRAT TD 12 [Bousher, 1999b], activity values for $^{241}$Am, $^{238}$Pu, and $^{239+240}$Pu can be extracted. The upper limit of the documented range was chosen and then converted into molar concentration. This gives an upper estimate for the Americium concentration in the aqueous phase of $4 \cdot 10^{-15}$ mol / L, whereas for Plutonium the maximum concentration is $8 \cdot 10^{-14}$ mol / L, assuming all activity can be attributed to $^{239}$Pu. Due to the lack of an overall cesium concentration value, as with the other RESTRAT example sites, 1 % of the Sodium

concentration value was assigned, giving estimates of $4 \cdot 10^{-4}$ mol / L, $4 \cdot 10^{-3}$ mol / L and $3 \cdot 10^{-3}$ mol / L for the Upper Bank, the Channel, and the Sediment compartment, respectively.

In the open literature no analytical data specific for this location is available. Extrapolations from nearby collected data sets [Dickson and Boelens, 1988] could be justified only for the composition of a typical water sample from the Irish Sea. In case of the Estuary itself, however, a sampling campaign became necessary. Therefore, as part of the RESTRAT project, Westlakes took several samples between July 1996 and March 1997, which were assigned to the various compartments as follows:

- one sample of water from 50 m outside the mouth of the Ravenglass Estuary, representing the Irish Sea (to be combined with generic data from [Dickson and Boelens, 1988]);
- two samples of water from 50 m inside the mouth and from the barrier of the mouth, both representing the channel;
- one sample of water from the Eskmeal viaduct, representing the lower banks;
- one sample of water from the Drigg stream confluence of the River Irt, representing the upper banks.

The sampling procedure was in most cases accompanied by in-situ determinations of pH, temperature, redox potential Eh and oxygen content. All samples were then shipped to and analysed at the FZ Rossendorf. Unfortunately, no sample could be obtained from the erosion zone. An additional sample was taken from the sediment of the estuary to allow analysing of the pore water. This uneven sample distribution to a certain degree also reflects the major changes that occurred in the BIOPATH compartment structure throughout most of the RESTRAT project. As anticipated, the Ravenglass Estuary turned out to be indeed the most complex test example case of the project.

Table 18: Selected best set of analytical values for the Ravenglass Estuary compartments, all concentrations are in mol / L.

| **Compartment:** | **Upper Banks** | | **Lower Banks** | | **Channel** | | **Sediment** | | **Irish Sea** | |
|---|---|---|---|---|---|---|---|---|---|---|
| **Label:** | **UB** | | **LB** | | **CH** | | **SD** | | **IS** | |
| Component: | Mean | STD | Mean | STD | Mean | STD | Mean | STD | Mean | STD |
| PO43- | 7.687E-05 | 7.446E-06 | | | | | | | | |
| NO3- | 5.645E-05 | 6.842E-06 | | | | | | | | |
| SO42- | 2.644E-03 | 1.472E-05 | 1.343E-02 | 5.796E-04 | 2.446E-02 | 7.361E-04 | 1.166E-02 | 1.031E-03 | 2.665E-02 | 5.889E-04 |
| CO32- | 1.085E-04 [1)] | | 1.327E-03 [1)] | | 2.073E-03 | 3.477E-05 | 1.999E-02 | 2.550E-03 | 1.196E-03 | 1.182E-03 |
| Cl- | 4.823E-02 | 3.989E-04 | 2.670E-01 | 4.002E-03 | 4.894E-01 | 1.396E-02 | 3.822E-01 | 4.986E-02 | 5.072E-01 | 7.978E-04 |
| SiO2 | 4.931E-05 | 5.791E-06 | 3.062E-05 | 7.711E-06 | 3.365E-05 | 8.977E-06 | 3.886E-04 | 8.484E-05 | 3.587E-05 | 1.120E-05 |
| K+ | 9.847E-04 | 3.617E-05 | 4.894E-03 | 1.937E-04 | 9.419E-03 | 3.546E-04 | 6.420E-03 | 9.043E-04 | 9.429E-03 | 2.735E-04 |
| Na+ | 4.226E-02 | 7.689E-04 | 2.310E-01 | 1.921E-03 | 4.138E-01 | 1.675E-02 | 3.006E-01 | 2.768E-02 | 4.186E-01 | 1.801E-02 |
| Ca2+ | 1.148E-03 | 1.023E-04 | 5.140E-03 | 2.380E-04 | 9.749E-03 | 4.290E-04 | 6.300E-03 | 3.705E-04 | 9.556E-03 | 7.485E-05 |
| Mg2+ | 4.567E-03 | 2.327E-04 | 2.584E-02 | 2.002E-03 | 4.680E-02 | 9.123E-04 | 3.473E-02 | 3.840E-03 | 4.800E-02 | 1.855E-03 |
| Fe | | | | | 2.387E-06 | 1.447E-06 | 5.300E-05 | 6.939E-05 | 2.507E-06 | |
| Al3+ | | | | | 3.781E-06 | 5.154E-06 | 4.429E-07 | 5.635E-07 | 2.075E-06 | 2.726E-06 |
| Zn2+ | 5.751E-07 | | 5.720E-07 | 1.428E-07 | 1.518E-07 | 3.333E-08 | | | 8.412E-08 | 1.082E-08 |
| U | 1.806E-09 | 9.506E-10 | 1.291E-08 | 3.216E-09 | 1.670E-08 | 1.470E-09 | 2.710E-08 | 1.159E-08 | 1.701E-08 | 8.912E-10 |
| Pb2+ | | | | | 3.620E-09 | 3.285E-09 | 1.448E-09 | 6.825E-10 | 2.896E-09 | 2.730E-09 |
| Ni2+ | 1.567E-07 | | 2.734E-07 | 4.457E-08 | | | | | | |
| Mn2+ | 8.710E-07 | 1.180E-06 | 3.595E-07 | 6.564E-08 | 1.256E-07 | 1.350E-07 | 3.012E-04 | 5.535E-05 | 1.005E-07 | 1.076E-07 |
| Cd2+ | | | | | 8.896E-09 | | | | | |
| As | 6.006E-08 | | 3.221E-07 | 3.624E-08 | | | | | | |
| pH: | 7.02 | 0.20 | 8.04 | 0.20 | 7.93 | 0.10 | 7.33 | 0.10 | 8.07 | 0.10 |
| Eh / mV: | | | | | 122.60 | 2.70 | 218 [1)] | | 129.10 | |

Table 18 combines the analytical results with the results from the speciation modelling, as discussed later, to yield a recommended best set of physico-chemical data. Superscript [1)] marks values set according to the modelling results when there is no experimental information available at the moment. Average values (MEAN) and standard deviations (STD) were calculated assigning equal weights to all listed values. There are no values given for Mercury, Chromium, Copper, and Cobalt, because the available data is either too widely scattered, or there are hardly measurements of those values above their respective detection limits.

The sediments can be divided into three categories (facies) reflecting their source of origin. The main classes are estuarine deposits (channel facies, erosional facies, and bank facies, the latter again subdivided into lower and upper bank facies) and relic facies. The channel facies mainly comprise coarse grained sand. Bank facies deposits consist mainly of fine grained sediments, of sandy silt and silt grade. Erosional facies have a mixed grain size of silty sand grade. Measured erosion rates vary from 0 to 6 mm / year.

For the channel facies a preliminary mean sedimentation rate is determined with 11 mm / year, but deposition is to be considered highly sporadic, partly in association with mobile beds. The main channel system is a high flow velocity environment. Lower bank facies have a relatively high sedimentation rate of 28 mm / year, whereas the upper bank facies (salt marshes and intertidal pastures) sediment with only 4 mm / year. The hydrology is strongly influenced by seasonal temperature changes and the circulation patterns of the Irish Sea.

Information about the mineralogical composition of the sediments can be drawn from Kelly and Emptage, 1992, also cited in RESTART TD12 [Bousher, 1999b]. Quartz is the dominant mineral, with smaller amounts of feldspars and clay / micas. Also Calcite is a common minor mineral in estuarine sediments, whereas river sediments contain some amphiboles. When considering the estuarine and marine clay minerals, the composition can be approximated with 66 % Illite, 8 % Chlorite and 10 % Kaolinite.

### 3.4.3. Chemical Speciation Modelling

The chemical composition of the main aqueous phases involved in the modelling clearly indicates, that the composition of the estuary water is nearly identical to the one of the Irish Sea, due to the strong tidal effects. That means a high ionic strength due to the large amounts of Sodium and Magnesium chlorides and sulfates. The pH becomes slightly more basic from the river through the estuary till the open sea. The redox potential of the sediments is in the reducing range, thus influencing especially the speciation of Plutonium, whereas in the flowing water the conditions are oxidizing. In all cases, Silica seems to be in equilibrium with either Quartz or Chalcedony. The waters are supersaturated with respect to several Manganese and Iron minerals, that, however, may not form due to kinetic hindrance.

For the Irish Sea, the modelling gave a ionic strength of 0.57 mol / L, with a total charge imbalance of only 3.7 %. The low redox potential value from the in-situ measurement could not be supported by the modelling, the water is expected to be much more oxidizing.

For the channel, the modelled ionic strength was with 0.56 mol / L very close to the value of the open sea, as expected. Here, the measured low Eh can be explained by interactions with a reducing sediment. This will influence especially the speciation of plutonium.

Water from the lower bank, although sampled at high tide, already show a significant decrease in ionic strength (here 0.32 mol / L). The carbonate content was not measured, modelling of an equilibrium with

the atmosphere gave the reasonable value of 1.33 mmol / L, corresponding to a charge imbalance of only 1.0 %.

The sample from the upper banks, also collected at high tide, has with 0.061 mol / L the lowest ionic strength. Similar to the upper bank situation, a carbonate content had to be found through modelling, the value in equilibrium with air is $1.085 \cdot 10^{-4}$ mol / L, corresponding to a charge imbalance of only 1.6 %.

In the case of the pore water sample from the mussel beds, reducing conditions were expected, the modelling yielded accordingly a redox potential of +218 mV. Contrary to all other compartments, Silica is not in equilibrium with Quartz, but strongly supersaturated. There are further supersaturations with respect to the solid phases Magnesite ($MgCO_3$) and Dawsonite ($NaAl(OH)_2CO_3$), that may precipitate in the long time frame selected for the risk assessment in RESTRAT. The ionic strength is 0.41 mol / L, close to the high mineralization values for marine waters. The quality of the chemical analyses is, for unknown reasons, not as good as for the other samples, indicated by a charge imbalance of 9.4 %.

Because the estuary compartments (except the Upper Banks) are so similar to each other and the Irish Sea, they are dealt with together when looking at the chemical speciation patterns of the main contaminants. Thus, only three cases had to be studied: Upper Banks, Channel (representing most of the estuary compartments), and Sediment.

Table 19: Speciation of radioactive contaminants in the Ravenglass Estuary, computed with EQ3NR.

| Upper Bank | Channel | Sediments |
|---|---|---|
| **Americium** | | |
| 33.9 % $AmOH^{2+}$ | 49.6 % $AmOH^{2+}$ | 69.8 % $AmCO_3^+$ |
| 24.2 % $Am^{3+}$ | 21.7 % $AmCO_3^+$ | 20.2 % $Am(CO_3)_2^-$ |
| 23.1 % $AmSO_4^+$ | 12.6 % $Am(OH)_2^+$ | 2.9 % $AmOH^{2+}$ |
| 8.6 % $AmCO_3^+$ | 5.7 % $AmOH^{2+}$ | 2.5 % $Am(CO_3)_3^{3-}$ |
| 3.6 % $Am(OH)_2^+$ | 3.9 % $Am(CO_3)_2^-$ | 2.0 % $Am^{3+}$ |
| 3.6 % $AmCl^{2+}$ | 3.6 % $AmSO_4^+$ | 1.1 % $AmSO_4^+$ |
| 2.3 % $AmH_2PO_4^{2+}$ | 2.3 % $AmCl^{2+}$ | |
| **Plutonium** | | |
| 58.3 % $Pu(HPO_4)_4^{4-}$ | 60.8 % $PuO_2(CO_3)_3^{4-}$ | 98.7 % $Pu(OH)_4$(aq) |
| 41.7 % $Pu(HPO_4)_5^{6-}$ | 11.9 % $PuO_2CO_3$(aq) | 1.2 % $Pu(OH)_5^-$ |
| | 11.8 % $PuO_2(CO_3)_2^{2-}$ | |
| | 8.0 % $PuO_2(OH)_3^-$ | |
| | 4.2 % $PuO_2(OH)_2$(aq) | |
| | 1.6 % $PuO_2^+$ | |

As already pointed out for the other RESTRAT example sites, Cesium is constantly occurring as the simple monovalent cation $Cs^+$. For the other two important contaminants, Americium and Plutonium, the typical speciations for them are given in Table 19, each compartment exhibits its own specific picture, most pronounced for Plutonium. For both elements, also the influence of pH, redox potential Eh, and carbonate concentration (via the $CO_2$ partial pressure) on their speciation were investigated.

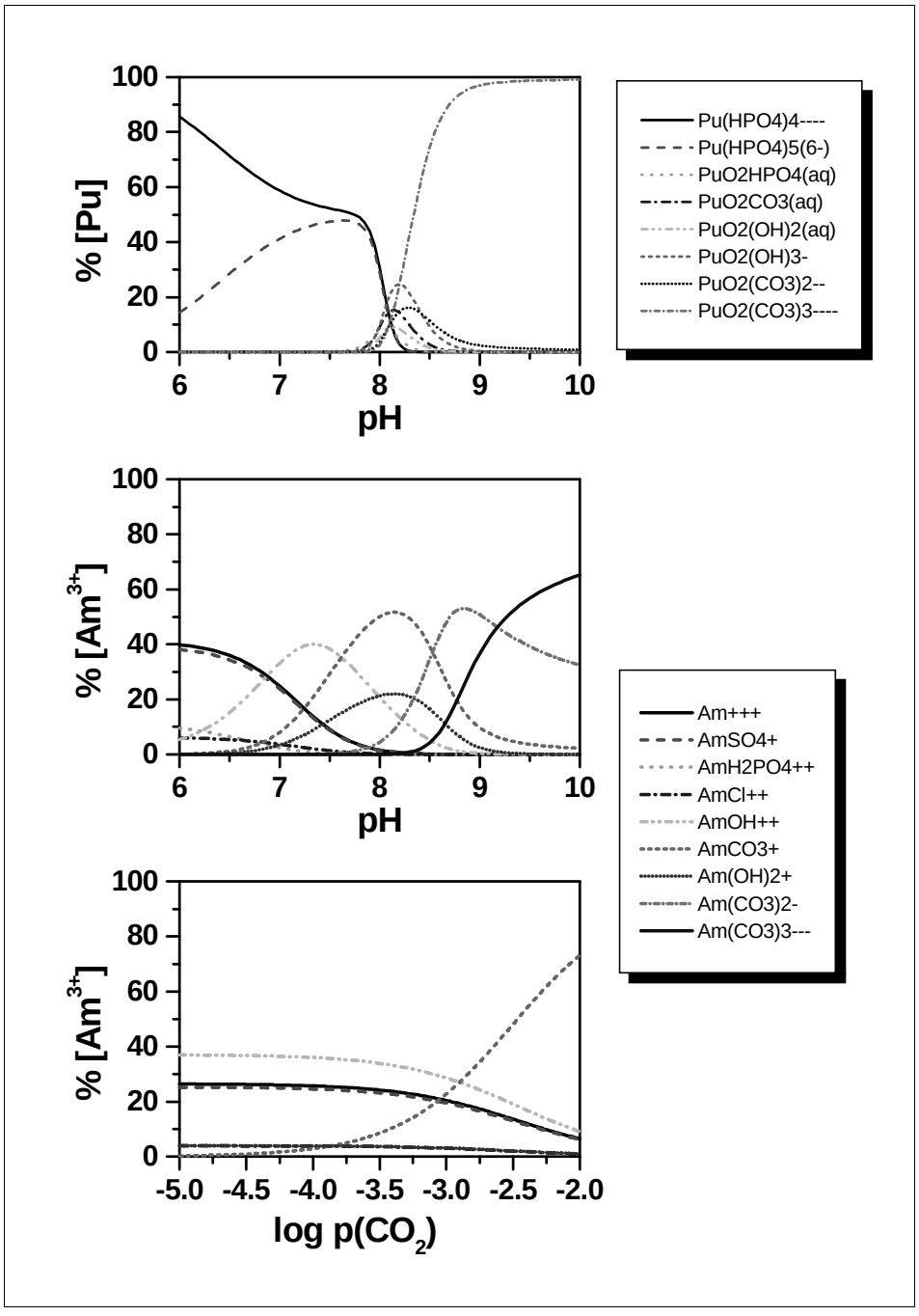


**Figure 26**: Americium and Plutonium speciation in waters from the upper banks of the Ravenglass Estuary as function of pH and $p_{CO2}$

Fig. 26 shows, for the Upper Bank compartment, the speciation of Americium as function of pH and the carbon dioxide partial pressure $p_{CO2}$ (no dependence on the redox potential could be observed, this is valid for all compartments) and of Plutonium as function of the pH (no dependence on $p_{CO2}$ or Eh could be observed).

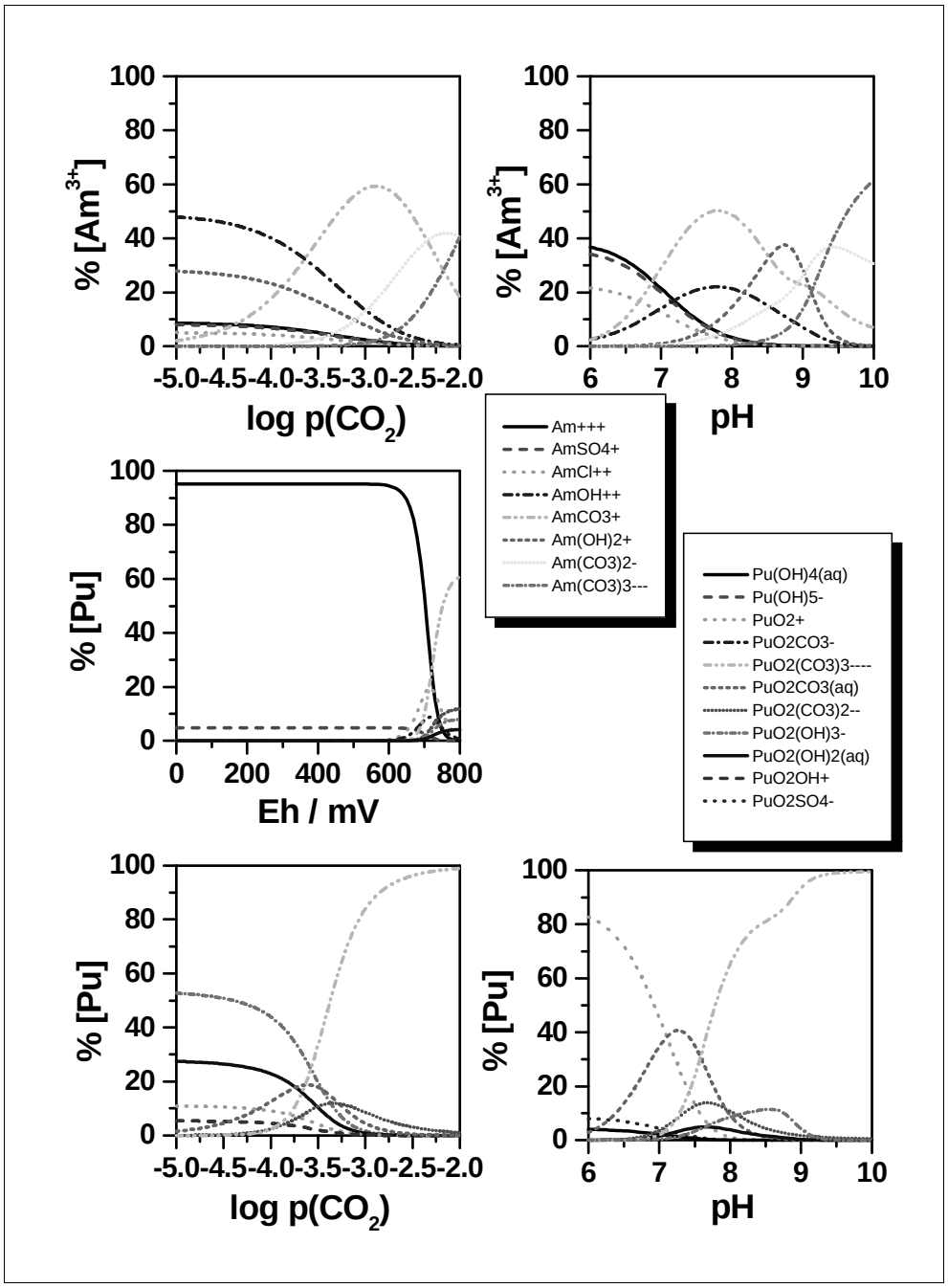


**Figure 27**: Americium and Plutonium speciation in the Channel of the Ravenglass Estuary as function of pH, Eh, and $p_{CO2}$

The next graph applies to the Channel compartment. Fig. 27 gives the Americium speciation as a function of pH and carbon dioxide partial pressure, and depicts the influence of pH, redox potential Eh, and carbon dioxide partial pressure on the Plutonium speciation.

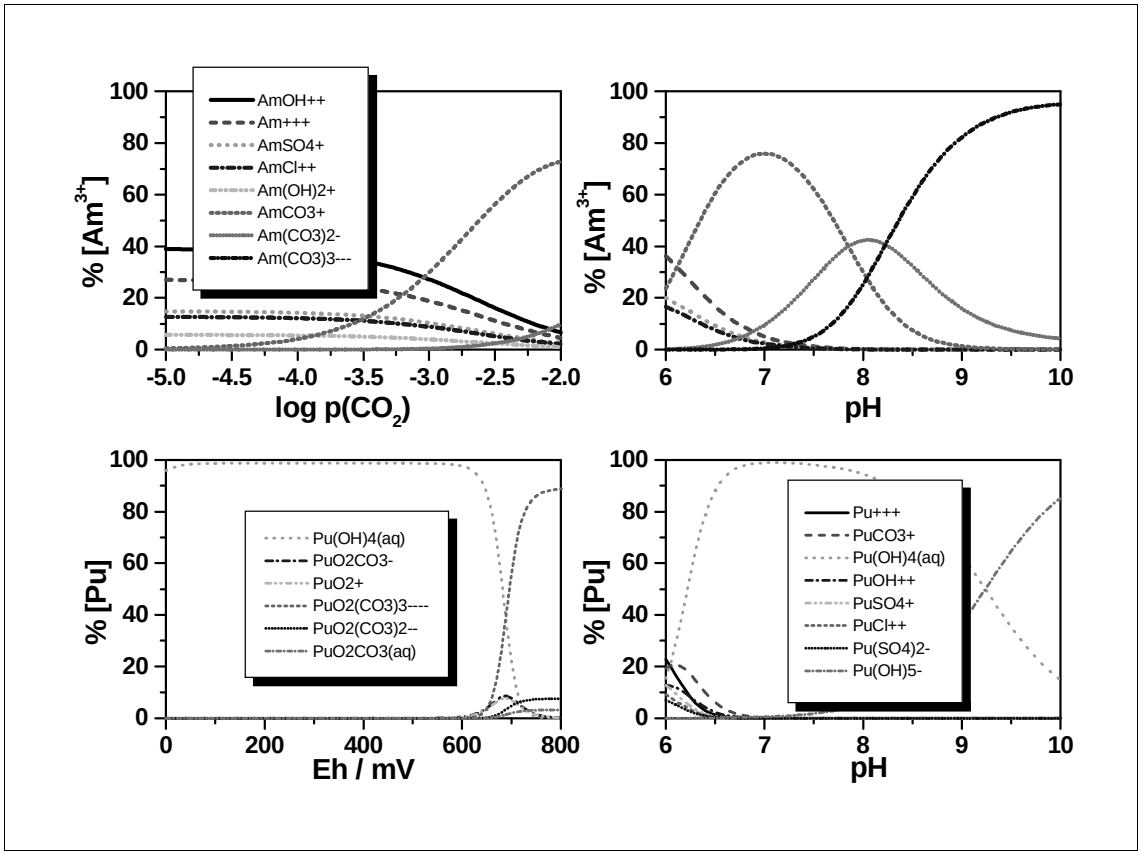


**Figure 28**: Americium and Plutonium speciation in sediment pore waters of the Ravenglass Estuary as a function of pH, Eh and $p_{CO2}$

Finally, Fig. 28 shows the Americium speciation (again as function of pH and carbon dioxide partial pressure) and the Plutonium speciation (as function of pH and Eh) for pore waters of the sediment.

### 3.4.4. $K_d$ Computations for the Basic Scenario

*Chemical data set*

The chemical data comprises of the contaminant, plus the major anions (chloride, sulfate, and carbonate) and cations (sodium, potassium, calcium and magnesium). In the case of the Upper Bank compartment, in addition phosphate must be considered. Silica and alumina are always assumed to be in equilibrium with Quartz and Kaolinite, respectively, as derived from mineralogical data and the chemical speciation modelling. The concentrations, as well as values for pH and Eh, are those listed in Table 18. The formation of the following minerals were suppressed due to kinetic considerations: Pyrophyllite, Diaspore, Leonhardite, Hydrapatite, Dolomite, Talc, Tremolite.

*Surface properties*

In order to obtain site-specific surface parameters, the total solid concentration in the Upper Bank and the Channel compartment was taken from the RESTRAT TD 12 [Bousher, 1999b] to be a suspension of 6.5±3.0 mg / L. According to solid phase analysis, the suspended material is mostly Quartz, with 5 % HFO as the sorbing admixture. This gives a sorbate concentration $C_S$ of 0.325±0.150 mg / L for both compartments. Using the specific site densities for HFO as given in Section 2.2.2., the following site concentrations $\Gamma_M$ in mol / L for strong and weak binding sites were obtained for the aqueous suspension: $1.755 \cdot 10^{-8}$ and $7.313 \cdot 10^{-6}$, respectively.

With regard to the estuary sediments, no data about porosity were available. From reported values of the bulk density of the sediments, a porosity of 80 % was derived. This, together with the data given in the above paragraph, translates into the following site concentrations $\Gamma_M$ in mol / L for strong and weak binding sites: $1.8 \cdot 10^{-3}$ and $7.48 \cdot 10^{-2}$, respectively. The resulting combined input parameter set was translated into the file model.chem as presented in Appendix D for the Americium case.

*Results*

In Fig. 29, the computed distribution coefficients for Americium and Plutonium are summarized, please refer to Fig. 7 in section 3.1.4 for explanations of the graph elements.

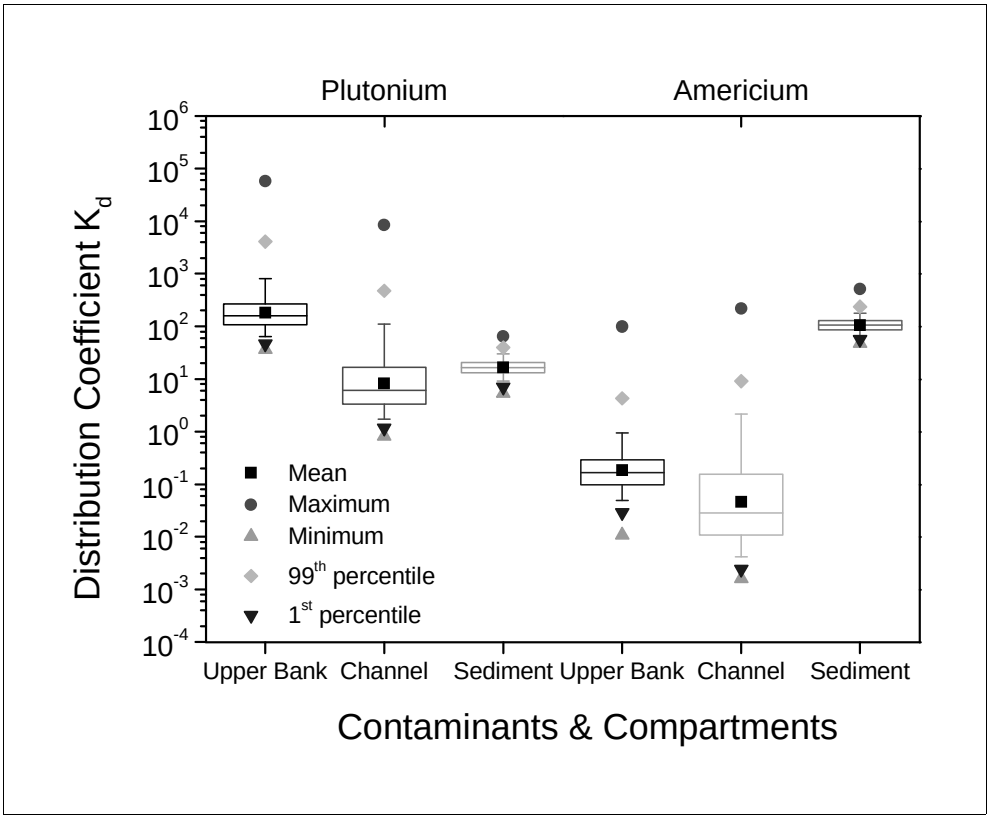


**Figure 29**: Computed $K_d$ values and their error distribution for the Ravenglass Estuary

Table 20 compares the calculated $K_d$ values with the ones used so far in the risk assessment. In the case of Plutonium in the sediment compartment (with expected reducing conditions) the results for both the tetra- and hexavalent actinide are reported, with the former being unusual high. The other $K_d$ values for Plutonium are on the lower limit of the generic range. For Americium, the site-specific computed $K_d$ values are even up to three orders of magnitude below the generic values. Obviously the high mineralization of those waters (with ionic strengths near to sea water levels) dislodges Americium from the available sorption sites. For both contaminants considered here the by far largest uncertainties (even compared with the other RESTRAT example sites) result from the Channel compartment.

Table 20: Comparison of computed and estimated distribution coefficients in $m^3$ / kg for Americium and Plutonium for the Ravenglass Estuary

| **$K_d$ in $m^3$ / kg** | **Computed** | | | | **Default** | | |
|---|---|---|---|---|---|---|---|
| **Compartment:** | *log $K_d$ ± σ* | *Geometric Mean* | *$5^{th}$ Percentile* | *$95^{th}$ Percentile* | *Mean* | *Lower Limit* | *Upper Limit* |
| Americium | | | | | | | |
| Upper Bank | -0.73 ± 0.41 | 0.19 | 0.05 | 0.94 | 552 | 30 | 790 |
| Channel | -1.33 ± 0.84 | 0.047 | 0.004 | 1.897 | | | |
| Sediment | 2.03 ± 0.13 | 107.7 | 65.7 | 179.2 | | | |
| Plutonium | | | | | | | |
| Upper Bank | 2.27 ± 0.36 | 185.5 | 64.4 | 806.5 | 1017 | 40 | 11000 |
| Channel | 0.93 ± 0.56 | 8.42 | 1.75 | 110.27 | | | |
| Sediment (VI) | 1.22 ± 0.16 | 16.8 | 9.2 | 30.6 | | | |
| Sediment (IV) | 6.60 ± 0.36 | $3.98 \cdot 10^6$ | $1.08 \cdot 10^6$ | $15.69 \cdot 10^6$ | | | |

The next table lists the results of a sensitivity analysis (ranked regression) to reveal the parameters mostly determining the overall uncertainty of the computed $K_d$ values. It turns out that in all cases the uncertainty in the solid concentration directly propagates to the computed $K_d$ error. It is an interesting fact, that in the sediment compartment the concentration error of the major cation, $Mg^{2+}$, also plays a certain role. The other important uncertainty impact factors are, as already known form the modelling for the previous examples cases, the pH and the carbonate concentration.

Table 21: Parameters responsible for the uncertainty of computed distribution coefficients for the Ravenglass Estuary.

| **Compartment:** | **1st Factor** | **$R^2$ Improvement** | **2nd Factor** | **$R^2$ Improvement** |
|---|---|---|---|---|
| Americium | | | | |
| Upper Bank | C(solid) | 63.0 % | $C(HCO_3^-)$ | 18.5 % |
| Channel | C(solid) | 94.7 % | pH | 4.2 % |
| Sediment | C(solid) | 59.9 % | $C(Mg^{2+})$ | 21.7 % |
| Plutonium | | | | |
| Upper Bank | C(solid) | 69.0 % | pH | 23.5 % |
| Channel | C(solid) | 96.2 % | pH | 2.8 % |
| Sediment | C(solid) | 38.6 % | $C(Mg^{2+})$ | 28.1 % |

### 3.5. Lake Tranebärssjön

#### 3.5.1. Compartment Structure

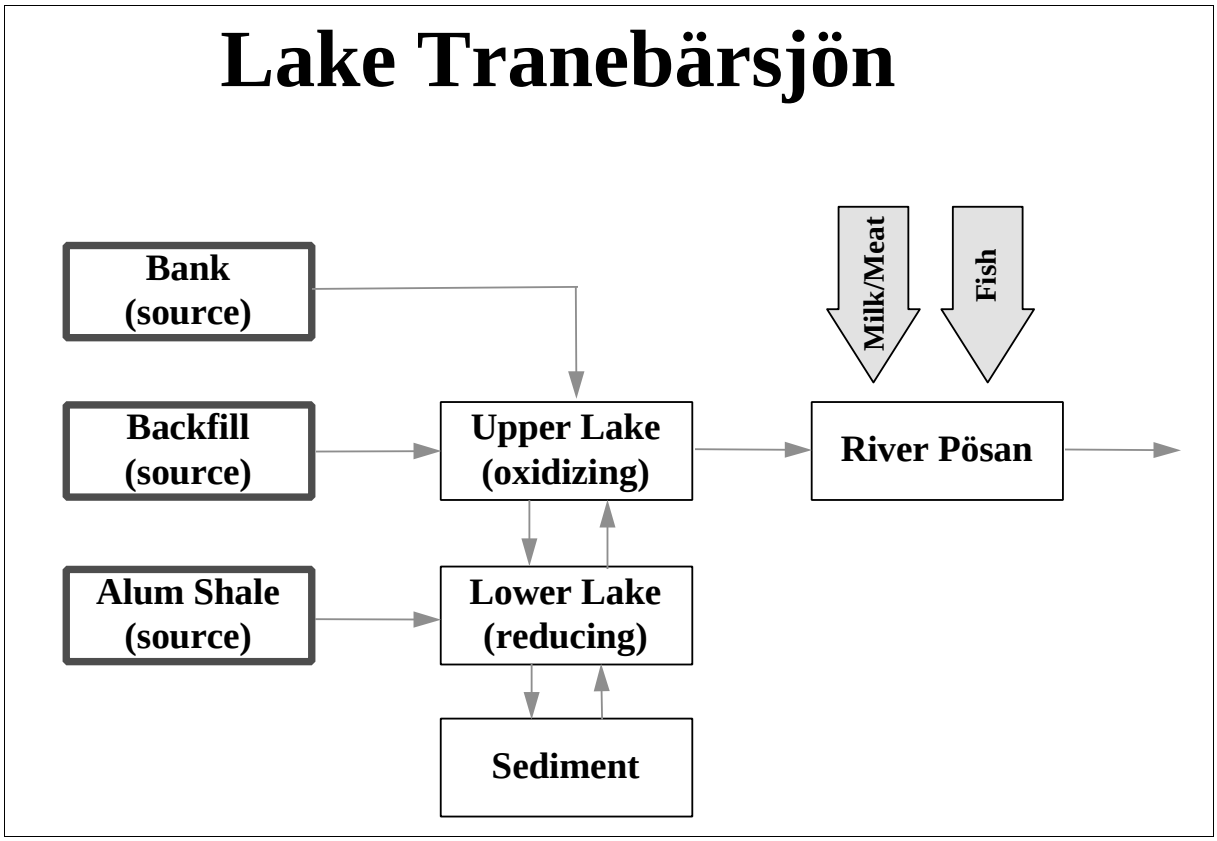


**Figure 30**. BIOPATH compartment structure for Lake Tranebärssjön

The compartment structure as shown in Fig. 30 includes several sections with an aquatic phase, either as an aqueous bulk phase with suspended solids or as pore water in a mineral matrix. Namely this involves four compartments: The upper layer of the lake itself, the respective lower layer, the backfill with its pore water, and the alum shale with its pore water. These are consequently the compartments where distribution coefficients have been computed.

#### 3.5.2. Physico-Chemical Characteristics

The surrounding of the lake differs on both shores. On one side it is mainly the undisturbed geological formation, with moraine on the top, then the limestone layer, the alum shale layer, and as the lowest layer of interest sandstone. The other side of the lake, including most of the lake bottom, consists of backfilled limestone and alum shale, covered by a thinner layer of backfilled moraine.

Based on the analytical values, the lake can be divided into two layers. The upper one has oxidising conditions and is dominated by sulfates and carbonates of calcium and sodium, with a slight basic pH. The water in the lower layer has a similar composition, with an increased amount of $Ca^{2+}$, $SO_4^{2-}$ and $CO_3^{2-}$ (and also manganese and nickel), and it is under reducing conditions and nearly neutral pH. There is a very

interesting phenomenon connected to it occurring twice a year on average. The colour of the upper layer changes drastically and fast to red, combined with an increased colloid content, probably iron oxides hydroxides. The situation is stable only for some days, then the original state of the lake system recovers. The reason for this sudden system changes are not known yet.

There have been extensive analytical campaigns starting as early as in 1965, with enforced activities after 1992. Most of their results are reported in Sundblad *et al.*, 1995, which also contains the data sets related to the Lake Tranebärssjön. These data are based on measurements of water samples taken from the lake at depths of 0.5 and 14 metres. River water samples from four points along the river Pösan, before and after the confluence with the outlet of the lake, were also collected and analysed. In addition, ten groundwater monitoring pipes are in operation. The analytics were performed independently in parallel by two laboratories. The monitoring campaign is continued until present, results from 1996 were available as spreadsheet files. Available primary (measured) data sets include:

- time series and annual averages for pH, T, conductivity and a number of anion and cation concentrations for the two lake water sampling points and the groundwater pipes;
- metal, sulfur and silica concentrations for pore water from the sediment of the lake;
- precipitation and temperature curves (1995 and longtime annual mean);
- annual curve of water discharge at various stations (surface, lake and ground water);
- annual curve of contents of sulfate, iron, nickel, cadmium, aluminium, manganese, magnesium, calcium, and uranium at various stations (surface, lake and ground water).

Based on these data sets, other values were computed, such as the amount of transported metals per year. The analytical values relevant for the afore mentioned aquatic compartments were taken from this data pool, supplemented by some additional material from Studsvik. Furthermore, in August 1996, new samples were taken by Studsvik as part of the RESTRAT project to close gaps in the previous investigations, and to verify the accuracy of those measurements. The pH was determined in-situ, then the new samples were shipped to and analysed at the FZ Rossendorf. All results, together with the results from the previous sampling campaigns, were checked for consistency. These values exhibit several general features:

- lack of data for several important anions in case of the pore water samples;
- unusually high values for iron and manganese, exceeding the saturation limit for many minerals of these elements;
- missing details about the sampling, conditioning, filtering and analytical procedures applied in the analysis from the Swedish contractors of Studsvik;
- ionic strengths higher then usually found in fresh water lakes, in a range between 0.03 and 0.05;
- well buffered pH values in the neutral range between 6.75 and 7.87.

To overcome at least some of the limitations and inconsistencies of the primary analytical data set, chemical speciation modelling with EQ3/6 (for details see next section) was applied to each of the aquatic system compartments. The thus obtained information was merged with the analytical findings, finally leading to the recommended best set of physico-chemical data as shown in Table 22. Superscript [1)] identifies values set as approximations based on general chemical considerations as explained above, whereas [2)] mark values set according to the modelling results when there is no experimental information available at the moment. Average values (Mean) and standard deviations (STD) were calculated assigning equal weights to all listed values. There are no values given for Cadmium, Arsenic, Thorium, Mercury, Chromium, Copper, and Cobalt, because the available data is either too widely scattered, or there are hardly measurements of those values above their respective detection limits.

Table 22: Selected best set of analytical values for the Lake Tranebärssjön compartments, all concentrations are in mol / L.

| **Compartment:** | **Lake: Top Layer** | | **Lake: Bottom Layer** | | **Backfill** | **Alum shale** | |
|---|---|---|---|---|---|---|---|
| **Abbreviation:** | **T** | | **B** | | **F** | **A** | |
| Component: | Mean | STD | Mean | STD | Mean | Mean | STD |
| F- | 2.874E-05 | 3.16E-05 | 3.195E-05 | 7.84E-06 | | | |
| PO43- | 3.791E-07 | 2.42E-07 | 4.422E-07 | 2.00E-07 | | | |
| NO3- | 8.816E-05 | 5.13E-05 | 5.806E-05 | 1.82E-05 | | | |
| NO2- | 2.174E-07 | 1.74E-07 | 1.304E-07 | 2.17E-07 | | | |
| NH4+ | | | 7.373E-06 | 2.88E-06 | | | |
| SO42- | 7.816E-03 | 7.44E-04 | 1.172E-02 | 1.25E-03 | 8.702E-03 | 1.517E-02 | 6.43E-05 |
| HCO3- | 2.991E-03 | 4.06E-04 | 5.203E-03 | 1.33E-03 | 4.55E-03 [2)] | 7.35E-03 [2)] | |
| Cl- | 3.582E-04 | 2.69E-05 | 3.648E-04 | 1.39E-05 | | | |
| Si | 8.771E-05 | 1.74E-05 | 1.656E-04 | 3.48E-05 | 1.673E-04 | 2.705E-04 | 6.60E-05 |
| K+ | 1.375E-04 | 1.28E-05 | 1.495E-04 | 2.35E-05 | 1.614E-04 | 2.654E-04 | 5.27E-06 |
| Na+ | 3.318E-04 | 1.42E-05 | 3.749E-04 | 4.57E-05 | 3.480E-04 | 5.459E-04 | 2.29E-05 |
| Ca2+ | 8.664E-03 | 8.29E-04 | 1.375E-02 | 1.49E-03 | 9.556E-03 | 1.455E-02 | 4.95E-04 |
| Mg2+ | 8.146E-04 | 8.84E-05 | 1.228E-03 | 2.86E-04 | 7.447E-04 | 1.469E-03 | 7.10E-05 |
| Fe | 1.934E-05 | 7.59E-06 | 3.612E-04 | 5.07E-04 | 4.297E-07 | 1.413E-03 | 5.22E-04 |
| Al3+ | 4.651E-07 | 3.90E-07 | 4.948E-07 | 3.49E-07 | 2.413E-07 | 3.244E-07 | 5.34E-08 |
| Zn2+ | 4.351E-07 | 5.16E-07 | 1.835E-07 | 1.86E-07 | 2.768E-07 | 4.971E-07 | 1.57E-07 |
| U | 5.560E-07 | 3.26E-08 | 1.039E-06 | 2.39E-08 | 7.016E-07 | 1.158E-06 | 1.01E-06 |
| Pb2+ | 4.344E-09 | 9.65E-10 | 6.757E-09 | 3.38E-09 | | | |
| Sr2+ | | | | | 8.411E-06 | 1.481E-05 | 6.35E-07 |
| Ni2+ | 7.058E-07 | 5.22E-07 | 2.834E-06 | 1.12E-06 | 2.385E-07 | 9.455E-07 | 3.39E-07 |
| Mn2+ | 9.338E-06 | 1.53E-05 | 1.141E-04 | 5.68E-05 | 2.803E-07 | 1.552E-04 | 7.77E-06 |
| Cd2+ | 3.558E-09 | 4.45E-09 | 8.896E-09 | 1.69E-08 | | | |
| As | 4.538E-08 | 5.20E-08 | 8.809E-08 | 1.09E-07 | | | |
| Th | 2.155E-09 | 1.22E-09 | 2.370E-09 | 1.52E-09 | | | |
| pH | 7.87 | 0.14 | 6.75 | 0.06 | 7.05 [2)] | 6.84 [2)] | 0.20 [2)] |
| Eh / mV | 800 [2)] | 50 | 200 [2)] | 200 | 800 [2)] | 200 [2)] | 200 |
| O2(aq) | 6.28E-04 | 1.29E-04 | 3.75E-06 | 5.63E-06 | | | |
| T / °C | 8.00 | 7.60 | 7.60 | 0.50 | 7.0 [1)] | 7.0 [1)] | |

The characterization of the relevant solid phases is not as satisfactory as compared to the aqueous phase. There are only rather general mineralogical investigations for this site published, mainly considering the alum shale. Analysis is complicated by a considerable content of organic matter of various origin and in different state of degradation. From the available data and speciation modelling based on them, the following conclusions can be drawn:

- The backfill consists of a ill-defined and varying mixture of alum shale debris, Limestone, and moraine constituents (Quartz and weathered alumosilicates such as Illite or Kaolinite).
- The alum shale composition was taken from Anderson *et al.*, 1985, on average it consists of Quartz (20 %), Illite (30 %), K-Feldspar (10 %), Chlorite (5 %), Pyrite (13 %), and Organics (22 %).
- The sediment at the bottom of the lake was analysed only with regard to the various elements, no mineralogical data could be drawn from that.

### 3.5.3. Chemical Speciation Modelling

All the following considerations will focus on Uranium as the most critical contaminant. Manganese and Nickel are also present at elevated levels that may harm humans. However, at present there is no unified approach available to assess simultaneously the health effects stemming from radioactive and non-radioactive contaminants, hence Manganese and Nickel will not be dealt with in the integrated risk assessment. There general speciation patterns are rather simple and have been already investigated thoroughly in the section about the Ranstad Tailing Site.

Before going into more detail for the four relevant aqueous phase compartments, table 23 gives the equilibrium speciation of uranium as modelled with EQ3NR. In all cases, the neutral complex $Ca_2UO_2(CO_3)_3$ binds the majority of the total available uranium.

Table 23: Species distribution for Uranium at the Lake Tranebärssjön (in % of total U), computed with EQ3NR.

| Species | Upper Lake | Lower Lake | Backfill | Alum Shale |
|---|---|---|---|---|
| $Ca_2UO_2(CO_3)_3(aq)$ | 96.8 % | 95.3 % | 94.8 % | 94.9 % |
| $UO_2(CO_3)_3^{4-}$ | 2.6 % | 2.2 % | 2.4 % | 2.6 % |
| $UO_2(CO_3)_2^{2-}$ | - | 2.4 % | 2.7 % | 2.4 % |

In the upper layer of the lake, the content of oxygen is large enough to transfer most of the element into their higher valency states, only manganese will stay at the $Mn^{2+}$ two-valent level. The measured oxygen content corresponds to a redox potential of +787 mV. The charge imbalance is small and well within the analytical uncertainty for the major components sulfate or calcium. The water is slightly oversaturated with respect to the mineral Calcite and has an ionic strength of 0.03 mol/L. The silica content seems to be determined by equilibrium with Quartz. In general, the available data set for this compartment is the one with the highest reliability and internal consistency. The only problem here is the inherent large fluctuations of the temperature, moving between a winter minimum of 0.3 °C and a summer maximum of 22.5 °C. The species distributions shown in Fig. 31 all relate to EQ3NR modellings with sulfate used for charge balancing. The system is redox indifferent towards uranium, only for the very unlikely situation of redox potentials below -100 mV $U^{VI}$ will be transformed into $U^{IV}$. The speciation dependence on pH and carbonate concentration is much more pronounced. The original system has a pH of 7.87 and a carbonate content corresponding to a $CO_2$ partial pressure of about $1.63 \cdot 10^{-3}$ bar ($\log p_{CO2} = -2.79$), i.e. five times the usual atmospheric value. Inside the experimental uncertainty ranges of these values the neutral complex $Ca_2UO_2(CO_3)_2$ will always dominate, however.

The lower layer of the lake exhibits a more complex chemistry and strongly reducing properties. Reasons may be the very slow mixing of the lake water, severely limiting the oxygen transport from the lake surface to its deeper parts, combined with various oxygen-consuming processes such as the oxidation of sulfide components of the alum shale or organic material sinking down to the bottom of the lake. In irregular time distances the chemistry of the lake shifts dramatically, with enormous amounts of iron (and probably manganese) particles moving upwards to the top layers of the lake, partly settling on its shores. All these phenomena make it complicated to assign a unique set of chemical parameter to this compartment. The momentary best approximations at hand is assuming a redox potential Eh between -190 mV, the transition zone from sulfide to sulfate, and +320 mV, the transition zone from $Fe^{2+}$ to $Fe^{3+}$. Eh will not be lower than

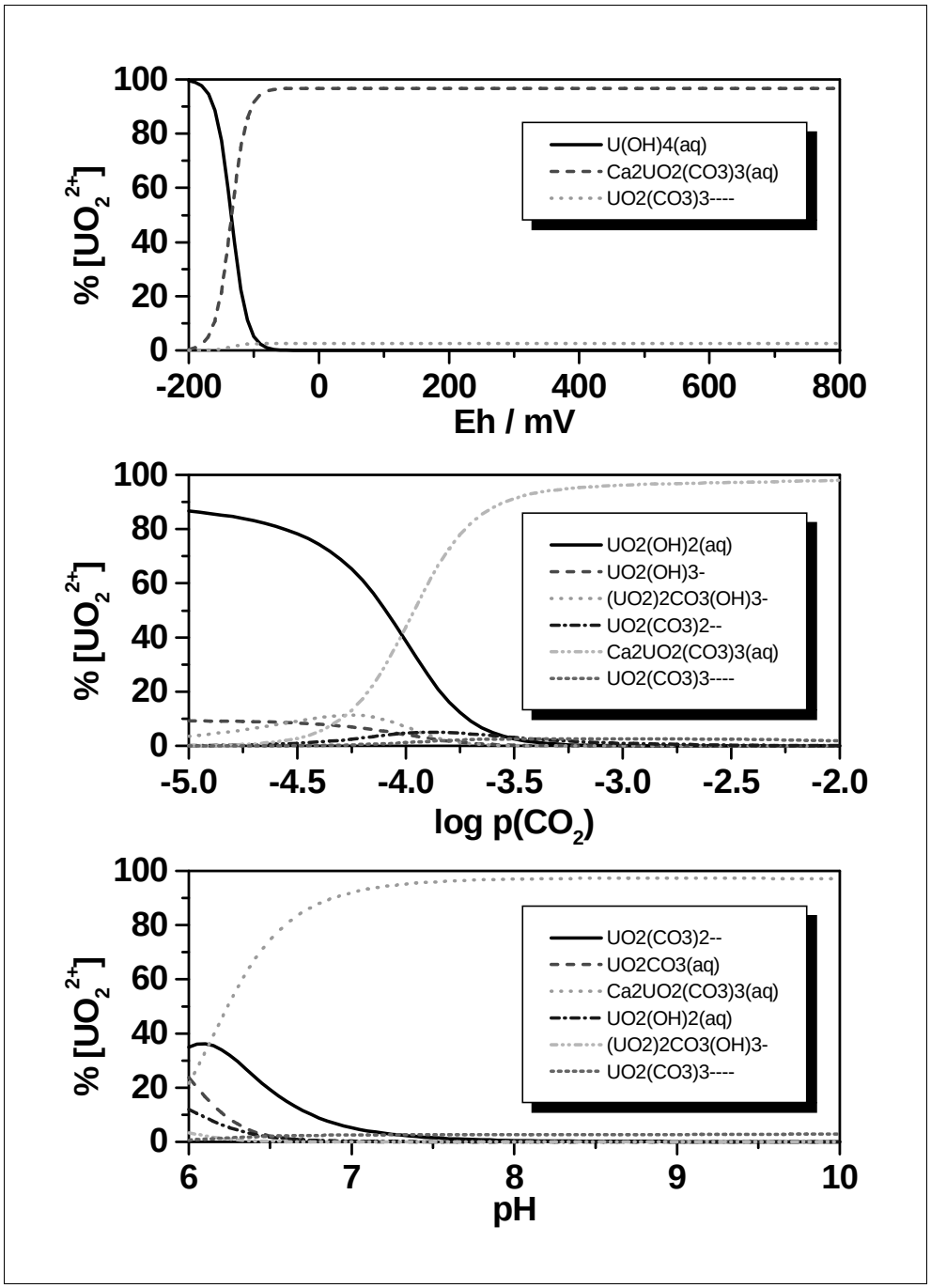


**Figure 31**: Uranium speciation as function of Eh, pH and $p_{CO2}$ for the upper water layers of Lake Tranebärssjön

-190 mV because most of the sulfides in the alum shale at the ground were already at least partly exposed to oxygen before the lake was filled, so oxidation could start. On the other hand the immense amount of iron dissolved in the waters can only be stable in the two-valent state, $Fe^{III}$ would precipitate as hydrous ferric oxides with a slow transformation to more stable products such as Haematite or Goethite. Unfortunately, the transition from $U^{4+}$ to $UO_2^{2+}$ at around -90 mV falls right into this proposed Eh range. For all

following modellings, thus, two scenarios must be considered for the contaminant uranium, one at an Eh of around -150 mV, and another at an Eh of around +150 mV. In the case of strongly reducing conditions, the speciation pattern is very simple, with $U(OH)_4$ making up nearly 100 % of all available uranium at all sensible values for pH (field value: 6.75) and the carbonate content (field value: $5.2 \cdot 10^{-3}$ mol/L). For the scenario with Eh = +150 mV, the carbonate content again is not really influencing the uranium speciation (dominated by $Ca_2UO_2(CO_3)_2$), but a decreasing pH may drastically change that pattern with the occurrence of pure uranyl carbonates. For details see Fig. 32. The modelling indicate, that silica and carbonate

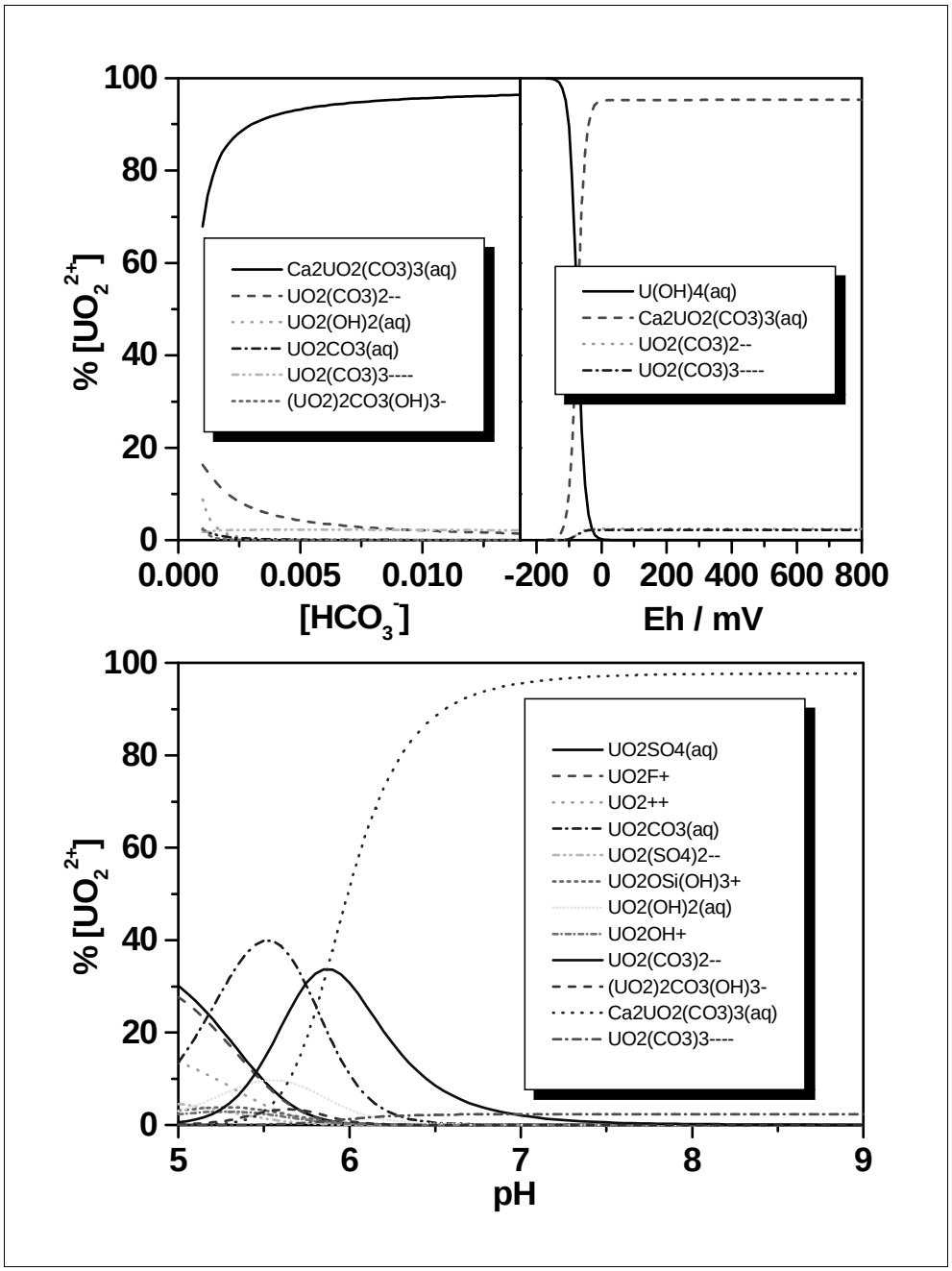


**Figure 32**: Uranium speciation as function of Eh, pH and carbonate concentration for the lower water layers of Lake Tranebärssjön

may be in equilibrium with Quartz and Calcite, respectively. The ionic strength of the water is with 0.046 mol/L substantially higher than in the upper layers of the lake. The charge imbalance derived from the

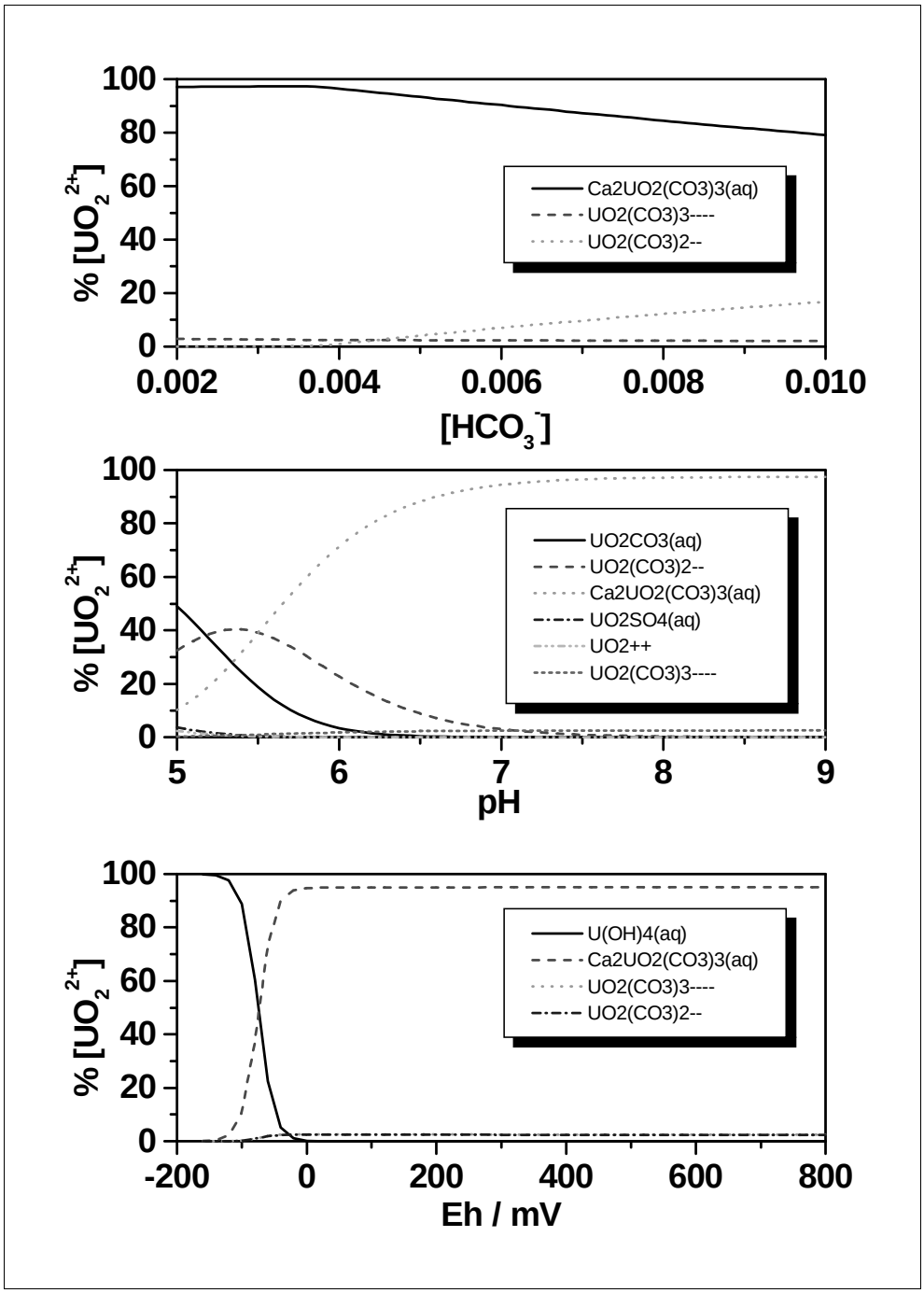


**Figure 33**: Uranium speciation as function of carbonate concentration (top) and pH (middle) for pore water from the backfill and as function of Eh (bottom) for pore water from the alum shale of Lake Tranebärssjön

measured concentrations is larger than the analytical uncertainty, implying partly incomplete or erroneous data.

Compared to the lake water data sets, the pore water analysis of both the backfill and the alum shale lacks data for all anions other than sulfate. Another gap is the pH, which was not determined. Nevertheless the situation is not hopeless. A comparison of the ionic water composition shows close relationships between the upper lake layer and the pore water from the backfill. The same is true for the lower lake layer and the pore water from the alum shale. This leads to the approximation that, besides sulfate, carbonate is the only other important anion. This is supported by the presence of Calcite as a major component of both the backfill and the alum shale. Finally, due to the composition of the alum shale, a reducing environment must be expected for the water in there. The water in the backfill will be considerably more oxidized. Based on these approximations and the available analytical information, modellings with EQ3/6 indeed gave reasonable values for the total carbonate concentrations in the backfill and alum shale pore waters of $4.6 \cdot 10^{-3}$ M (total ionic strength of 0.0325 M) and $7.4 \cdot 10^{-3}$ M (total ionic strength of 0.052 M), respectively. Moreover, the pH was computed from the charge balance to be 7.04 and 6.83, respectively, again values that fall well into the expected range. And the uranium speciation pattern is rather unsensitive with respect to these values, as demonstrated in the upper part of Fig. 33. Finally, the analytical results for Silica gave in the speciation modelling saturation indices of Quartz very close to one, so this mineral may be in equilibrium with silica content of the pore waters. The temperature of the pore water should be rather constant throughout the year and similar to the value measured for the lower layer of the lake, thus it was set to 7.0 °C. Whereas pH is a critical factor for the uranium speciation in the backfill, Eh may strongly influence the respective speciation in the alum shale due to possible very low redox potentials. Both aspects are dealt with in the middle and lower part of Fig. 33.

### 3.5.4. $K_d$ Computations for the Basic Scenario

*Chemical data set*

The chemical data comprises of the contaminant uranium plus all components with concentrations larger than $1 \cdot 10^{-5}$ mol/L. An exceptions is the omission of nitrate that does not interact significantly with uranium. Silica and alumina (only relevant for the pore water solutions) are assumed to be in equilibrium with Quartz and Kaolinite, respectively, as derived from mineralogical data and the chemical speciation modelling. The concentrations, as well as values for pH and Eh, are those listed in Table 22. When there is no uncertainty given, a default value of 20 % is assigned. The formation of the following minerals is suppressed due to kinetic considerations: Pyrophyllite, Diaspore, Leonhardite, Dolomite, Talc, and Tremolite. For the backfill and alum shale compartments, pH and the carbonate concentration are coupled through a 0.6 correlation to account for their mutual dependence based on the Calcite dissolution / precipitation equilibria!

*Surface properties*

As for all the other example sites, 5 % of each solid concentration is assigned to the complexing phase HFO, with the exception of the suspended material in the lower part of the lake, which has a much higher iron content, approximated by 50 % HFO. The solid concentrations for the three tailing layers were computed according to Eqn. 1. Densities are calculated from Table 3 based on the approximated solid phase composition for the Backfill and the Alum shale, yielding approximately 2.4 g/cm$^3$ for both. The respective porosities are 0.3 and 0.1, which eventually translates into sorbate concentrations $C_S$ of 280 g / L and 1080 g / L. In case of the two lake water layers, experimental values for the total suspended solid

concentration are available: 2.9 mg / L for the upper part and 59 mg / L for the lower part of the lake. All the resulting binding site concentrations (for both strong and weak binding sites) can be extracted from Appendix E.

*Results*

The computed distribution coefficients are shown in Fig. 34 for all compartments, for a detailed graph explanation see the respective statements for the Drigg Site (section 3.1.4).

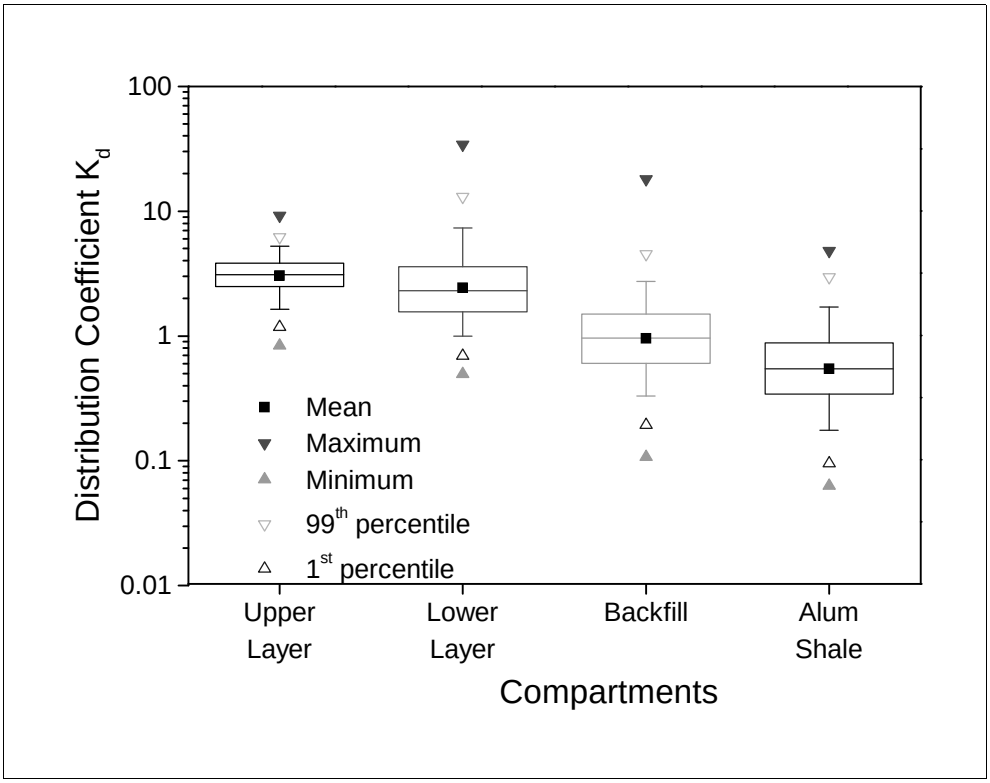


**Figure 34**: Computed $K_d$ values and their error distributions for the Lake Tranebärssjön

Table 24 summarized all results and compares them with the default value used so far in the risk assessment modelling. As with the other example sites, also for the Lake Tranebärssjön the distribution coefficients show a lognormal distribution. The default values used before were characterized by a logtrigonal error function. The distribution coefficients specific to the two aqueous compartments fall well inside the range of the generic values, whereas for the pore water compartments the site-specific $K_d$ values are larger than the generic ones.

Table 24: Comparison of computed and conventional distribution coefficients for Uranium in the Lake Tranebärssjön compartments

| **$K_d$ in $m^3$ / kg** | **Computed** | | | | **Default** | | |
|---|---|---|---|---|---|---|---|
| **Compart-ment:** | *log $K_d \pm \sigma$* | *Geometric Mean* | *$5^{th}$ Percentile* | *$95^{th}$ Percentile* | *Mean* | *Lower Limit* | *Upper Limit* |
| Upper Lake | 0.48 ± 0.15 | 3.01 | 1.62 | 5.16 | 2 | 0.2 | 20 |
| Lower Lake | 0.38 ± 0.27 | 2.4 | 0.98 | 7.3 | | | |
| Backfill | -0.02 ± 0.29 | 0.944 | 0.326 | 2.714 | 0.015 | 0.01 | 0.1 |
| Alum Shale | -0.27 ± 0.30 | 0.538 | 0.172 | 1.678 | | | |

Finally, table 25 identifies those physico-chemical parameters influencing the $K_d$ distribution strongest. Contrary to nearly all the other cases involving Uranium as a contaminant (for the Drigg Site and the Ranstad Tailing), here pH is not the dominating impact factor for the overall $K_d$ uncertainty. With the exception of the lower lake water layer, the $K_d$ is most sensitive to changes in the carbonate content instead. Also the solid concentration has an important influence.

Table 25: Parameters responsible for the uncertainty of computed Uranium distribution coefficients for the Lake Tranebärssjön

| **Compartment:** | **$1^{st}$ Factor** | **$R^2$ Improvement** | **$2^{nd}$ Factor** | **$R^2$ Improvement** |
|---|---|---|---|---|
| Upper Lake | C(solid) | 36.8 % | pH | 34.6 % |
| Lower Lake | $C(HCO_3^-)$ | 84.9 % | C(solid) | 11.1 % |
| Backfill | $C(HCO_3^-)$ | 78.3 % | C(solid) | 9.3 % |
| Alum Shale | $C(HCO_3^-)$ | 79.7 % | pH | 8.8 % |

## 4. Conclusions

Most of the calculated distribution coefficients ($K_d$ values in $m^3/kg$) for uranium, americium, plutonium and cobalt fall well into the range used so far for modelling of these sites, see e.g. in Puigdomenech and Bergström 1994, but exhibit much smaller uncertainties. Where there were significant deviations, they could always be attributed to site-specific conditions. It should be noted, that all $K_d$ values exhibit a log-normal distribution.

The following contaminant-specific conclusions can be drawn:
- $K_d$ values for uranium are especially sensitive towards uncertainties in pH and carbonate content, controlling the amount of hydrolysis species and carbonate complexes that reduce the sorbed portion of uranium;
- $K_d$ values for americium are very small for highly mineralized waters;
- plutonium sorption is best described assuming hexavalent plutonyl ions.

These first results for the example sites prove the applicability of the concept of substitution of empirical $K_d$ values by a theory-based sorption and speciation model. The software implementation is now tested and documented. From the currently available results, several general conclusions can be drawn:
- in many cases the solid concentration $C_{solid}$ is a major impact factor for the distribution coefficient modelling, in case of porous aquifers mainly reflecting the uncertainty of the rock porosity and lacking knowledge about that portion of rock which is not accessible to sorption processes inside the various layers;
- the thermodynamic database situation is far from being satisfactory, especially for redox reactions;
- the sorption data for actinides at lower oxidation states is very sparse and of questionable quality;
- the collection of analytical data for the solid phases, i.e. mineralogical characterization of rocks, sediments, and suspended solids, deserves more attention.

In order to better account for the mineralogical inhomogeneity of natural solids (rocks and minerals) the sorption model should be expanded to several instead of just one mineral surface per compartment. To further speed up computation times it seems worthwhile to change the present external call of the speciation code to a fully incorporated subroutine inside PRISM / BIOPATH.

As it turned out from at least two of the five examples sites, and as is demonstrated in the site classification chapter of the RESTRAT Manual (RESTRAT TD 14, Zeevaert *et al.*, 1999), many real-world contaminations are in fact a mixture of radionuclides with chemical-toxic contaminants, such as heavy metals, arsenic or organic compounds. Thus the effects of such mixed contaminations need to be modelled, too.

The approach towards a better incorporation of physico-chemical phenomena governing the source term at contaminated sites must be further elaborated by inclusion of other aspects that may be important at certain sites. Here, the addition of interactions between contaminants, solids and humics to the integrated model is the most obvious case. Another topic to be included in future versions of the integrated risk assessment would be the co-precipitation of contaminants with “bulk” mineral phase precipitation.

Theoretical considerations, models and appropriate software are only one side of the metal, the other side is a high-quality database. In case of site-specific parameters this mainly targets at improvements in sampling and the treatment before and during analytical procedures. Recommendations with regard to such methods are given in the RESTRAT TD 2 [Brendler, 1999], but this must be handled by the investigators of a certain site specifically. However, when it comes to reaction-specific data, the urgently required

improvements in quantity and quality of appropriate thermodynamic and kinetic databases, a coordinated European action would give greatest benefits.

## 5. References

Allison JD, Brown DS and Novo-Gradac KJ (1991). MINTEQA2/PRODEFA2 Version 3.0 user's manual. U.S. EPA, Environmental Research Laboratory, EPA/600/3-91/021

Altmann R, Brandis G, Regen O and Schneider J (1984). Chemisch-technische Stoffwerte - eine Datensammlung. VEB Deutscher Verlag für Grundstoffindustrie, Leipzig

Anderson A, Dahlman B, Gee DG and Snäll S (1985). The Scandinavian Alum Shales. Sveriges Geologiska Undersökning, Uppsala

Ball JW, Jenne EA and Cantrell MW (1981). WATEQ3: A geochemical model with uranium added. U.S. Geological Survey Open File Report 81-1183, Washington, DC

Baston GMN, Berry JA, Brownsword M, Heath TG, Tweed CJ and Williams SJ (1995). Sorption of Plutonium and Americium on repository, backfill and geological materials relevant to the JNFL low-level radioactive waste repository at Rokkasho-Mura. Mat.Res.Soc.Symp.Proc. 353:957-964

Bergström U, Edlund O, Evans S and Röjder B (1982). BIOPATH - A computer code for calculation of the turnover of nuclides in the biosphere and the resulting doses to man. Report, Studsvik Energiteknik AB, Studsvik/NW-82/261, Nyköping

Bernhard G, Geipel G, Brendler V and Nitsche H (1996). Speciation of uranium in seepage waters from a mine tailing pile studied by time-resolved laser-induced fluorescence spectroscopy (TRLFS). Radiochimica Acta 74:87-91

Bond KA, Cross JE and Ewart FT (1990). Thermodynamic modelling of uranium(VI) sorption onto London clay. Nirex Safety Studies NSS/R207, UKAEA, Harwell

Bond KA, Moreton AD and Heath TG (1992). The HATCHES User Manual, UKAEA, Harwell

Bond KA, Ilett DJ and Tweed CJ (1996). HATCHES database, NEA Release 9 (28th November 1996), UKAEA, Harwell

Bousher A (1999a). Drigg Site: Basic characteristics and evaluation of restoration options. RESTRAT Technical Deliverable TD 9, Report Westlakes Scientific Consulting, Cumbria, UK

Bousher A (1999b). Ravenglass Estuary: Basic characteristics and evaluation of restoration options. RESTRAT Technical Deliverable TD 12, Report Westlakes Scientific Consulting, Cumbria, UK

Brendler V (1999). Physico-chemical phenomena governing the behaviour of radioactive substances. State-of-the-art description. RESTRAT TD 2, Issue 3, Rossendorf / Dresden

Brendler V, Stiglund Y and Nordlinder S (1999). Risk assessment model for use in site restoration. Software and user instructions. RESTRAT TD 7, Issue 1, Rossendorf / Dresden

Cornell RM and Schwertmann U (1996). The Iron Oxides. Structure, Properties, reactions, Occurence and Uses. VCH, Weinheim

Cremers A and Maes A (1985). Radionuclide partitioning in environmental systems: A critical analysis. In: Sibley TH and Myttenaere C (eds.). Application of distribution coefficients to radiological assessment models. Elsevier Applied Science, London

Cross JE and Ewart FT (1991). HATCHES - a thermodynamic database and management system. Radiochim.Acta 52/53:421-422

Davis JA, James RO and Leckie JO (1978). Surface Ionization and Complexation at the Oxide/Water Interface 1. Computation of Electrical Double Layer Properties in Simple Electrolytes. Journal of Colloid and Interface Science 63:481-499

Davis JA and Kent DB (1990). Surface complexation modelling in aqueous geochemistry. In: Hochella MF and White AF (eds.): Reviews in Mineralogy 23:177-260

Davis JA and Leckie JO (1978). Surface Ionization and Complexation at the Oxide/Water Interface II. Surface properties of Amorphous Iron Oxyhydroxide and Adsorption of Metal Ions. Journal of Colloid and Interface Science 67:90-107

Davis JA and Leckie JO (1980). Surface Ionization and Complexation at the Oxide/Water Interface 3. Adsorption of Anions. Journal of Colloid and Interface Science 74:32-43

Dicke C and Smith RW (1996). Surface Complexation Modelling of Uranium Adsorption on Naturally Occurring Iron Coated Sediments. Presentation given at the American Chemical Society Annual Meeting in New Orleans on March 28, 1996

Dickson RR and Boelens RGV (1988). The status of current knowledge on anthropogenic influences in the Irish Sea. International Council for the Exploration of Sea, Cooperative Research Report 155

Dzombak DA and Morel FMM (1990). Surface complexation modeling. Hydrous ferric oxide, Wiley, New York

Falck WE, Read D and Thomas JB (1996). Chemval 2: thermodynamic database, EU Report EUR 16897 EN, Luxembourg

Gardner RH, Röjder B and Bergström U (1983). PRISM - A systematic method for determining the effect of parameter uncertainties on model predictions. Report, Studsvik Energiteknik AB, Studsvik/NW-83/555, Nyköping

Geipel G, Brachmann A, Brendler V, Bernhard G and Nitsche H (1997). Uranium(VI) sulfate complexation studied by time-resolved laser-induced fluorescence spectroscopy (TRLFS). Radiochimica Acta, 75:199-204

Goldberg S (1991). Sensitivity of Surface Complexation Modeling to the Surface Site Density Parameter. Journal of Colloid and Interface Science 145:1-9

Grenthe I, Fuger J, Lemire RJ, Muller AB, Nguyen-Trung C and Wanner H (1992). Chemical Thermodynamics of Uranium, Elsevier, Amsterdam

Gunneriusson L and Sjöberg S (1993). Surface Complexation in the $H^+$ - Goethite (α-FeOOH) - Hg(II) - Chloride System. Journal of Colloid and Interface Science 156:121-128

Hayes KF and Leckie JO (1987). Modeling Ionic Strength Effects on Cation Adsorption at Hydrous Oxide/Solution Interfaces. Journal of Colloid and Interface Science 115:564-572

Hayes KF, Redden G, Ela W and Leckie JO (1990). Application of Surface Complexation Models for Radionuclide Adsorption - Sensitivity Analysis of Model Input Parameters. NUREG/CR-5547, PNL-7239

Higgo JJW (1987). Radionuclide interactions with marine sediments. NIREX Safety Studies Report NSS/R142, London

Higgo JJW (1988). Review of sorption data applicable to the geological environments of interest for the deep disposal of ILW and Llw in the UK. NIREX Safety Studies Report NSS/R162, London

Hsi CD and Langmuir D (1985). Adsorption of uranyl onto ferric oxyhydroxides: Application of the surface complexation site-binding model. Geochimica et Cosmochimica Acta 49:1931-1941

Hsu PH (1989). Aluminium hydroxides and oxyhydroxides. In: Dixon JB and Weed SB (eds.). Minerals in Soil Environments, 2nd ed. Soil Science Society of America, Madison, Wisc.

Hummel W (1991). Thermodynamic data base for organic ligands, PSI Internal report TM-41-91-43

Kelly M and Emptage M (1992). Distribution of radioactivity in the Esk estuary and its relationship to sedimentary processes. DoE Report No. DoE/HMIP/RR/92/015, UK DoE, London.

Ludwig C and Schindler PW (1995). Surface Complexation on $TiO_2$ I. Adsorption of $H^+$ and $Cu^{2+}$ Ions onto $TiO_2$ (Anastase). Journal of Colloid and Interface Science 169:284-290

Lumsdon DG and Evans LJ (1994). Surface Complexation Model Parameters for Goethite (α-FeOOH). Journal of Colloid and Interface Science 164:119-125

Olin M and Lehikoinen J (1997). Application of surface complexation modelling: Nickel sorption on quartz, manganese oxide, kaolinite and goethite, and thorium on silica. Posiva report 97-10

Östhols E (1995). Thorium Sorption on amorphous silica. Geochimica et Cosmochimica Acta 59:1235-1249

Pearson FJ (1994). NAGRA Chemical Thermodynamic Database: Redox coupled versions for EQ3/EQ6 and PHREEQE, NAGRA Internal report 94-66, Wettingen

Pearson FJ and Berner U (1991). NAGRA Thermochemical Data Base. I. Core Data, NAGRA Technical report 91-17, Wettingen

Puukko E and Hakanen M (1997). Surface complexation modelling: experiments on the sorption of nickel on quartz, kaolinite and goethite, and preliminary results on sorption of thorium on quartz. Posiva report 97-06, Helsinki

Pearson FJ, Berner U and Hummel W (1991). NAGRA Thermochemical Data Base. II. Supplemental Data 05/92, NAGRA Technical report 91-18, Wettingen

Persson P and Lövgren L (1996). Potentiometric and spectroscopic studies of sulfate complexation at the goethite-water interface. Geochimica et Cosmochimica Acta 60:2789-2799

Puigdomenech I and Bergström U (1994). SKB Technical Report 94-32, Stockholm

Schwertmann U and Cornell RM (1991). Iron oxides in the laboratory. Preparation and characterization. VCH, Weinheim

Silva RJ, Bidoglio G, Rand MH, Robouch PB, Wanner H and Puigdomenech I (1995). Chemical Thermodynamics of Americium, Elsevier, Amsterdam

Smith RM, Martell AE and Motekaitis RJ (1997). NIST Critically Selected Stability Constants of Metal Complexes Database, Version 4.0, NIST Standard Reference Database 46, Gaithersburgh

Smith GM, Fearn HS, Smith KR, Davis JP and Klos R (1988). Assessment of the radiological impact of disposal of solid radioactive waste at Drigg. National Radiological Protection Board, NRPB-M148, Oxon.

Sposito G (1983). On the Surface Complexation Model of the Oxide-Aqueous Solution Interface. Journal of Colloid and Interface Science 91:329-340

Sposito G (1989). Surface Reactions in Natural Aqueous Colloidal Systems (1989) Chimia 43:169-176

Stiglund Y (1999a). Ranstad Tailing Site: Basic Characteristics and Evaluation of Restoration Options. RESTRAT TD 10, Report Studsvik Eco & Safety AB, Nyköping

Stiglund Y (1999b). Lake Tranebärssjön: Basic Characteristics and Evaluation of Restoration Options. RESTRAT TD 13, Report Studsvik Eco & Safety AB, Nyköping

Strübel G and Zimmer SH (1991). Lexikon der Minerale, 2nd ed., Ferdinand Enke Verlag, Stuttgart

Sundblad B, Stiglund Y, Mathiasson L and Odenstedt S (1996). Efterbehandling Ranstad - Utsläpps- och recipientkontroll 1995. Report Studsvik Eco & Safety AB, Studsvik/ES-96/23, Nyköping

Sweeck L and Zeevaert T (1999). Molse Nete river: Basic characteristics and evaluation of restoration options. RESTRAT Technical Deliverable TD 11, Report SCK-CEN, Mol, Belgium

van Cappellen P, Charlet L, Stumm W and Wersin P (1993). A surface complexation model of the carbonate mineral mineral-aqueous solution interface. Geochimica et Cosmochimica Acta 57:3505-3518

van Geen A, Robertson AP and Leckie JO (1994). Complexation of carbonate species at the goethite surface: Implications for adsorption of metal ions in natural waters. Geochimica et Cosmochimica Acta 58:2073-2086

Waite TD, Davis JA, Payne TE, Waychunas GA and Xu N (1994). Uranium(VI) adsorption to ferrihydrite: Application of a surface complexation model. Geochimica et Cosmochimica Acta 58:5465-5478

Wolery TJ (1992). EQ3/6 Manual, UCRL-MA-110662 Part I, Lawrence Livermore National Laboratory

Wolery TJ (1995). EQ3/6, a software package for geochemical modeling, Version 2b, Software distribution, LLNB, Livermore

Wu L, Forsling W and Schindler PW (1991). Surface complexation of calcium minerals in aqueous solution. Journal of Colloid and Interface Science 147:178-185

Zeevaert T, Jensen PH, Brendler V, Nordlinder S and Bousher A (1999). Manual on restoration strategies for radioactive-contaminated sites. RESTRAT Technical Deliverable TD 14, Report SCK-CEN, Mol, Belgium

Zhang Q, Xu Z and Finch JA (1995a). Surface ionization and complexation at the sphalerite / water interface I. Computation of electrical double-layer properties of sphalerite in a simple electrolyte. Journal of Colloid and Interface Science 169:414-421

Zhang Q, Xu Z and Finch JA (1995b). Surface ionization and complexation at the sphalerite/water interface II. Computation of electrical double-layer properties of sphalerite in the presence of iron ions in a simple electrolyte. Journal of Colloid and Interface Science 175:61-67

Appendix A: Computation of distribution coefficients: Plutonium input parameter set for the Drigg Site.

```
Drigg Site (RESTRAT PROJECT)
fzr
V.Brendler
25.6.1999
2
TCELSIUS  0  c  7
PuO2+2
Drain
7
HFO_DDL.DBS
ADS1CONC  0  n  2.25E-03   2.00E-04
ADS1AREA  0  c  600
2
ADS1TYP1  0  c  1.215E-07
ADS1TYP2  0  c  5.063E-06
Eh        -1    n          0.417     0.2
pH        0  n  6.45       0.5
11
PuO2+2    0  n  2.00E-14   2.00E-15  2.00E-20
SO4-2     0  n  5.67E-04   3.12E-05
CO3-2     0  n  7.41E-03   2.00E-03
Cl-1         0  n          2.40E-03  1.69E-04
PO4-3     0  n  2.00E-06   4.20E-07
H4SiO4    19    QUARTZ
K+1          0  n          1.23E-04  2.56E-06
Na+1         0  n          2.36E-03  1.74E-05
Ca+2         0  n          1.85E-03  1.37E-04
Mg+2         0  n          5.51E-04  1.23E-05
Al+3         19             KAOLINITE
0
4
PYROPHYLLITE
DIASPORE
LEONHARDITE
HYDRAPATITE
CO3-2
Drigg Stream
7
HFO_DDL.DBS
ADS1CONC  0  n  1.56E-02   5.00E-03
ADS1AREA  0  c  600
2
ADS1TYP1  0  c  8.430E-07
ADS1TYP2  0  c  3.513E-05
Eh        -1    n          0.401     0.2
pH        0  n  6.80       0.53
11
PuO2+2    0  n  2.00E-14   2.00E-15  2.00E-20
SO4-2     0  n  4.02E-04   4.47E-05
CO3-2     0  n  2.87E-03   5.00E-04
Cl-1         0  n          1.63E-03  7.20E-05
PO4-3     0  n  1.26E-06   1.35E-06
H4SiO4    19    QUARTZ
K+1          0  n          2.11E-04  3.88E-05
Na+1         0  n          1.44E-03  1.71E-04
Ca+2         0  n          1.30E-03  1.98E-04
Mg+2         0  n          3.06E-04  6.90E-05
Al+3      19    KAOLINITE
0
4
PYROPHYLLITE
DIASPORE
LEONHARDITE
HYDRAPATITE
CO3-2
```

Appendix B: Computation of distribution coefficients: Uranium input parameter set for the Ranstad Tailing Site.

```
Ranstad Tailing Site (RESTRAT PROJECT)
fzr
V.Brendler
14.07.1999
4
TCELSIUS 0 c 9
UO2+2
Tailing Layer (Box 1)
7
HFO_DDL.DBS
ADS1CONC 0 n 327 65
ADS1AREA 0 c 600
2
ADS1TYP1 0 c 0.01764
ADS1TYP2 0 c 0.735
Eh -1 n 0.346 0.02
pH 0 n 7.46 0.15
12
UO2+2 0 n 1.004e-6 2.36e-7 1.0e-15
NO3-1 0 c 1.188e-4
SO4-2 0 n 2.248e-2 1.92e-3
CO3-2 0 n 3.584e-3 1.10e-3
Cl-1  0 n 5.639e-4 6.47e-5
H4SiO4 19 QUARTZ
K+1   0 n 1.175e-3 8.91e-5
Na+1  0 n 8.647e-4 4.44e-5
Ca+2 19 CALCITE
Mg+2  0 n 1.038e-2 3.33e-4
Al+3 19 MUSCOVITE
Mn+2  0 n 8.670e-5 2.98e-5
0
4
PYROPHYLLITE 1
LEONHARDITE 1
KAOLINITE 1
DIASPORE 1
SO4-2
Moraine Layer (Box 2)
7
HFO_DDL.DBS
ADS1CONC 0 n 532 110
ADS1AREA 0 c 600
2
ADS1TYP1 0 c 0.02873
ADS1TYP2 0 c 1.197
Eh -1 c 0.8
pH 0 n 6.93 0.2
12
UO2+2 0 c 5.128e-9 1.0e-15
NO3-1 0 c 1.097e-5
SO4-2 0 c 2.567e-4
CO3-2 0 c 3.715e-3
Cl-1  0 c 3.798e-4
H4SiO4 19 QUARTZ
K+1   0 n 3.363e-5 8.14e-6
Na+1  0 n 2.736e-4 9.66e-5
Ca+2 19 CALCITE
Mg+2  0 n 1.446e-4 3.46e-5
Al+3 19 MUSCOVITE
Mn+2  0 c 5.646e-6
0
4
DIASPORE 1
PYROPHYLLITE 1
LEONHARDITE 1
KAOLINITE 1
CO3-2
Limestone Layer (Box 3)
7
HFO_DDL.DBS
ADS1CONC 0 n 2.57e3 500
ADS1AREA 0 c 600
2
ADS1TYP1 0 c 0.139
ADS1TYP2 0 c 5.79
Eh -1 c 0.8
pH 0 n 7.85 0.12
11
UO2+2 0 n 4.887e-9 1.15e-9 1.0e-15
SO4-2 0 n 5.350e-4 7.29e-5
CO3-2 0 n 2.991e-3 5.79e-5
Cl-1  0 n 3.244e-4 1.99e-5
H4SiO4 19 QUARTZ
K+1   0 n 3.775e-5 9.18e-6
Na+1  0 n 2.913e-4 2.85e-5
Ca+2 19 CALCITE
Mg+2  0 n 2.092e-4 2.85e-5
Al+3 19 MUSCOVITE
Mn+2  0 n 7.077e-6 2.72e-6
0
5
PYROPHYLLITE 1
LEONHARDITE 1
KAOLINITE 1
HAUSMANNITE 1
DIASPORE 1
CO3-2
M-Lake (Box 4)
7
HFO_DDL.DBS
ADS1CONC 0 n 0.015 0.003
ADS1AREA 0 c 600
2
ADS1TYP1 0 c 8.70e-7
ADS1TYP2 0 c 3.38e-5
Eh -1 n 0.318 0.02
pH 0 n 7.8 0.2
12
UO2+2 0 n 3.033e-8 1.02e-9 1.0e-15
NO3-1 0 n 1.84e-5 7.42e-6
SO4-2 0 n 5.815e-3 5.65e-4
# CO3-2 21 n -3.5 1e-3
# CO3-2 0 n 1.593e-3 1.35e-4
CO3-2 19 CALCITE
Cl-1  0 n 2.191e-4 8.14e-6
H4SiO4 19 QUARTZ
K+1   0 n 3.954e-4 2.60e-5
Na+1  0 n 1.139e-3 4.27e-4
Ca+2  0 n 5.291e-3 5.65e-4
Mg+2  0 n 7.634e-4 6.75e-5
Al+3 19 MUSCOVITE
Mn+2  0 c 8.513e-6
0
4
PYROPHYLLITE 1
LEONHARDITE 1
KAOLINITE 1
DIASPORE 1
SO4-2
```

Appendix C: Computation of distribution coefficients: Cobalt input parameter set for the Molse Nete river.

```
Molse Nete river (RESTRAT PROJECT)
fzr
V.Brendler
23.6.1999
1
TCELSIUS  0  c  12
Co+2
River
7
HFO_DDL.DBS
ADS1CONC  0  n  7.00E-04   1.00E-04
ADS1AREA  0  c  600
2
ADS1TYP1  0  c  3.78E-08
ADS1TYP2  0  c  1.575E-06
Eh        -1    n          0.500     0.3
pH        0  n  7.11       0.15
11
Co+2      0  n  1.0E-07    2.00E-08
PO4-3     0  n  4.05E-06   1.81E-06
SO4-2     0  n  8.71E-04   9.53E-05
CO3-2     0  n  1.43E-03   1.82E-04
Cl-1      0  n  1.21E-03   2.86E-04
H4SiO4    19    QUARTZ
K+1       0  n  2.23E-04   5.24E-05
Na+1      0  n  1.40E-03   3.15E-04
Ca+2      0  n  1.18E-03   1.36E-04
Mg+2      0  n  2.69E-04   7.01E-05
Al+3      19    KAOLINITE
0
4
PYROPHYLLITE
DIASPORE
LEONHARDITE
HYDRAPATITE
Cl-1
```

Appendix D: Computation of distribution coefficients: Americium input parameter set for the Ravenglass Estuary.

```
Ravenglass Estuary (RESTRAT PROJECT)
fzr
V.Brendler
14.7.1999
3
TCELSIUS  0   c  10
Am+3
Upper Banks
7
HFO_DDL.DBS
ADS1CONC  0   n  3.25E-04   2.00E-04
ADS1AREA  0   c  600
2
ADS1TYP1  0   c  1.755E-08
ADS1TYP2  0   c  7.313E-07
Eh        -1  n  0.700      0.2
pH        0   n  7.02       0.2
11
Am+3      0   n  4.000E-15  2.00E-16
SO4-2     0   n  2.644E-03  1.47E-05
CO3-2     0   n  1.085E-04  2.00E-05
Cl-1      0   n  4.823E-02  3.99E-04
PO4-3     0   n  7.687E-05  7.45E-06
H4SiO4    19  QUARTZ
K+1       0   n  9.850E-04  3.62E-05
Na+1      0   n  4.226E-02  7.69E-04
Ca+2      0   n  1.148E-03  1.02E-04
Mg+2      0   n  4.567E-03  2.33E-04
Al+3      19  KAOLINITE
0
4
PYROPHYLLITE
DIASPORE
LEONHARDITE
HYDRAPATITE
Cl-1
Channel
7
HFO_DDL.DBS
ADS1CONC  0   n  3.25E-04   5.00E-03
ADS1AREA  0   c  600
2
ADS1TYP1  0   c  1.755E-08
ADS1TYP2  0   c  7.313E-07
Eh        -1  n  0.123      0.1
pH        0   n  7.93       0.1
9
Am+3      0   n  4.000E-15  2.00E-16
SO4-2     0   n  2.446E-02  7.36E-04
CO3-2     0   n  2.073E-03  3.48E-05
Cl-1      0   n  4.894E-01  1.40E-02
H4SiO4    19  QUARTZ
K+1       0   n  9.419E-03  3.55E-04
Na+1      0   n  4.138E-01  1.68E-02
Ca+2      0   n  9.749E-03  4.29E-04
Mg+2      0   n  4.680E-02  9.12E-04
0
4
DOLOMITE
TALC
TREMOLITE
LEONHARDITE
Cl-1
Sediment
7
HFO_DDL.DBS
ADS1CONC  0   n  33.25 6.6
ADS1AREA  0   c  600
2
ADS1TYP1  0   c  1.796E-03
ADS1TYP2  0   c  7.481E-02
Eh        -1  n  0.218      0.1
pH        0   n  7.33       0.1
10
Am+3      0   n  4.000E-15  2.00E-16
SO4-2     0   n  1.166E-02  1.03E-03
CO3-2     0   n  1.999E-02  2.55E-03
Cl-1      0   n  3.822E-03  4.99E-02
H4SiO4    19  QUARTZ
K+1       0   n  6.420E-03  9.04E-04
Na+1      0   n  3.006E-01  2.77E-02
Ca+2      0   n  6.300E-03  3.70E-04
Mg+2      0   n  3.473E-02  3.84E-03
Al+3      19  KAOLINITE
0
4
DOLOMITE
PYROPHYLLITE
DIASPORE
LEONHARDITE
Cl-
```

Appendix E: Computation of distribution coefficients: Uranium input parameter set for the Lake Tranebärssjön.

```
Lake Tranebärsjön (RESTRAT PROJECT)
fzr
V.Brendler
14.7.1999
4
TCELSIUS 0   c  7
UO2+2
Upper Layer
7
HFO_DDL.DBS
ADS1CONC  0   n  1.45E-04   2.90E-05
ADS1AREA  0   c  600
2
ADS1TYP1  0   c  7.830E-09
ADS1TYP2  0   c  3.263E-07
Eh        -1  n  0.800      0.05
pH        0   n  7.87       0.14
9
UO2+2     0   n  5.560E-07  3.26E-08
SO4-2     0   n  7.816E-03  7.44E-04
CO3-2     0   n  2.991E-03  4.06E-04
Cl-1      0   n  3.582E-04  2.69E-05
H4SiO4    19  QUARTZ
K+1       0   n  1.375E-04  1.28E-05
Na+1      0   n  3.318E-04  1.42E-05
Ca+2      0   n  8.660E-03  8.29E-04
Mg+2      0   n  8.146E-04  8.84E-05
0
0
SO4-2
Lower Layer
7
HFO_DDL.DBS
ADS1CONC  0   n  2.95E-02   5.90E-03
ADS1AREA  0   c  600
2
ADS1TYP1  0   c  1.593E-06
ADS1TYP2  0   c  6.638E-05
Eh        -1  n  0.200      0.2
pH        0   n  6.75       0.06
9
UO2+2     0   n  1.039E-06  2.39E-08
SO4-2     0   n  1.172E-02  1.25E-03
CO3-2     0   n  5.203E-03  1.33E-03
Cl-1      0   n  3.648E-04  1.39E-05
H4SiO4    19  QUARTZ
K+1       0   n  1.495E-04  2.35E-05
Na+1      0   n  3.749E-04  4.57E-05
Ca+2      0   n  1.375E-02  1.49E-03
Mg+2      0   n  1.228E-03  2.86E-04
0
3
DOLOMITE
TALC
TREMOLITE
SO4-2
Backfill
7
HFO_DDL.DBS
ADS1CONC  0   n  280        56
ADS1AREA  0   c  600
2
ADS1TYP1  0   c  1.512E-02
ADS1TYP2  0   c  6.300E-01
Eh        -1  n  0.800      0.2
pH        0   n  7.05       0.2
9
UO2+2     0   n  7.016E-07  1.40E-07
SO4-2     0   n  8.702E-03  1.70E-03
CO3-2     0   n  4.550E-03  9.10E-04
H4SiO4    19  QUARTZ
K+1       0   n  1.610E-04  3.20E-05
Na+1      0   n  3.480E-04  7.00E-05
Ca+2      0   n  9.556E-03  1.90E-03
Mg+2      0   n  7.447E-04  1.50E-04
Al+3      19  KAOLINITE
0
4
DOLOMITE
PYROPHYLLITE
DIASPORE
LEONHARDITE
SO4-2
Alum Shale
7
HFO_DDL.DBS
ADS1CONC  0   n  1080       220
ADS1AREA  0   c  600
2
ADS1TYP1  0   c  5.832E-02
ADS1TYP2  0   c  2.430
Eh        -1  n  0.200      0.2
pH        0   n  6.84       0.2
9
UO2+2     0   n  1.158E-06  1.10E-06
SO4-2     0   n  1.517E-02  6.43E-05
CO3-2     0   n  7.350E-03  1.50E-03
H4SiO4    19  QUARTZ
K+1       0   n  2.654E-04  5.27E-04
Na+1      0   n  5.459E-04  2.29E-05
Ca+2      0   n  1.455E-02  4.95E-04
Mg+2      0   n  1.469E-03  7.10E-05
Al+3      19  KAOLINITE
0
4
DOLOMITE
PYROPHYLLITE
DIASPORE
LEONHARDITE
SO4-2
```